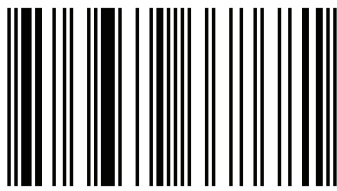


## Wireless Power by Magnetic Resonance

The subject of wireless power has been of great fascination since antiquity. First proposed in modern times by Nikola Tesla, it has intrigued and challenged the academic world. While there have been many attempts to describe this work, the mathematical explanation of wireless power can be traced to J. Clerk Maxwell's original equations and the behavior of wireless power in the circuit is due to Joseph Larmor's fundamental works on the dynamics of the field concept. Once you experience the unlimited nature of wireless power, it captures your imagination. One can build devices big and small at a range of frequencies, from small implants to industrial and robotic applications. This book is written for those who thrive on innovation and the unforetold limits of the evolution of the human spirit.



Dr. Tucker was born in Chicago, Illinois and attended the University of Reading, where he received his PhD. Fascinated by wireless power and robotics at a young age, he spent much of his formative years winding coils and assembling circuits in the basement of his family house in an attempt to understand the invisible force known as electromagnetism



978-3-639-66868-1

Wireless Power by Magnetic Resonance

Tucker

Scholars'  
Press

Christopher A. Tucker

## Wireless Power by Magnetic Resonance

Theory, application, and control

**Christopher A. Tucker**

**Wireless Power by Magnetic Resonance**

FOR AUTHOR USE ONLY



**Christopher A. Tucker**

# **Wireless Power by Magnetic Resonance**

**Theory, application, and control**

FOR AUTHOR USE ONLY

**Scholar's Press**

## **Impressum / Imprint**

Bibliografische Information der Deutschen Nationalbibliothek: Die Deutsche Nationalbibliothek verzeichnet diese Publikation in der Deutschen Nationalbibliografie; detaillierte bibliografische Daten sind im Internet über <http://dnb.d-nb.de> abrufbar.

Alle in diesem Buch genannten Marken und Produktnamen unterliegen warenzeichen-, marken- oder patentrechtlichem Schutz bzw. sind Warenzeichen oder eingetragene Warenzeichen der jeweiligen Inhaber. Die Wiedergabe von Marken, Produktnamen, Gebrauchsnamen, Handelsnamen, Warenbezeichnungen u.s.w. in diesem Werk berechtigt auch ohne besondere Kennzeichnung nicht zu der Annahme, dass solche Namen im Sinne der Warenzeichen- und Markenschutzgesetzgebung als frei zu betrachten wären und daher von jedermann benutzt werden dürften.

Bibliographic information published by the Deutsche Nationalbibliothek: The Deutsche Nationalbibliothek lists this publication in the Deutsche Nationalbibliografie; detailed bibliographic data are available in the Internet at <http://dnb.d-nb.de>.

Any brand names and product names mentioned in this book are subject to trademark, brand or patent protection and are trademarks or registered trademarks of their respective holders. The use of brand names, product names, common names, trade names, product descriptions etc. even without a particular marking in this work is in no way to be construed to mean that such names may be regarded as unrestricted in respect of trademark and brand protection legislation and could thus be used by anyone.

Coverbild / Cover image: [www.ingimage.com](http://www.ingimage.com)

Verlag / Publisher:

Scholar's Press

ist ein Imprint der / is a trademark of

OmniScriptum GmbH & Co. KG

Heinrich-Böcking-Str. 6-8, 66121 Saarbrücken, Deutschland / Germany

Email: [info@scholars-press.com](mailto:info@scholars-press.com)

Herstellung: siehe letzte Seite /

Printed at: see last page

ISBN: 978-3-639-66868-1

Zugl. / Approved by: Reading, University of Reading, 2013Diss., 2013

Copyright © 2014 OmniScriptum GmbH & Co. KG

Alle Rechte vorbehalten. / All rights reserved. Saarbrücken 2014

## Dedication

This work is dedicated to my family. Without their strength, support, and belief in me this book would not have been possible.

FOR AUTHOR USE ONLY

FOR AUTHOR USE ONLY

## Table of Contents

1	Introduction .....	15
1.1	Maxwell and Larmor .....	22
1.2	Poynting and Tesla .....	32
1.3	Wireless power as concept .....	38
2	Power transmission and magnetic-resonant modes in an inductively-coupled circuit .....	40
2.1	A single coupled-mode with projection .....	53
2.1.1	The coupling coefficient .....	60
2.1.2	Coupled-mode power .....	69
2.1.3	Efficiency, quality, and loss .....	72
2.1.4	The magnetic potential.....	75
2.2	The circuit model .....	89
2.2.1	The push-pull oscillator .....	92
2.2.2	Simulation and construction of the circuit .....	96
2.2.3	Equations of the circuit model .....	99
2.2.4	The circuit model with acceleration.....	104
2.3	The propagation model.....	108
2.3.1	The receiving antenna .....	115
2.3.2	Radiated power .....	122
2.3.3	Field emissions.....	127
2.3.4	Energy derived by forces over areas.....	128
2.4	The circuit experiments.....	130
2.4.1	Measured power at a distance with a single loop transmitter and receiver .....	130

2.4.2	Measured power at a distance with an enhanced magnetic field at the potential .....	141
2.4.3	The circuit experiment performed in human proximity.....	144
2.4.3.1	Coupled-power delineation.....	150
2.4.3.2	ac mode.....	151
2.4.3.3	dc mode.....	152
2.4.4	Optimization of the circuit .....	154
3	Two coupled-modes without projection.....	159
3.1	The theoretical model.....	162
3.1.1.1	The transmitter coils .....	163
3.1.1.2	The receiver coils.....	164
3.1.1.3	The coupling coefficient .....	165
3.1.1.4	Determination of mutual inductance in the model.....	167
3.1.1.5	On quality and loss .....	168
3.2	The propagation of magnetic currents.....	169
3.3	The circuit experiment .....	173
3.4	Observations of behaviors present in the circuit of two coupled- modes.....	178
4	The dipole concept and accelerated electrons in matter .....	181
4.1	Basic assumptions .....	183
4.2	Point-charge representation and forces under separation.....	184
4.3	Mapping of dipole energy circulation .....	188
5	Application and control .....	192
5.1.1	A brief discourse on the potential of medical device applications.....	193
5.1.2	Featured power and choice in the machine.....	200

5.1.2.1	General model of robotic feeding and the application of choice .....	203
5.1.2.2	Decision-making embedded within transformation logic.....	207
5.1.2.3	A wireless-power model of robotic feeding.....	209
5.1.2.4	The entropic circuit.....	212
5.1.2.5	Thoughts on featured power and choice .....	214
5.1.3	Solar panels for spacecraft.....	216
5.1.3.1	Theory of operation .....	218
5.1.3.2	A sample application .....	219
5.1.3.3	Thoughts about wireless power for space activities .....	224
6	Conclusion.....	225
6.1	Coupled-modes .....	227
6.2	Circuit model and propagation.....	227
6.3	Antenna at the interface.....	229
6.4	Commentary on the magnetic potential and final words.....	230
7	Appendix – Table, figure, and code .....	234
8	References .....	237

## Table of Figures

Fig.1.1. Maxwellian (left) and Tesla (right) description of transmission by circuit discharge.....	17
Fig.1.2. Tesla's vision of wireless power. ....	36
Fig.2.1. The prototypical model for the transmission of wireless power by magnetic resonance.....	41
Fig.2.2. Demarcation of the field force in the medium displacing energy to a fall-off threshold. ....	43
Fig.2.3. Ray relationships between the magnetic field, radial vector, and infinitesimal current.....	45
Fig.2.4. Geometry of the coupling-mode magnetic field.....	46
Fig.2.5. Projection of energy by a current impressed on the loop. ....	49
Fig.2.6. Field lines following an axis of displacement. ....	50
Fig.2.7. Flux linkage between two inductively-coupled coils. ....	51
Fig.2.8. Field geometry extending away from the projection.....	52
Fig.2.9. Projection field forming the mid-field region by intensity.....	53
Fig.2.10. Projection of field and its geometry between two inductively-coupled coils. ....	53
Fig.2.11. FEM model workspace layout.....	58
Fig.2.12. Calculator values for (a) resonance frequency, and (b) inductance of the transmission loop.....	62
Fig.2.13. Coil properties describing (51). ....	63

Fig.2.14. Magnetic coupling of low- $\kappa$ modes of distant resonators in space and time. ....	67
Fig.2.15. Theoretical coupling coefficient over a distance given (45). ....	68
Fig.2.16. (a) The vector potential in the magnetic field, (b) the potential component on the loop interface.....	78
Fig.2.17. A single loop projecting a magnetic field.....	80
Fig.2.18. Two circular loops with accretion discs. ....	81
Fig.2.19. (a) Magnetic flux of loop antenna, (b) disc adds flux strength....	87
Fig.2.20. Propagating energy in $\mathbf{B}$ . ....	88
Fig.2.21. Density of azimuthal $\mathbf{B}$ field. ....	89
Fig.2.22. The regenerative oscillator. ....	91
Fig.2.23. Inductively-coupled push-pull oscillator. ....	93
Fig.2.24. The n-channel MOSFET structure. ....	94
Fig.2.25. Schematic representation of accelerating electrons split across a tank circuit. ....	94
Fig.2.26. Phase-shift amplifier on coils. ....	95
Fig.2.27. The transmission element with a coupled-mode. ....	96
Fig.2.28. (a) The receiving element with a coupled-mode, (b) an example receiver. ....	97
Fig.2.29. The broadcasting model for simulation. ....	98
Fig.2.30. Simulated signal seen by the receiver. ....	98

Fig.2.31. Simplified circuit diagram.....	103
Fig.2.32. The constructed oscillator.....	104
Fig.2.33. Representation of oscillator cycle circulating charges in the antenna conductor.....	105
Fig.2.34. Radiation emissions of a magnetic loop antenna.....	111
Fig.2.35. Wave propagation for the modal coupling scheme of wireless power transfer.....	111
Fig.2.36. Schematic representation of a virtual transmission line of an antenna to a region of space.....	112
Fig.2.37. Angular motion of the oscillator transition phase. ....	113
Fig.2.38. The transmitter coil.....	114
Fig.2.39. (a) Schematic of the receiving loop antenna. (b) Loop antenna connected to a capacitor at the voltage gap. The white arrows are surface currents. .....	116
Fig.2.40. Modified schematic of RWG edge elements and dipole interpretation for curvature $\theta$ .....	119
Fig.2.41. Two loop meshes: (a) 288 triangles and (b) 1152 triangles. ....	119
Fig.2.42. (a) Triangle quality of the loop mesh, (b) current density on the loop. ....	120
Fig.2.43. Directional power density of field on its approaching wave front, white shows higher intensity.....	121
Fig.2.44. Projection of magnetic currents with highest potential coupling points $H_\theta$ .....	126

Fig.2.45. Average power-over-space antenna radiation pattern looking into the coil. ....	127
Fig.2.46. Maxwell's vortices at the interface of a loop. ....	128
Fig.2.47. Diagram of the circuit for a single coupled-mode. ....	131
Fig.2.48. Power over distance showing the projection field $\bar{\mathbf{H}}$ , where $C_i \approx C_j$ . ....	132
Fig.2.49. Power transmission over a longer distance.....	133
Fig.2.50. The power over distance using a thicker antenna wire.....	134
Fig.2.51. The power intensity over distance showing linear falloff, where $C_i > C_j$ . ....	135
Fig.2.52. Radiation pattern observed at the receiver. ....	137
Fig.2.53. Prototypical wireless-power oscillator demonstrating the theoretical model. ....	140
Fig.2.54. Experimentally-tested orientation of multiple receivers $r$ and $s$ with reference to each position at the transmitter $t$ when there is no angle of rotation away from axial alignment $a_n = 0$ . The standing height of all coils are equal.....	148
Fig.2.55. Experimentally tested orientation of multiple receivers $r$ and $s$ , through with an angle of rotation $\theta$ away from axial alignment, with reference to each position at the transmitter $t$ . The standing height of all coils is equal. ....	149
Fig.2.56. The dc power intensity seen by the receiving antenna with axial alignment. ....	153
Fig.2.57. Operational oscillator powering multiple lamps. ....	157

Fig.3.1. Tesla's wireless power model.....	160
Fig.3.2. Transmitter coil package.....	164
Fig.3.3. Receiver coil package.....	164
Fig.3.4. Schematic diagram of the circuit for two coupled-modes.....	166
Fig.3.5. The virtual waveguide comprised of a coherent field in the model based on Fig.2.17.....	168
Fig.3.6. Magnetic field intensity and flux density between two secondary spiral coils.....	170
Fig.3.7. Magnetic field intensity and flux density at greater distance.....	171
Fig.3.8. Receiver package and third coil. Component breadboard shown.	
.....	173
Fig.3.9. The efficiency of the Tesla resonator over a distance. ....	174
Fig.3.10. Comparison of the Tesla resonator with Kurs [10]. .....	174
Fig.3.11. The efficiency of the Tesla resonator with enhanced quality factor.....	176
Fig.4.1. Point-charge dipole under separation. ....	185
Fig.4.2. Point-charges and the wake pattern of forces.....	186
Fig.4.3. Electrostatic dipole model emitting shearing forces, $\vec{F}_E, \vec{F}_B$ , fixed about the moment m and creating the projection $\vec{H}$ . .....	187
Fig.4.4. Photon reflection and absorption primitives.....	188
Fig.4.5. Propagation zones for dipole energy circulation. ....	189
Fig.4.6. Dipole preservation circuit. ....	192

Fig.5.1. EEG measurement over the Psoas Major/Minor under ordinary conditions.....	197
Fig.5.2. EEG measurement over the Psoas Major/Minor 15 minutes after exposure.....	197
Fig.5.3. EEG measurement over the Psoas Major/Minor 76 minutes after exposure.....	198
Fig.5.4. EEG measurement over the Psoas Major/Minor 149 minutes after exposure.....	198
Fig.5.5. EEG measurement over the Psoas Major/Minor 160 minutes after exposure.....	199
Fig.5.6. EEG measurement over the Psoas Major/Minor 180 minutes after exposure.....	199
Fig.5.7. Featured power environment using choice control.....	200
Fig.5.8. Activity of robotic feeding behavior. ....	203
Fig.5.9. Activity of robotic feeding behavior – Pseudocode. ....	204
Fig.5.10. Finite-state diagram of robotic power-seeking behavior. ....	205
Fig.5.11. Runtime choice-weights for consequential decision-making....	207
Fig.5.12. Finite-state diagram of power seeking behavior for charging station and wireless power. ....	209
Fig.5.13. Runtime choice-weights for consequential decision-making in complex power-signaling.....	211
Fig.5.14. Functional diagram of an entropic circuit.....	213
Fig.5.15. Common solar paddle array.....	221

Fig.5.16. Flexive joints using wireless-power couplings.....222

Fig.7.1. Effect on the simulated output based on changing the value of the coupling coefficient  $\kappa_y$ . .....235

FOR AUTHOR USE ONLY

## Table of Tables

Table 2.1. Loop coils theoretical specification.....	65
Table 2.2. Energy, quality, and loss specification.....	74
Table 2.3. Simulation circuit properties.....	97
Table 2.4. Oscillator state by $\mathcal{Q}$ and $\zeta$ .....	101
Table 2.5. Oscillator traveling wave parameters.....	102
Table 2.6. Computational elements from mesh to field solutions. ....	115
Table 2.7. Transmission and receiving coils physical specification.....	116
Table 2.8. Matlab computed input characteristic antenna data.....	121
Table 2.9. Experimental coils calculated electrical specification I.....	131
Table 2.10. Experimental coils calculated electrical specification II. ....	133
Table 2.11. Calculated antenna characteristics based on [29]. .....	139
Table 2.12. Calculated quantities in the projected magnetic field.....	143
Table 2.13. Calculated quantities in the projected magnetic field.....	143
Table 2.14. Experimental quantities of the magnetic loop antenna.....	144
Table 3.1. Resonant coils physical specification.....	165
Table 3.2. Resonant coils calculated electrical specification.....	167
Table 3.3. Resonant coils measured electrical specification.....	175
Table 7.1. Values of factor $u^2$ [31].....	234
Table 7.2. Instructions to create an antenna mesh file.....	236

# Wireless power by magnetic resonance

Theory, application, and control

FOR AUTHOR USE ONLY

## 1 Introduction

Before the proven success of Marconi's 1902 transatlantic radio transmissions to what later became the sole means of the wireless art, various methods investigated the transport of energy and information over long distances without wires. The most well-known practical experiments preceding this were performed by Lodge [119] and Tesla [103]; the latter discussed wireless transmission as early as his 1892 lectures delivered before the American Institute of Electrical Engineers in New York and the Institute of Electrical Engineers in London [13]. His methods focused on non-radiative and capacitive discharge, while Lodge centralized around inductive discharge following Hertz and the treatment of the Maxwellian theory of light [2, 108, 121].

Marconi, inheriting ideas from Lodge and supported by the work of Heaviside, would go on to establish the practical Hertzian model of radio transmission. Tesla's work, by contrast, would lay dormant. The core of Tesla's experiments to a large extent were supported by Poynting and Larmor, which had two features in common: 1. The Earth acts as a conductor corridor, a charged shell capable as a transmission medium, and, 2. By designing a suitable circuit, pathways could be created allowing electrical currents to pass between distant locations. A more subtle conclusion is that the coils could be designed in such a manner as their magnetic fields resonate, at least in part, with the Schumann resonance [110]. A centerpiece is the treatment of free-space in the manner described by Maxwell's non-radiative magnetic vortices [99, 100, 109], and of a displacement of current contained in a structure [23, 47]. Haus observed and mathematically incorporated these ideas into his notion of evanescent waves in the late 20<sup>th</sup> Century [94].

Wireless energy transfer, in the present scope of understanding, is most effective in near or mid-field regions, arguably in some radiative form. Near-field transfer is of the type exhibited in the transformer effect and usually obtained through mutually-inductive coils and capacitive effects. Mid-field regions exhibit behavior where the falloff is rapid, yet linear. It has been proposed that distances achievable by this scheme are generally very short, limited to a few times the diameter of the coils [31], losses occurring due to resistive and radiative effects. Transmission in the far-field involves higher frequencies where distances achieved are much greater than the radius of the coils and can involve complex tracking systems. The conclusion if this is theoretical and practical methods of the wireless transfer of energy, distinguished by the broadcast frequency and circuit geometry, are distinguished by scope and application.

The purpose of the research described in this work is to investigate two forms of efficient medium-range coupling using small-scale antennas without tracking systems where the transmitter and receiver can lie at a distance, where one must lie in axial alignment, the other regardless of position and orientation. By the construction of highly-efficient resonance transformers which facilitate stable transmission of power and information at useful distances, these two distinct forms—one with a single set of coils exhibiting a projection field, a second with two sets of tuned circuits exhibiting energy distribution regardless of coil orientation demonstrate the velocity of electrons and their acceleration in their conductors establish the well-known concept of relativity while illustrating the interpretation of free-space manifesting differential time in resonant coupling could be incorrect.

This begins with Tesla's idea of velocity-inhibition, in response to the Fitzgerald-Lorenz contraction, dividing types of wireless transmission into two categories: One where devices are radiative, manifest a projection from the acceleration of electrons [6], and non-radiative where the exchange of energy is along a power series of standing planar waves between the coils relative to their positions on the surface of the planet [103]. The power series is underpinned by the power transformation in family time of the exchange of magnetic fields at resonance [21, 26, 52, 84]. Along the length of the planar waves constituting a virtual waveguide, lie regions of strong coupling where a coil and a load extract electrical energy to perform work.

In the view of the wireless transfer of power by projection, wireless transmission of energy through signaling [99, 122], the model relies on the creation of an inductive link which is maximized at a particular resonance frequency  $\omega_0$  given the physical characteristics of sets of tuned coils, e.g., the angular momentum of the electrons in the conductor. The transmission can be accomplished by discharge at a coil, described by the Maxwellians, shown on the left-side of Fig.1.1, or by discharge at a capacitor, described by Tesla, shown on the right-side of Fig.1.1.

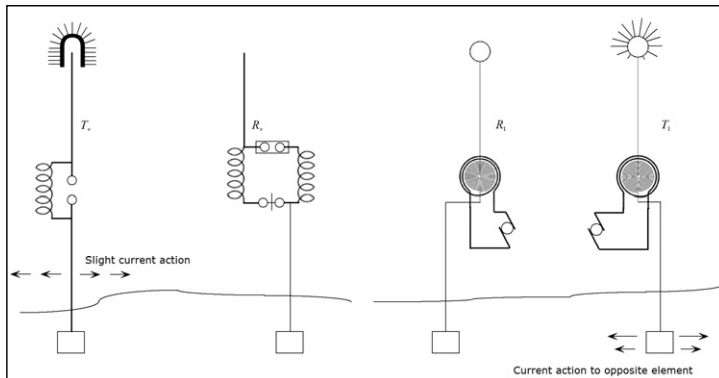


Fig.1.1. Maxwellian (left) and Tesla (right) description of transmission by circuit discharge.

It is commonly viewed the transformer model discovered by Michael Faraday and Joseph Henry permits the transfer of energy between circuits in close proximity. But can it also be assumed a similar phenomenon is responsible over longer distance transmission using same or similar mechanisms? Is there a universal phenomenon which allows transfer? It could be argued that the near-field for these schemes does not exist, rather, the energy is expressed in the far-field exclusively, dependent on the type of antenna which typically are loops of a few turns, transforming energy to free-space from a sinusoidal source. In the most restricted sense, energy is stored in the field by the exchange between the inductive and capacitive components contained in the circuit, through damping of the frequency. Consequently, a contiguous field has presence over the distance between the coupled elements that cannot be simply divided into near and far-field descriptions. Therefore, for the purposes of correctness, clarity, and exactness all fields resulting from electrical reactions in circuits discussed in this work will be denoted as having a presence in the mid-field region.

James Clerk Maxwell proposed mathematical solutions to the experimental observations of Michael Faraday and built a framework around what was to become field theory between the years of 1855 to 1873. Poynting further developed the mathematical context of the free-space field concept to include energy and its distributions in 1884, Hertz first experimental confirmed the existence of electromagnetic waves in 1886, Larmor described the electron and its behavior under acceleration by a current in 1895, Lodge demonstrated the first prototype of what would be called “the radio” in 1894, and Tesla, using more refined devices at higher potentials, demonstrated this work to the public at the IEE in London in 1892 and at the Chicago World’s Fair in 1893, culminating his vision in Colorado

Springs in 1899 and the Wardenclyffe Tower in 1901 for the World Wireless System [112, 113].

In the electrical age of the Victorian Era, the development of power transmission was reinforced by many imaginative scenarios in the hope of an encompassing and complete description. The most powerful of these being that of the aether to support the transmission of electromagnetic waves, later subtended by relativity following the First World War. From the 1920s to the 1960s, the concept of signaling was isolated into its own category separate from power transmission, due primarily to the development of the field of radio engineering following Marconi. Wireless power, as a transmitted radio-frequency signal, would reappear in the early 21<sup>st</sup> Century.

The description of a method and means of wireless power transmission, facilitated primarily by the phenomenon of magnetic resonance, in this work will focus on the most pressing question: what constitutes free-space as a transmission medium, given the set of historical conditions the fields of physics and engineering have imposed upon it? In order to begin addressing this question, the proposition of a model of the transportation of energy across free-space by magnetic resonance will be provided. The concept of signaling is relevant to the work as a more descriptive body of theory regarding radio-wave propagation and computational strategies, as opposed to purely electromechanical forces such as voltage and current. The emphasis will be that the dynamics of the field is of greater interest than simple expressions of power ratios transforming between distant points.

The model discussed in this work is to be structured as:

- modular components of an idealized architecture, each of the components forming a part of the entire argument,
- in the attempt to demarcate a cross-compatibility between the circuit and field model,
- to propose methods which demonstrate linear granularity,
- to propose experiments to test the methods, in order to,
- discover a measurement criterion of performance of a physical model, and,
- discuss the results and extended components learned during the process to aid in future development.

The presentation will be an engineering-centric, scientific investigation where the material is organized appropriate for the subject matter. The work is divided into three categories: circuits, fields, and waves; each chapter serves to disseminate the contribution into distinct, yet interconnected, parts. As the author is aware of the divergence between circuit and field analytics, the circuit model will be tested in an experiment of a working prototype and the antenna at the interface will be where the author will attempt to converge the concept. This will not only provide a concrete expression for the theoretical musings, but to also make the concept more tangible. For such an abstract concept, a cast of the meaning of the expression should exhibit both a form and a function. This process will enumerate

- a circuit with antenna emitting radiation in a geometrically-defined pattern,
- as an ambient free-space field of a uniform structure, and,
- a behavior depiction in terms of Maxwell, Larmor, Poynting, and Tesla,

- which leads to a characteristic prototype of device,
- which has numerous direct applications in the current state-of-the-art,
- however, it will be recalled that the device is not unto itself, rather, a representation of a method and means to *transform* energy in the aforementioned context as a method of control,
- useful to serve many ambitions as manifested in technology.

In an attempt to be concise as possible, the remainder of the introduction will be to trace the specific parts of Maxwell's *original* equations that are directly relevant to the arguments and mathematical descriptions pursued in the following chapters. The work of Joseph Larmor will be discussed in terms of his point of view of time-contraction in context with these equations. Next, how these equations are utilized by Poynting to mathematize the electromagnetic field in terms of circuits and how Tesla was able to verify experimentally these theoretical concepts on a large scale. The focus of this book, then, is to draw the reader to consider how reliant the science is on past works to yield insights to modern problems [1], while demonstrating recent innovations following these works. While there is a dependence upon the past, the freedom of context it provides expands possibilities in overcoming the dogma of orthodoxy which is the only way to foster innovation. Therefore, it is useful to consider also how control plays a significant role in helping to define the work in two distinct aspects: one of the phenomenon and its manifestation, and one of how it solves problems by functioning as a piece of middleware.

## 1.1 Maxwell and Larmor

Maxwell's equations have been widely discussed in the literature since their first appearance in *A Dynamical Theory of the Electromagnetic Field* in 1865. These equations address five basic phenomena:

- The electric field  $\mathbf{E}$ , (in V/m),
- The magnetic field  $\mathbf{B}$ , (in T),
- The magnetic field intensity  $\mathbf{H}$ , (in A/m),
- The density of electric charge  $\rho$ , (in C/m<sup>3</sup>),
- The density of electric current  $\mathbf{J}$ , (in A/m<sup>2</sup>),

which, in the microscopic case, take the vector forms:

$$\begin{aligned}\nabla \times \mathbf{E} + \frac{\partial \mathbf{B}}{\partial t} &= 0, \\ \nabla \cdot \mathbf{E} &= \frac{\rho}{\epsilon_0}, \\ \nabla \times \mathbf{B} - \frac{1}{c^2} \frac{\partial \mathbf{E}}{\partial t} &= \mu_0 \mathbf{J}, \\ \nabla \cdot \mathbf{B} &= 0,\end{aligned}\tag{1}$$

and in the macroscopic case, with Ampère's circuital law,

$$\nabla \times \mathbf{H} = \mathbf{J} + \frac{\partial \mathbf{D}}{\partial t},\tag{2}$$

where the constants are tied by the relationship to free-space,

$$\epsilon_0 \mu_0 c^2 = 1,\tag{3}$$

where,

- $\epsilon_0$  is the electric permittivity of the vacuum, (in F/m),

- $\mu_0$  is the magnetic permeability of the vacuum, (in H/m), and,
- $c$  is the speed of light in a vacuum, (in m/s).

In the present era, there exist two distinct embodiments of what is commonly attributed to be “Maxwell’s equations”. Those by Maxwell himself and those by the Maxwellians [2]: Heaviside, Fitzgerald, Lodge, and Hertz. The modern and ubiquitous form of the Maxwell equations are the result of a vectorization of the original twenty equations with twenty unknowns, in quaternion format, by the Maxwellians with an emphasis to capture an approximation of moving charges and rotations of energy in the field, notably Maxwell’s idea of the “curl”. Accounting of electromagnetic interactions outside the context of the localized field were discarded. While the reasons for the truncation allowed a simpler representation which suited the newborn field of electrical engineering in the 19<sup>th</sup> Century, such a notion is not reasonable in the present era of the computational arts. The Maxwellians, driven primarily by the work of Heaviside, banished the vector and scalar potential functions from the original equations. As a result, the concept of the displacement current  $\mathbf{D}$ , central to describing energy transfer as the consequence of coupling by magnetic resonance, and the real-valued magnetic potential,  $\mathbf{A}$ , were omitted [3, 4]. The reason being since neither these nor the resulting magnetic fields are associated with moving charges, contrary to the position later argued by J.J. Thomson in his theory of corpuscles, or what Larmor called electrons, the construct was viewed as simply not necessary and purely mathematical conveniences. To this day, the displacement current and a real-valued magnetic potential in classical systems theory is a controversial, rather unclear [104, 105], but central aspect of electromagnetic theory.

For the purposes of explanation in terms of the experiments introduced later in this book, both the Maxwellian and Maxwell equations are not complete to describe the antenna at its interface for particular types of oscillators. Rather, because of the central role of accelerated electrons in these operations, the dynamics needed to be understood from a different point of view, namely that offered by Joseph Larmor in a series of publications from 1893 – 1897 [5, 6, 43]. In examining both theories—the Maxwellians on one side, Larmor on the other—it becomes clear where the two procedures share commonality and differences. The points of view, however, are distinct and not directly compatible, therefore by their nature, divergent. The divergence essentially revolves around Thompson's interpretation of the description of the electron, which Larmor had described as [6]: dissecting the problem from the point of view of radiation on the basis of electric actions, the other, electric actions on the basis of a mechanical theory of radiation—of radiant structures or field objects emitted by the exchange of energy at a distance between coupled conductors. The Maxwellians were to take the former while Larmor undertook the latter.

Maxwell's original expression of electromagnetic quantities, following *Dynamical Theory*, consists of two systems A and B where one has influence on the other and the effects are compounded by coefficients of force. In terms of induction, Maxwell states that L, M, and N depend on the distribution of the magnetic effects due to two circuits, their relative position and subject to variation given its velocity.

Of the original twenty Maxwell equations, only six will be treated by this work for their relevance to the topic at hand.

- (A) The relation between electric displacement, true conduction, and the total current, compounded of both as a means of reduced momentum,

$$\begin{aligned} C \frac{dw}{dt} \delta z &= X \delta x + Y \delta y, \\ X &= \frac{d}{dt} (C p^2 q u + C p q v), \\ Y &= \frac{d}{dt} (C p q u + C q^2 v), \end{aligned} \quad (4)$$

where the momentum of the system referred to as A is  $Lu + Mv$  and B is  $Mu + Nv$ .

- (B) The relation between the lines of magnetic force and the inductive coefficients of a circuit, as already deduced from the laws of induction and the resistive forces  $R$  and  $S$ , the equation of the current in  $x$  in A will be,

$$\xi = Rx + \frac{d}{dt} (Lx + My), \quad (5)$$

and that the current in  $y$  in B is,

$$\eta = Sy + \frac{d}{dt} (Mx + Ny). \quad (6)$$

- (C) The relation between the strength of a current and its magnetic effects, according to the electromagnetic system of measurement.  
 (D) The value of the electromotive force in a body, as arising from the motion of the body in the field, the alteration of the field itself, and the variation of electric potential from one part of the field to another.

- (E) The relation between electric displacement, and the electromotive force which produces it, as the work done in a unit of time arising from the variations of L, M and N of the conducting circuits A and B,

$$\frac{1}{2} \frac{dL}{dt} x^2 + \frac{dM}{dt} xy + \frac{1}{2} \frac{dN}{dt} y^2. \quad (7)$$

- (F) The relation between and electric current, and the electromotive force which produces it.
- (G) The relation between the amount of free electricity at any point, and the electric displacements in the neighborhood.
- (H) The relation between the increase or diminution of free electricity and the electric currents in the neighborhood.

Only those indicated above with equations, e.g., (A), (B), and (E), will be discussed in greater detail for their contributions. The others will be absorbed into the discussion only where necessary. It is relevant now to examine the expression of the terms as quantities of intrinsic energy of the field and show the applicability of this method, as opposed to strictly the Maxwellian equations (1) and (2), tied to unity in (3) for a more thorough mathematical description of the field more agreeing in geometry and by inspection, which has resulted in this particular wireless power scheme.

In order to do this, it will take the assumption where Larmor and Maxwell agree on the electric displacement (A and E). Larmor states regarding this term from the point of view of the medium:

The problem of the aether has been first determinedly attacked from the side of electrical phenomena by Clerk Maxwell in quite recent times; his great memoir on a 'Dynamical Theory of the Electromagnetic Field' is of

date 1865. It is in fact only comparatively recently that the observation of Ørsted, and the discoveries and deductions of Ampère, Faraday, and Thomson had accumulated sufficient material to allow the question to be profitably attacked from this side. Even as it is, our notions of what constitute electric and magnetic phenomena are of the vaguest as compared with our ideas of what constitutes radiation, so that Maxwell's views involve difficulties, not to say contradictions, and in places present obstacles which are to be surmounted, not by logical argument or any clear representation, but by the physical intuition of a mind saturated with this aspect of the phenomena. Many of these obstacles may, I think, be removed by beginning at the other end, by explaining electric actions on the basis of a mechanical theory of radiation, instead of radiation on the basis of electric actions. The strong point of Maxwell's theory is the electromotive part, which gives an account of electric radiation and of the phenomena of electromagnetic induction in fixed conductors; and this is in keeping with the remark just made. The nature of electric displacement, of electric and magnetic forces on matter, of what Maxwell calls the electrostatic and the magnetic stress in the medium, of electrochemical phenomena, are all left obscure [4, pp.445-6].

Which assumes a potential energy structure of imperfect consistency called free-space. The term will be restricted to a charged dielectric: A theoretical representation of a specific type of phenomenon extant between free-space conductors on a planetary surface. It is this structure the author argues is an accurate representation.

A line of agreement between Larmor and Maxwell begins both the foundation and the angle of approach to the problem-space for the formulations in this work, namely the displacement current. From this beginning point, the work will explore those tools from both sets of the arguments to explain the physical model of a wireless power scheme which exhibits magnetic resonance in the mid-field region, that is, at the end of its

projection field  $\bar{\mathbf{H}}$ . At present, this seems the best tool to yield an accurate mathematical representation. This work will restrict the discussion of this when it approaches quantum field theory, deferring the model to an example of sufficiently large dielectric medium given a transmission frequency. Simply, moving charges in the experiment are described by the Larmor formula and Bloch waves for an irregular medium.

Rather than directly called using the Fitzgerald-Lorentz conjecture of retarded time used as a foundation in relativity, family time [26] is used to describe length contraction given forces, velocities, and wave propagation, guised in Poincare's [42] non-Euclidean approach. This is possible because the use-case is restricted to that of two resonant conductors having a conduction-current between them.

Some questions to answer are the following:

- What forces allow the propagation of the free-space wave of electric and magnetic components resulting from action in parallel conductors, or resonant objects?
- What forces counteract the propagation of the free-space wave of electric and magnetic components resulting from action in parallel conductors, or resonant objects?
- While it is clear such objects exchange energy across free-space, how does the nature of the disturbance and the displacement taking place mirror what is being observed in the experiment?
- Can it be argued that the corridor of wave propagation is demarcated as a virtual waveguide with properties analogous to its physical analogue?

The significance of the displacement current lies in the inclusion of a strain on the medium, which could be filled with charged matter of either a light or dark predisposition, depending on how it is defined. Particularly, this work will describe the medium which can experience electric strain where a magnetic field is impressed. Maxwell's derivation of strain is unrelated to the modern day derivation for displacement current in the vacuum, which is based on consistency between Ampère's law for the magnetic field and the continuity equation for electric charge. Maxwell imagined the displacement as a sea of molecular vortices existing in free-space and the displacement a strain on the medium. However, when considering polarized circuits, the ambiguity in Maxwell's derivation clears—the current is the displacement. The consequences of clarity are costs in the form of an exchange of forces at the boundary whose periodicity suggests the ability to create artificial electrical structures with a polarization.

Once Maxwell's sea of molecular vortices had been abandoned, along with it the aether, an interpretation of displacement current evolved that treated free-space explicitly as a separation of free-space from material media, unlike Maxwell's original concept.<sup>1</sup> This is a feature associated with the potentials, relative to free-space [7, 8], which yields the curl to describe linear displacement. If the vector  $(f, g, h)$  denotes the curl of the medium, or twice the absolute rotation of the portion of the medium at the point considered, and the medium is supposed of crystalline-like quality, in that

---

<sup>1</sup> The final disengagement of “vacuum” from real media occurred with the international agreement to use the material-unrelated terms *electric constant* and *magnetic constant* to replace the seemingly material-related terms *permittivity* of vacuum and *permeability* of vacuum. These constants have *defined* (not measured) values that refer to free-space, which is viewed as an unattainable idealization; not as a real, observable medium, not equivalent to a quantum vacuum.

the geometry is distributed and well-ordered along its principal axes. Under such an assumption the field object,  $\Omega_0$ , takes the form,

$$\Omega_0 = \frac{1}{2} \int (a^2 f^2 + b^2 g^2 + c^2 h^2) d\nu, \quad (8)$$

where  $d\nu$  is an element of volume inclusive of the boundary. It follows that for an internal equilibrium of the structure, it must have,

$$a^2 f dx + b^2 g dy + c^2 h dz = -d\varphi, \quad (9)$$

a complete differential and that over any boundary enclosing a region devoid of elasticity the value  $\varphi$  must be constant. Such a boundary is the surface of a conductor;  $\varphi$  is the electric potential in the field due to charges on the conductors;  $(f, g, h)$  is the electric displacement in the field, circuital by its very nature as a rotation, and  $(a^2 f, b^2 g, c^2 h)$  is the electric force derived from  $\varphi$ . The charge on a conductor is the integral of  $\int (f, g, h) dS$  over a surface  $S$  enclosing it and cannot be altered except by opening up a channel devoid of elasticity, in the medium, between this conductor and another containing like properties so that electric discharge occurs only by the impression of force on the elastic quality of the medium [6].

At the interface between two dielectric media, taken to be crystalline as above, the condition reveals the tangential electric force is continuous. When the circumstances are those of equilibrium, and therefore an electric potential may be introduced, this condition allows discontinuity in the value of the potential in crossing the interface, but demands that the amount of this discontinuity shall be the same all along the interface; these are

precisely the circumstances of the observed phenomena of voltaic potential differences. The component, normal to the interface, of the electric displacement is of course always continuous, from the nature of that vector as a flux. This will be used to imply that calculation of the **B** field at the interface along with its projection  $\bar{\mathbf{H}}$ , given  $\mathbf{D}$  will describe the type of emitted field and its relative geometry.

The magnetic field, calculated as a function of its intensity, is subject to a property called velocity-inhibition. In free-space, it is,

$$\begin{aligned}\mathbf{B} &= \nabla \times \mathbf{A} = \frac{\mu_0}{4\pi} \int_0^{120\pi} \frac{\mathbf{J}\alpha \times r}{r^3} dv, \\ \bar{\mathbf{H}} &= \epsilon_0 \frac{\partial \mathbf{D}}{\partial t} \cdot \frac{4}{3} \pi r^3,\end{aligned}\tag{10}$$

where the energy revealed at the boundary of the antenna and the free-space boundary is given by  $\bar{\mathbf{H}}$ ,  $\alpha = \left( t - \frac{v}{c} \right)$  a component called family time [26],  $dv$  an element of volume. In area enclosed by  $\bar{\mathbf{H}}$ ,  $\epsilon_\phi$  is free-electricity where the field is considered ambient; its motion is given by the direction of  $\mathbf{A}$ . The application of this hypothesis is illustrated by characteristics of stored and distributed energy properties shown in ordinary geometries of a simple loop antenna, the restriction of such properties to this arrangement exclusively.

Larmor states the energy given off by the acceleration of an electron can transform its energy at the interface of an antenna to sustain a magnetic field. When accelerating or decelerating the electron releases the force applied by acceleration, the energy radiated is given by,

$$P = \frac{e^2 a^2}{6\pi\epsilon_0 c^3}. \quad (11)$$

Given in terms of the scalar and vector potential, addressed in §2.1.4,

$$\mathbf{E} = -\nabla\varphi - \frac{\partial\mathbf{A}}{\partial t}. \quad (12)$$

Equation (12) illustrates the expectation that the energy in the field is due primarily to both potentials at the interface of the antenna to free-space. Also, that the transmission path which yields the energy *must* contain some inherent structure for transfer to occur. This will be known as the “virtual transmission line” later in the work.

## 1.2 Poynting and Tesla

John Henry Poynting would describe the energy in the field and Nikola Tesla would experimentally-verify these mathematical works [9, 13, 14, 15, 52]. By the end of the 19<sup>th</sup> Century, the stage was set for later experimenters and inventors to create what became known as “the wireless art” or radio. Poynting commented [9] on Maxwell’s theory which alludes to later descriptions by Larmor [6]:

I am not sure that there has hitherto been any distinct theory of the way in which the energy developed in various parts of the circuit has found its way thither, but there is, I believe, a prevailing and somewhat vague opinion that is some way it has been carried along with the conductor by current. Probably Maxwell’s use of the term ‘displacement’ to describe one of the factors of the electric energy of the medium has tended to support this notion. It is very difficult to keep clearly in mind that this ‘displacement’ is, as far as we are yet warranted in describing it, merely something with direction, which has some of the properties of an actual displacement in incompressible fluids or solids. When we learn that the ‘displacement’ in a

conductor having a current in it increases continually with time, it is almost impossible to avoid picturing something moving along the conductor, and it then seems only natural to endow this something with energy-carrying power. Of course, it may turn out that there is an actual displacement along the lines of electromotive intensity. But it is quite as likely that the electric ‘displacement’ is only a function of the true displacement, and it is conceivable that many theories may be formed which this is the case, while they may all account for the observed facts. ... It seems to me then that our use of the term is somewhat unfortunate, as suggesting to our minds so much that is unverified or false, while it is so difficult to bear in mind how little it really means.

I have therefore given several cases in considerable detail of the application of the mode of transfer of energy in current-bearing circuits according to the law given above, as I think it is necessary that we should realize thoroughly that if we accept Maxwell’s theory of energy residing in the medium, we must no longer consider a current as something conveying energy along the conductor. A current in a conductor is rather to be regarded as consisting essentially of a convergence of electric and magnetic energy from the medium upon the conductor and its transformation there into other forms. The current through a seat of so-called electromotive force consists essentially of a divergence of energy from the conductor into the medium. The magnetic lines of force are related to the circuit in the same way throughout, while the lines of electric force are in opposite directions in the two parts of the circuit—with the so-called current in the conductor, against it in the seat of electromotive force. It follows that the total E.M.I. round the circuit with a steady current is zero, or the work done in carrying a unit of positive electricity round the circuit with the current is zero. For work is required to move it against the E.M.I. in the seat of energy, this work sending energy out into the medium, while an equal amount of energy comes in the rest of the circuit where it is moving with the E.M.I. This mode of regarding the relations of the various parts of the circuit is, I am aware,

very different from that usually given, but it seems to me to give us a better account of the known facts.

It may seem at first sight that we ought to have new experimental indications of this sort of movement of energy, if it really takes place. We should look for proofs at points where the energy is transformed into other modifications, that is, in conductors. Now in a conductor, when the field is in a steady state, there is no electromotive intensity, and therefore no motion and no transformation of energy. The energy merely streams round the outside of the conductor, if in motion at all in its neighborhood. If the field is changing, energy can pass into the conductor, as there may be temporary E.M.I. set up within it, and there will be a transformation. But we already know the nature of this transformation, for it constitutes the induced current. Indeed, the fundamental equation describing the motion of energy is only a deduction from Maxwell's equations, which are formed so as to express the experimental facts as far as yet known. Among these are the laws of induction in secondary circuits, and they must therefore agree with the law of transfer. We can hardly hope, then, for any further proof of the law beyond its agreement with the experiments already known until some method is discovered of testing what goes on in the dielectric independently of the secondary circuit.

The passage above, in the opinion of the author, is trying to compartmentalize the notion that the size, shape, and space taken by an electromotive force appearing in free-space as a field is wholly dependent upon the apparatus, or antenna, projecting it. Poynting's comments infer that plane waves propagate on a transmission line driven by the currents and its field is distributed along a surface, even if the line and surface are virtual. The length of transmission is dependent upon the intensity of the field and the permittivity of the waveguide. In free-space at 20C and one atmosphere, attenuation of the field past the mid-field region, described in detail in Section 2, occurs at a ratio of the coil radius to the distance,

typically sixteen times [10]. The number is a conservative estimate. A simple experiment showing a measurably-powered state of a loop and receiver illustrates the propagation of photons in an emission pattern constituting a free-space field containing a periodic structure created by the presence of the coils [11] and that the emitted field is quantized [12].

Tesla undertook experimental verification of these theories as early as 1892 [13], and presented his results in 1900 [103]. Tesla was to focus his efforts on wireless power transmission, first through stationary waves then by signaling, sending power to remotely light bulbs and turn motors, in a body of research over a period of years from 1894 to 1908 at his laboratories in New York and Colorado Springs. Tesla's method was to project waves by magnetically coupling coils acting as an interface between the oscillator circuit and free-space. It is Tesla's method that is the founding principle of this work. However, it is also interesting to understand what phenomenon is driving the dielectric of free-space by using such "indirect" methods. It is the author's opinion that a direct test can only be useful when there is a framework describing a quasi-definite medium, i.e., the aether or dark matter.

Tesla's macroscopic vision was to use stationary waves to broadcast between antipodes on the surface of the planet as a means to send power, which differed from the radiative model constructed by Hertz. In brief, the difference is subtle; Tesla espoused the transfer of energy at a distance without wires by standing waves, Hertz espoused the transfer of energy in the same manner via radiation. The Hertz model supposed discharge at an inductor while the Tesla model supposed discharge at a capacitor.

Tesla's notion of wireless power transfer was to use the planet as both source and conductor with towers at positions of an antipode to excite energy dispersed in the ionosphere while the wave transmitted along the surface of the planet. Receivers were constructed with aerials to absorb these currents. In terms of propagation, Tesla's main emphasis was the use of standing waves, similar to those observed in waveguides, to accomplish power transmission. He noted the advantage of these waves is their omnipresence on the planet surface and long wavelength; coupled with the use of the grounding plane, it is possible in this method to use single-wire receivers. The planet can be considered as a resonant cavity due to the high conductivity between altitudes. In practical terms, this means anything with an antenna can absorb currents where the wire length is directly proportional to the magnitude. Tesla introduced a profound concept that to this day has been largely unexplored. If history had unfolded as Tesla had envisioned, the modern electrical grid would look like that represented in Fig.1.2.



Fig.1.2. Tesla's vision of wireless power.

After experimental trials at Wardenclyffe from a period of 1899 – 1903, some sporadic work as late as 1911, Tesla's work went unfinished. The

tower was demolished during the First World War. Afterwards, Tesla abandoned his standing-wave hypothesis and exclusively experimented with radiative, or radiation-based emission, models [14]. At the time, prevailing attention was toward Marconi's broadcasting system for information and not the transmission of power. After the publication of the work on the Yagi antenna [15] in 1926 and the development of shortwave [16], wireless power would fade from view. Forty years passed before interest in wireless power resurfaced. In the 1960s, short-wavelength transmission experiments [17] and the modeling of prototypical forms showed positive results [18]. A rethinking of inductive transfer began to surface in solving problems associated with subcutaneous implants [19].

While many divergent types of wireless power transmission have resulted, especially since 2004, this work will focus on a quantized emission of power in the form of plane waves from loop antenna. The focus will be exemplified by the exploration of two distinct expressions of wireless power: That of a single primary loop transmitter/receiver system, and that of a primary/secondary loop pair transmitter/receiver system. The former will exhibit the author's notion of the mid-field region of the radiation model of a single coupled-mode, while latter will exhibit Tesla's stationary or standing waves and tunable wave cavity of two coupled-modes.

An important contribution of this work is to contrast the use of the Maxwell-Heaviside version of Maxwell's equations in the literature survey, and using the 1865 versions to begin the formation of the theoretical framework from where the arguments and analytics are derived from it. Thereby tracing through three concepts, selected because of their appropriateness to the subject: 1. The relation between electric displacement, conduction and current, 2. Between the lines of magnetic

force and inductive forces, and 3. Between electric displacement and electromotive force. It will be shown in the work that novel contributions are framed in these expressions.

This work will discuss the geometry and ambience of the magnetic field in terms of Joseph Larmor and John Henry Poynting's conception of field objects. Outside of some works in the early 20<sup>th</sup> Century, it appears the state-of-the-art has ignored what is otherwise a very powerful set of tools to quantify the forces responsible for magnetic resonant coupling. This work will choose a set of equations and force-representations that are utilized to explain the *why* of the phenomenon.

### **1.3 Wireless power as concept**

Wireless power in the context of this work is not considered to be a core component of physics, rather, a means allowing a transformation of energy from one state to another. While it is obvious this work will describe wireless power by magnetic resonance in terms of physics and mathematics, the author views the subject from the point of view of a control system.

Wireless power operates in the realm of transformation and control theory. This is because the way wireless power is used does not contribute anything significantly new, instead, it is merely a tool whereby to transform electrical currents from their wired analogues. Therefore, it is an insistence in this work that the circuit manifests a specific behavior given the nature of its arrangement.

A brief outline of what is to be presented in this work is the following.

Chapter 2 describes the theoretical and mathematical model of a circular loop antenna consisting of two primary coils in a single coupled-mode. Section 2.1 will discuss a coupled-mode with a projection and the forces that are contiguous. Section 2.2 will discuss the behavior as also embedded in the unique circuit which drives the coupled-mode. Section 2.3 will discuss the propagation model and the equations which are capable of describing it. Section 2.4 will discuss several sets of experiments, relevant to a single coupled-mode, in various forms. In light of what is described in the introduction regarding humans and wireless power, biomedical implants will be one such experiment. This chapter will also discuss optimization of the model.

Chapter 3 describes the theoretical and mathematical model of a circular loop antenna consisting of two primary coils and two secondary coils with two coupled-modes. This is discussed in terms of a reconstructed Tesla resonator, described in U.S. Patent #645,546 of 1900. The model is tested experimentally and compared with other works in the literature. An innovative modification is presented to control the magnetic field on the secondary coil tying directly into control of the order of the fields traversing the coils.

Chapter 4 discusses a novel model of the dipole, given the theory and experimental evidence presented in the previous chapters. It introduces a modified model based on the research conducted for this work. It reveals the possibility of dipole preservation given the parameters of the oscillator and circuits discussed in Chapter 2.

Chapter 5 presents applications and controls for the wireless power model such as featured power for robotic power, and power distribution for space

activities. Featured power is an important contribution to behavioral robotics with the introduction of transitive power through state negotiation where robots can learn by manipulation of their own causality, the ramifications of choice, its consequence, and cost.

Chapter 6 reveals conclusions based on the pace of the work and iterates the important points of the work while leaving the subtleties of the arguments intact in their individual chapters.

Chapter 7 contains appendices of figures and tables too large to place in line with the text.

Chapter 8 contains the references used throughout the work.

With the introduction setting the stage, the next section begins the journey into the world of wireless power, not only envisioned by Tesla and his contemporaries, but through the lens of scientific discourse vis the realization of theory through exhaustive empiricism.

## **2 Power transmission and magnetic-resonant modes in an inductively-coupled circuit**

Chapter 1 discussed in brief and with a few equations, the tenets of theory for wireless power transmission by magnetic resonance. This chapter will apply what has been discussed to a physical model. In order to accomplish this, a specific set of assumptions are to be applied to the notion of a circuit and a field. The circuit model will be a restricted case where the details of its behavior are given in a very particular context. The model is thus: A circuit consists of two distinguishable parts, a transmitter and a receiver. The transmitter is comprised of regulated amplification and timing components connected to a loop antenna and a capacitor. The amplifier is

connected to a source of direct current (dc) power. The receiver is comprised of a loop antenna, a capacitor, and a load such as a lamp or motor. The receiver is placed at a distance away from the transmitter. The circuit will transmit radio-frequency electrical energy into free-space the form of photons exchanged between two or more coupled resonators, depending how they are chained together [106]. At certain distances and antenna orientations, work performed by the energy transfer can be observed at a receiver by an illuminated lamp or turning motor. A pair of circular loops of a sufficiently similar geometry but with a fixed wire length set at a distance form a closed induction circuit illustrated in Fig.2.1. These loops form a resonant circuit with a free-space presence constituting a waveguide in the form of a virtual transmission-line.

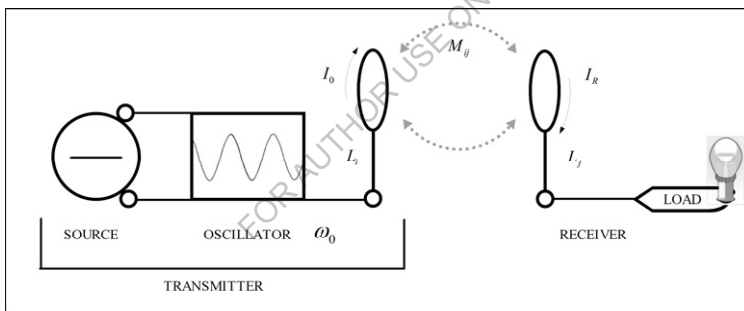


Fig.2.1. The prototypical model for the transmission of wireless power by magnetic resonance.

By examination of Fig.2.1, current flows from source to oscillator to coil loop  $L_i$ , accelerating electrons at a rate given loop curvature and ratio of loop circumference to wavelength. Torque is given as a function of the current  $I_0$ . In this model, the current is at sufficient levels, as a property of the components used to construct the oscillator, to supply enough torque so that photons are projected into free-space in the form of radiation at a characteristic angular frequency  $\omega_0$ . The number of photons emitted by a

given arrangement is shown by the energy,  $\gamma_0$ , of the photons emitted by the antenna, as,

$$\gamma_0 = \hbar\omega_0, \quad (13)$$

and the number of photons per second,  $\gamma_t$ , is given by the presence of circuital power  $J_0$ ,

$$\gamma_t = \frac{J_0}{\gamma_0}. \quad (14)$$

At a distance, the receiving coil loop  $L_j$  absorbs the photons converting them back into electron currents via a voltage gap. The current is then considered bound to the circuit to perform work powering a load. The process involves:

1. The transfer of energy between input current contained in the oscillator, accelerated to an amplitude impressed as a magnitude on the coil wire of the transmission antenna,
2. the transit of photons,  $\gamma_0$ , across free-space at a characteristic frequency  $\omega_0$ , and,
3. the transfer of energy between free-space and the constitution of electrical currents in the coil wire of the receiving antenna.

The flow pattern is similar to shock waves occurring at locations where the energy is not contained in the field,  $(E_\theta, H_\theta)$ , nor where the magnetic flux approaches zero, as,  $\Phi_M \rightarrow 0$ . Rather, at these points where packets of energy are moving, the field manifests itself as a projection encompassing an area  $\bar{\mathbf{H}}$  which extends at a length from the antenna,  $L_t$ , to a surface in

free-space,  $S_\theta$ , at its boundary with respect to the axial normal,  $\bar{n}$ . The boundary consists of an equilibrium in the force exerted by the displacement,  $\mathbf{D}$ , and the counter-forces exerted by the medium to resist it.  $\bar{\mathbf{H}}$  denotes the furthest edge mid-field region where energy transfer is at a peak. At  $S_\theta$ , the far field begins and so does the fall-off of the intensity. The parameters  $\epsilon_0$ ,  $\mu_0$ , and  $\sigma_0$  are invariant with position except at  $S_\theta$  [20]. This phenomenon is depicted in Fig.2.2.

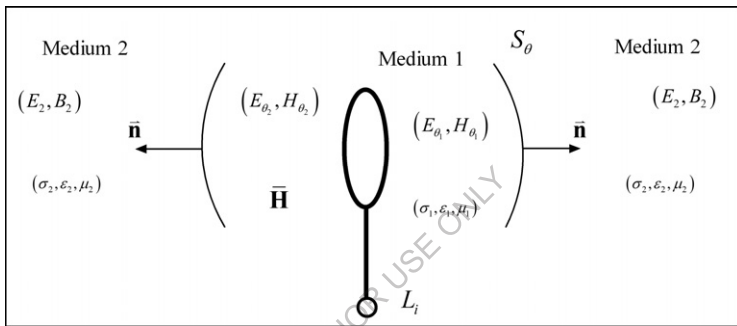


Fig.2.2. Demarcation of the field force in the medium displacing energy to a fall-off threshold.

For the conservation of electric charge, a difference in the flux at the axial normal,  $\bar{n}$ , to the antenna must imply a change in the total electric charge  $q$  contained within the volume denoted by  $S_\theta$  as  $\frac{\partial q}{\partial t}$ . Power in the form of photons projected toward the boundary yields the displacement of energy from the loop in combination with its circuit. Concurring with Larmor, the boundary has elasticity and is susceptible to strain. In addition, concurring with the original Maxwell, the boundary is the point of displacement. Ideally, the field is considered homogenous across the space with charges considered evenly distributed exhibiting a uniform motion. The antenna therefore creates a disturbance as a deformation of the medium. At the

boundary of the displacement, the rotational property of  $S_\theta$  or instantaneous torque,  $\tau_0$ , is given by,

$$\tau_0 = \nabla \times \mathbf{D}, \quad (15)$$

because of Fitzgerald's proposition of the identity of electromagnetic radiation as an exchange of force [21],

$$\nabla \times \mathbf{F} = \nabla (\nabla \cdot \mathbf{F} - \delta \mathbf{F}), \quad (16)$$

when, with respect to (1),

$$\rho = 0, \text{ and } \mathbf{J} = 0, \quad (17)$$

(11) will yield a wave equation in the form of,

$$\frac{1}{c^2} \frac{\partial^2 \psi}{\partial t^2} = \Delta \psi. \quad (18)$$

The field is therefore subject to uniform external forces dependent upon conditions of temperature and pressure and has a susceptibility, which is expected. Therefore, energies and frequencies limited by a given geometry share a common state of equilibrium. The effect of the equilibrium is analogous to inflating a balloon. The tension at the surface holding the energy inside is given by the shearing forces between the field at its border and the medium. Gauss's theorem transforms the surface into a changing flux of the electric field through the closed surface formed by the volume of open surfaces. More precisely, any "missing" flux of the current density  $\mathbf{J}$  is absorbed from the flux of the vector  $\epsilon_0 \frac{\partial \mathbf{E}}{\partial t}$  or at the potential vector

**A.**

Considering magnetic flux, an energized circular loop emits a magnetic field,  $\mathbf{B}$ , of a given intensity and geometry according to the well-understood Biot-Savart and Neumann principles. Both propose that the contribution of each piece of the wire contained in the loop varies inversely as the square of the distance. Over the entire length of the wire, each contribution adds up to a total field that varies inversely as the distance from the loop. The contribution to the magnetostatic field at the origin of a current element,  $\delta I$ , at position  $\mathbf{r}$  is,

$$\delta\mathbf{B} = \frac{\mu_0 \mathbf{r} \times \delta I}{4\pi r^3}, \quad (19)$$

given by the relationship of its radial length and the infinitesimal of the magnetic field, shown in Fig.2.3.

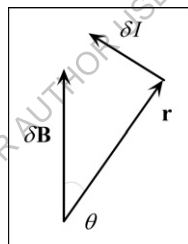


Fig.2.3. Ray relationships between the magnetic field, radial vector, and infinitesimal current.

The quantity,  $\delta I$ , is the current multiplied by the length of travel resulting from integrating the current density,  $\mathbf{J}$ , along the surface over a small element of volume, from (8). In particular, for a thin wire whose length element  $\delta s$  has a total current  $I_0$  traversing it in the direction of  $\delta s$ ,  $\delta I = I \delta s$ , and negatively otherwise. This proposition holds for mono-directional currents only. In the bi-directional case, an oscillator creates a rotational force through  $\pi$  phases, the direction of the current changes

twice in a cycle throughout all of  $\delta s$ . The displacement at the molecular level of the conductor is given by Maxwell in (4).

The model of wireless power transfer, illustrated in Fig.2.1, consists of two distinct views of operation: that of a system of coupled modes and that of projection. The first view is expressed by the utilization of a pair of coils, one acting as a transmitter or primary coil, the other as a receiver or secondary coil. The combination of these two [107], or more [106], antenna is considered a coupled-mode [23]. The second view is an antenna projecting a force. In the model, the magnetic field is assumed to have a simple symmetry as in the case of free-space fields.

The first view, a coupled-mode, is manifest as a flux-linkage between symmetrical antennas, it is by design dependent upon the  $\mathbf{B}$  field. Geometry of the coupling mode is shown in Fig.2.4.

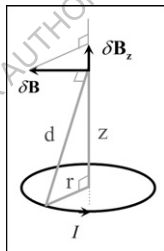


Fig.2.4. Geometry of the coupling-mode magnetic field.

For the case of a circular current loop, all radial contributions will cancel out. The resulting magnetic induction,  $\mathbf{B}$ , is oriented along the axis where  $\mathbf{B} = \mathbf{B}_z$ . Because of the symmetry of the triangles consisting the interior of the loop, shown in Fig.2.4, the contribution  $\delta\mathbf{B}_z$  is  $r/d$  times (19), as,

$$\delta\mathbf{B}_z = \frac{r}{d} \frac{\mu_0 I}{4\pi d^2} \delta s. \quad (20)$$

All the elements,  $\delta s$ , add up to the circumference,

$$\mathbf{B}_z = 2\pi r \frac{r}{d} \frac{\mu_0 I}{4\pi d^2} = \frac{1}{2} \frac{\mu_0 I r^2}{d^3}, \quad (21)$$

while the field at the center of the loop is,

$$\mathbf{B} = \frac{\mu_0 I}{2r} \cos(\theta), \quad (22)$$

at peak value where  $z = \frac{r^2}{d^2}$ . Note the addition of a cosine theta term to

(22), it will be discussed in greater detail in §2.1.4.

Analogous to a pair of Helmholtz coils, consider two loops shown in Fig.2.1 sharing the same horizontal axis, or in axial alignment. Let their respective latitudes be  $+a$  and  $-a$ , magnetic induction is along the axis of axial alignment at distance  $z$ , as,

$$\mathbf{B} = \frac{1}{2} \mu_0 I r^2 \left\{ \left[ r^2 + (a-z)^2 \right]^{-3/2} + \left[ r^2 + (a+z)^2 \right]^{-3/2} \right\}. \quad (23)$$

The second derivative of (23) with respect to  $z$  at  $z=0$ , is

$$\mathbf{B}''(0) = 3\mu_0 I r^2 (4a^2 - r^2) (r^2 + a^2)^{-7/2}. \quad (24)$$

The value  $a = \frac{1}{2}r$  is where the magnetic induction is singularly valued

along the trajectory of the axis. When values of  $a$  are large,  $\mathbf{B}''$  is positive at the center where  $z=0$  indicating a minimum value present. The configuration where the separation between the two loops is equal to their

radius,  $2a = r$ , yields a magnetic field, which is almost uniform, near the center of the loop, as,

$$\mathbf{B} = \left(\frac{4}{5}\right)^{3/2} \frac{\mu_0 I}{r} \approx .071554 \frac{\mu_0 I}{r}. \quad (25)$$

The scalar potential of the magnetic field at the center of the loop, and where it is equidistant between two loops are examples of a current-free region. It takes the form of a multivalued function whose gradient is the magnetostatic induction. For a simply-connected region under coupled-modes, such a potential is well-defined up to a uniform additive constant. Otherwise, an ambiguity arises whenever the region contains loops which are interlocked with loops of outside current. In that case a continuous potential can only be defined with a modulo operation for a certain number of discrete quantities, each of which corresponds to one piece of the outside current.

The method described above fits to (19) that in static distributions, all currents must circulate in closed loops where  $\nabla \times \mathbf{J} = 0$ . Equation (19) cannot express with dynamic distributions where local electric charges may vary according to the inbound flux of current. A more sophisticated method is required.

By the Kelvin-Stokes formula, the circulation of a vector around an oriented loop is equal to the flux of its rotational element, or curl, through any smooth oriented surface bordered by that loop. The solution yields Ampère's law in integral form,

$$\mu_0 I \equiv \mu_0 \iint_S \mathbf{J} \cdot d\mathbf{S}, \quad (26)$$

which is the same as the geometry in the plane,

$$\int_{\partial S} \mathbf{B} \cdot d\mathbf{r}. \quad (27)$$

The simplest and most direct application of Ampère's law is to first formulate under the Biot-Savart and Neumann principles, then extend the flow of magnetic induction,  $\mathbf{B}$ , analogous to a straight wire or a waveguide keeping in mind the intensity is inversely proportional to the distance.

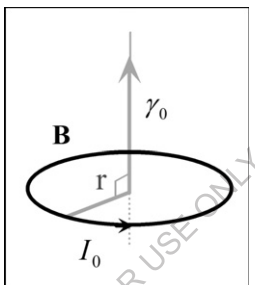


Fig.2.5. Projection of energy by a current impressed on the loop.

Consider a circular loop of radius  $r$  whose axis is a straight wire carrying an instantaneous current  $I_0$ . The magnetic induction,  $\mathbf{B}$ , at the loop is tangential. The projection of the motion is constant as long as  $I(t)$  is.

The magnetic circulation and Ampère's law then gives,

$$2\pi r \mathbf{B} = \mu_0 I, \quad (28)$$

or equivalently,

$$\mathbf{B} = \frac{\mu_0 I}{2\pi r}. \quad (29)$$

Maxwell amended the static law of Ampère into the following generalization that holds in all cases including changing charge distributions [22],

$$\nabla \times \mathbf{B} - \frac{1}{c^2} \frac{\partial \mathbf{E}}{\partial t} = \mu_0 \mathbf{J}, \quad (30)$$

which agrees with the vectorized version of Faraday's law,

$$\nabla \times \mathbf{E} + \frac{\partial \mathbf{B}}{\partial t} = 0. \quad (31)$$

The curl of  $\mathbf{B}$ , given (30), is the characteristic of a rotating component of  $\mathbf{B}$ . The curl is illustrated in Fig.2.6.

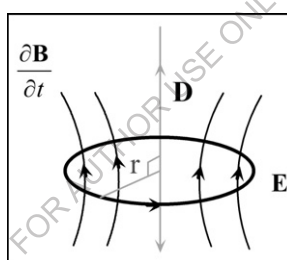


Fig.2.6. Field lines following an axis of displacement.

By the action of the curl, the forces consisting propagation take the form of the displacement  $\mathbf{D}$ . The displacement has a component, called directional current, or group velocity in terms of waves, along the magnetic flux lines. The intensity of  $\mathbf{D}$  linearly decreases with distance.  $\mathbf{B}$  couples to perform work where  $\frac{\partial \mathbf{B}}{\partial t}$  can flow in a second coil. The measurement of the intensity  $\mathbf{D}$  will be determined by the velocity of field flow. For example, let  $\mathbf{v}$  be the vector field of a fluid flow. At a given point in the flow, a small wheel with blades whose axis is oriented in the direction of  $\nabla \times \mathbf{v}$  at

any point is placed in the flow in order to measure radial intensity. Then the angular velocity  $\nu_1$  of the wheel's rotation from the action of the current will maximize where its value is equal to  $\frac{|\nabla \times \mathbf{v}|}{2}$ . Assuming  $\mathbf{v}$  has arbitrary coordinates  $P(x, y, z)$ ,  $Q(x, y, z)$ , and  $R(x, y, z)$ , then  $\nabla \times \mathbf{v}$  has the coordinates,

$$\frac{\partial R}{\partial y} - \frac{\partial Q}{\partial z}, \frac{\partial P}{\partial z} - \frac{\partial R}{\partial x}, \frac{\partial Q}{\partial x} - \frac{\partial P}{\partial y}. \quad (32)$$

The arcs cast by (23) form boundaries in three-dimensions of  $\nabla \times \mathbf{v}$  at the interface with the antenna and feedback from the receiving object, illustrated in Fig.2.7.

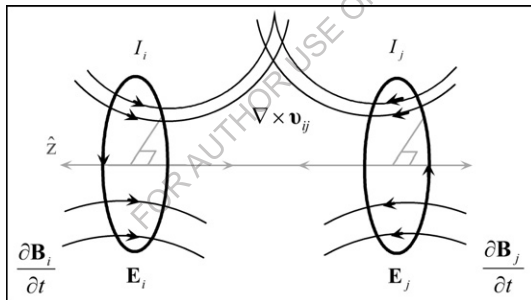


Fig.2.7. Flux linkage between two inductively-coupled coils.

The magnetic scalar potential,  $\varphi_0$ , for  $\mathbf{B}$  created by the loops illustrated in Fig.2.7 is proportional to the currents,  $I_{i,j}$ , in the loop and to the solid angle-space,  $\Omega_0$ , subtended by the side of the loop facing the observer, as,

$$\begin{aligned} \mathbf{H} &= -\nabla \varphi_0, \\ \varphi &= -\frac{\mu_0 I}{4\pi} \Omega_0. \end{aligned} \quad (33)$$

An ambiguity arises in the solid angle because there is a modulo operation of  $4\pi$ . The angle is an approximation that becomes loses precision each time the value is taken. The sign convention is such that the side of a small loop is seen at a solid angle, which exceeds a multiple of  $4\pi$  by a small positive quantity.

The second view, of projection, is manifest as a shock wave from a single transmission antenna. The length and intensity of the projection,  $\bar{\mathbf{H}}$ , is due to both the properties of the antenna and the power applied by the circuit. Modification of Fig.2.4 to include projection is shown in Fig.2.8, and is discussed in greater detail in §2.1.4.

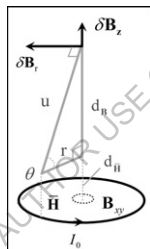


Fig.2.8. Field geometry extending away from the projection.

The projection is the evidence of the virtual waveguide, carrying energy across free-space displacing it as it exhibits motion away from the antenna in both the positive and negative directions of  $\hat{z}$ . For convenience, it is divided up into amplitude zones,  $A_i$ , where measurements are taken to obtain the geometry of the emission by mapping its intensity. The projection of the loop is illustrated in Fig.2.9.

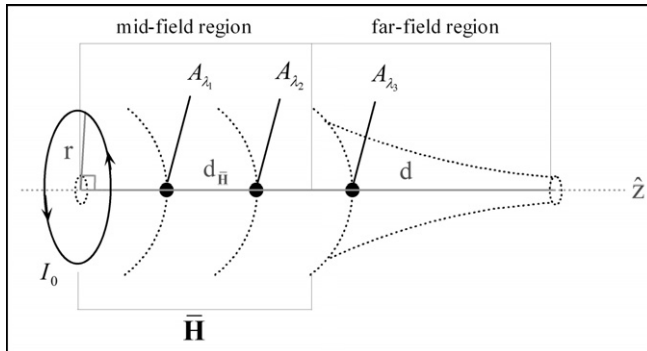


Fig.2.9. Projection field forming the mid-field region by intensity.

A composite of both the coupled-mode and projection is shown in Fig.2.10.

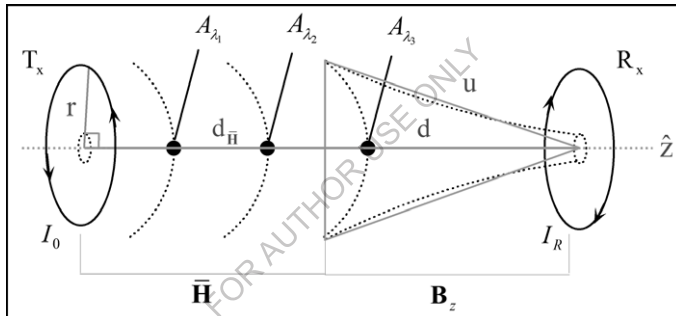


Fig.2.10. Projection of field and its geometry between two inductively-coupled coils.

The description of the system, in terms of its characteristic partial differential equation, will be elliptic, where its spatial solutions take a hyperbolic form consisting of *sinh* and *cosh* functions. Quantization of the field components and manifesting them in an experiment will be the aims of the following sections.

## 2.1 A single coupled-mode with projection

The relationship between the loops and the amount of energy transported between them is most effectively described by how they are coupled [24].

Coupling, in the direct sense, refers to the relationship *between loops* and not to free-space. Energy across free-space and its impedance is not created the phenomenon of coupling, rather, it is the *consequence* of coupling between the objects which allows the transit of energy. This is a subtle but important point. Magnetic loops of a relatively small size and number of turns exhibit a magnetic field density sufficient to be an excellent model for experimentation.

A mode describes the energy in patterns of electric, magnetic, and force generated by the loops. The magnetic field intensity  $\mathbf{H}$ , is related to the magnetization,  $\mathbf{M}$ , of the surrounding space on the antenna by its susceptibility,  $\chi_v$ , as,

$$\mathbf{M} = \chi_v \mathbf{H}. \quad (34)$$

The boundary condition will be the surface  $S_\theta$ , from Fig.2.2. Analogous to the case of the thin current sheet the assumption is the thickness of the loop structure is negligible. Therefore, Ampère's law will yield the instantaneous power density on an "approximately-closed" contour,

$$J_{\bar{\mathbf{H}}} = H_{A_\lambda} r_i^3 + H_i \ell_i^2, \quad (35)$$

If the medium is assumed homogenous and isotropic and the surface impedance of the boundary linearly approaches zero, it is considered a primitive waveguide. Any discontinuity in a waveguide facilitates a coupling between some or all desirable modes in varying magnitudes. Two electrical objects, consisting of inductive and capacitive components of relative value to each other, form a closed induction circuit. The linking is due to attractive resonators in a waveguide of characteristic impedance is imbued, purely by intuition, as sharing properties with transmission-line

resonator with small losses [23, 24, 25]. A single coupled-mode can be identified by placing a receiving loop at an amplitude zone  $A_\lambda$ .

$L_i$  is a circular loop with a voltage gap no greater than the size of its radius.  $L_i$  is connected in parallel to a capacitor powered by a switching amplifier. Comparably, the loop antenna  $L_j$  can also be connected in parallel to a capacitor whose value is no greater than that of  $L_i$ .

The wave impedance is set by the ratio of the transverse components of the electric  $E_0$  and magnetic  $H_0$  fields. For a transverse-electric-magnetic (TEM) plane wave traveling through a nearly-homogeneous medium at a given temperature and pressure, wave impedance is everywhere equal to the intrinsic impedance of the medium. The wave impedance, in terms of fields is

$$\mathbf{Z} = \frac{|\mathbf{E}|}{|\mathbf{H}|}, Z_0 = \frac{E_0^-(x)}{H_0^-(x)}. \quad (36)$$

Disassembling the components of (36) into finer parameters, the free-space impedance is

$$Z_0 = \sqrt{\frac{j\omega_0\mu_0}{\sigma_0 + j\omega_0\epsilon_0}}, \quad (37)$$

In (37),  $j$  is an imaginary unit, and  $\omega_0$  is the angular frequency. In the case of a dielectric where the conductivity is zero, the equation reduces to,

$$Z_0 = \sqrt{\frac{\epsilon_0}{\mu_0}}. \quad (38)$$

Calculated at 20C and one atmosphere,

$$\begin{aligned} Z_0 &= 376.73\Omega \\ &= 119.92\pi\Omega, \end{aligned} \quad (39)$$

isolated from the conductivity of free-space for the value considered in the present definition of the unit of the Ampère. For any waveguide in the form of a hollow metal tube of conductivity  $\sigma_0$ , such as circular guide, the wave impedance of a traveling wave is dependent on the resonance frequency  $f_0$ , but is assumed uniform throughout the guide. For transverse electric (TE) modes of propagation the wave impedance is

$$Z_e = \frac{Z_0}{\sqrt{1 - \left(\frac{f_c}{f_0}\right)^2}}, \quad (40)$$

where  $f_c$  is the cut-off frequency of the mode. For transverse magnetic (TM) modes of propagation this value is

$$Z_m = Z_0 \sqrt{1 - \left(\frac{f_c}{f_0}\right)^2}. \quad (41)$$

Above the cut-off ( $f_0 > f_c$ ), the impedance is real (resistive) and the wave carries energy. Below cut-off the impedance is imaginary (reactive) and the wave is evanescent, the latter shown to be an effective scheme [30]. These expressions neglect the effect of resistive loss in the walls of the waveguide, or at the surface boundary  $S_\theta$ . The presence of a dielectric resulting from atmospheric phenomena chaotically shifts in impedance through  $\pi$  modifying  $f_c$ .

To retain narrow selectivity, only single-frequency emission is discussed. The choice comes at a cost: impedance is not a function of the properties

the circuit, rather, combined with that of free-space. The radiation pattern exhibits a topological surface from an energized oscillator. The field is quantifiable at certain lengths from the antenna but has fractal dispersion geometry, similar to task of calculating the length of a shoreline, so what constitutes the observable boundary is relative to the technical sophistication of the laboratory of the experimenter. Generally, the observable free-space electromagnetic field has its boundary at an edge where the energy stored at the horizon vanishes, as  $\Phi_M \rightarrow 0$ . Depending on the geometry of the coils and the intensity of energy stored, the boundary shifts.

Some applications where the waveguide or transmission-line containing more than one type of dielectric medium occurs, such as complex microstrip [26], in terms of the boundary conditions, the wave impedance will in general vary over the cross-section of the line, as a waveguide transient [27]. A similar notion, investigated by Aharonov-Bohm [28], suggests such a scheme at lower temperatures reveals interesting conclusions about the nature of  $S_\theta$ . The dipole, as the supporting phenomenon of a coupled-mode in both its real and imaginary valued term, interacts with the space surrounding the loop causing the displacement **D**.

Referring to Fig.2.1, consider a system of resonators consisting of a pair of magnetic dipole loop antenna  $L_i, L_j$  separated by a distance, which contain a single coupled-mode.  $L_i, L_j$  are set on a work-plane as to contain a periodic structure. To perform an analysis, a software package called *Comsol Multiphysics* is used to simulate the electromagnetic characteristics of the scheme. The work-plane consists of two circular loops of a material with conductivity  $\sigma_m$  and radius  $r_i$ . These loops are aligned in such a way

so that the center of their radii shares a common axis or an axial alignment. The FEM layout is illustrated in Fig.2.11.

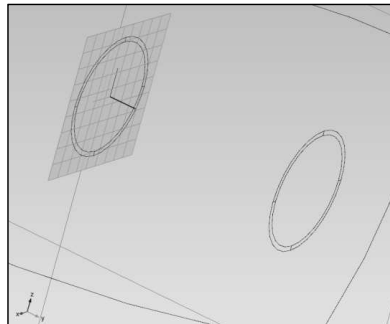


Fig.2.11. FEM model workspace layout.

The goal of this investigation is to consider small antenna sizes with a high efficiency. In the model, the loop size is the most critical property. If coil loop is wound at a specific ratio of circumference to wavelength, it is equivalent to an antenna connected to an electrically-short transmission line. To maximize the emission of radiation, the magnetic loop should be at a ratio of its circumference to its quarter wavelength. Such a magnetic loop will be shown to have the ideal ratio,  $\Re_0$ , in terms of maximum transmission efficiency, is when this ratio falls on an exponential scale,

$$\begin{aligned}\Re &= \frac{2\pi r_i}{0.25\lambda}, \\ \Re_0 &= 10^x, \\ x &= -1, -2, -3 \dots n,\end{aligned}\tag{42}$$

yielding loops with a radius of 3 centimeters that are set apart at a distance of 6 centimeters. The loop surface lies on the  $x, y$  plane while  $z$  between the loops forms the axial line. In consideration of the efficiency of energy transfer, the receiving antenna collects electromagnetic photons, the

amount given the area its surface occupies and the influence, in the form of feedback, it imposes on the space surrounding it [29]. With the introduction of a voltage gap, electrical energy is extracted in the form of power and work is performed by this method.

In consideration of the surrounding medium of free-space, the arrangement of the antenna in space is a periodic locally-approximated waveguide with implicit time-dependence  $e^{j\omega t}$ ; uncoupled spatial dependences are  $e^{-j\beta_i z}$  and  $e^{-j\beta_j z}$ . In a coupled-mode, the spatial equations [23] are,

$$\begin{aligned}\frac{d}{dz}a_i &= -j\beta_i a_i - j2\kappa_{ij} \cos\left(\frac{2\pi z}{l}\right) a_j, \\ \frac{d}{dz}a_j &= -j\beta_j a_j - j2\kappa_{ji} \cos\left(\frac{2\pi z}{l}\right) a_i,\end{aligned}\tag{43}$$

given their coupling with a weak time dependence,

$$\begin{aligned}\frac{da_i}{dt} &= j\omega_i a_i + j\kappa_{ij} a_j, \\ \frac{da_j}{dt} &= j\omega_j a_j + j\kappa_{ji} a_i,\end{aligned}\tag{44}$$

relative to the coupled state of the resonators,

$$\kappa_{ij} = \kappa_{ji} = \frac{M_{ij}}{\sqrt{L_i L_j}},\tag{45}$$

as a weakly-coupled system, where  $\kappa_{ij} < 0.01$ . This is in contrast to a “strongly-coupled” scheme [30]. The attention on weak-coupling is referring to the weak time dependence (44) for a system taking an

assumption low coupling coefficient  $\kappa_{ij}$  affects efficiency  $\eta_{ij}$  weakly and properties of the circuit affect  $\eta_{ij}$  strongly.

### 2.1.1 The coupling coefficient

In consideration of the geometry of the scheme presented in the previous sections, the variables to be solved are: the coupling coefficient  $\kappa_{ij}$ , the mutual inductance  $M_{ij}$ , the quality factors  $Q_i$  and  $Q_j$  expressed by coils  $L_i$  and  $L_j$ , by the contributions of their fields  $E_0$  and  $H_0$ . To understand the effectiveness of the scheme and the work done at a distance, the energy-storage ability of the system is determined by the coupling coefficient in transfer mode. The intensity of flow of the energy across the distance is determined by  $\kappa_{ij}$  between coils  $L_i$  and  $L_j$  at a distance  $d$ . When a current  $I_0$  is applied to coil  $L_i$ , the power transfer flows from coils  $L_i$  to  $L_j$ , and  $L_j$  to  $L_i$ . The coupling coefficient in (45) is solved for a series of coils of characteristic size and geometry. The linkage between the series of magnetic resonant coils is defined at each coupling where  $M_{ij}$  is the mutual inductance,  $L_i$  and  $L_j$  are the self-inductances of the coils. The inductance can be calculated since its size and geometry are already specified, by the approximation of the inductance of a circular loop [31, 32]:

$$L_i \approx \mu_0 \mu_r n_i^2 r_i \left( \ln \frac{8r_i}{a_i} - 2 + Y \right), \quad L_j \approx \mu_0 \mu_r n_j^2 r_j \left( \ln \frac{8r_j}{a_j} - 2 + Y \right), \quad (46)$$

Where  $r_i, r_j$  is the loop radius,  $a_i, a_j$  the wire radius,  $n_i, n_j$  the number of turns, and  $Y$  the flow constant of the skin-effect of the emitted radiation, given the resonance frequency, which is approximated to be the same at the surface of both coils. The resonance frequency of the system,

$$f_0 = \frac{1}{2} (f_i + f_j), \quad (47)$$

is comprised of the resonance frequency  $f_i, f_j, \dots f_n$  of each of the coils,

$$f_{i,j} = \frac{1}{2\pi\sqrt{L_{i,j}C_{ij}}}, \quad (48)$$

and the frequency error between each half of the circuit,

$$f_e = |f_i - f_j|. \quad (49)$$

A consideration of the design is not only to keep the antenna small but also to keep the resonance frequency  $f_0$  low enough as to not to be deleterious to human tissue. Studies have shown that a frequency spectrum between 100 kHz and 4 MHz is suitable [33]. The theoretical specification of the antenna is calculated where,

$$\begin{aligned} n &= 3, \\ r &= 30 \text{ mm}, \\ a &= 0.4 \text{ mm}, \\ \varepsilon_0 &= 8.85 \cdot 10^{-12} \text{ F} \cdot \text{m}^{-1}, \\ \mu_0 &= 4\pi \cdot 10^{-7} \text{ H} \cdot \text{m}^{-1}, \\ \mu_r &= 0.99994, \\ Y &= 0. \end{aligned} \quad (50)$$

The material properties of the coil is for an insulated copper wire wound in concentric loops so the total loop surface is comprised of a number of turns. Equal to a Litz winding, each turn insulated from the other reduces the contribution of the skin effect  $Y$ . The winding has legs of a given length as to allow the loop to be mounted into a circuit board and projected along a plane linear to the ground plane. The additional inductance of the

legs is taken into consideration. A C#.NET program called *Circuit calculator*, built specifically for performing and visualizing the relationships of the values of components used in the wireless power by magnetic resonance, calculates the theoretical specification of the model. Given (48), a capacitance of 100nF is chosen so the frequency is below the MHz threshold—the calculation sequence is shown in Fig.2.12. The table of values for the model loops  $L_{i,j}$  and resonance frequencies  $f_{i,j}$  is listed in Table 2.1.

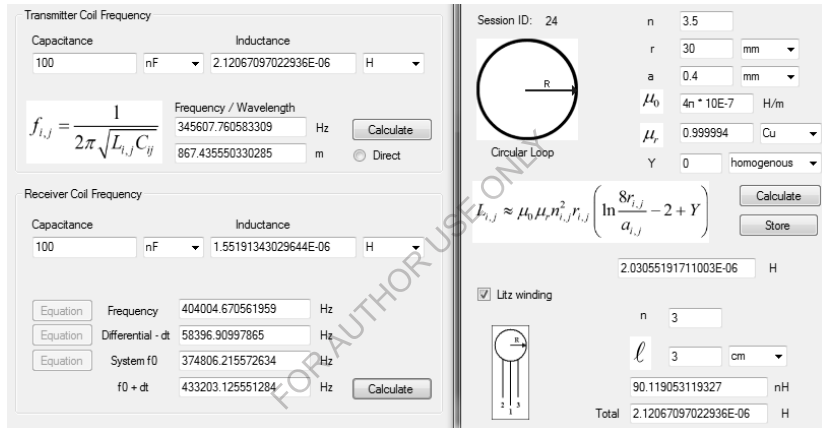


Fig.2.12. Calculator values for (a) resonance frequency, and (b) inductance of the transmission loop.

A frequency of approximately 400 kHz is expected to be the resonance frequency for the physical loop antenna. Having calculated the self-inductance of the coils, the mutual inductance will be solved next.

The mutual inductance between two coils is dependent purely on the geometry of the scheme [32]. An energized loop affects action at a distance. Its attraction, or mutual inductance, is given by the Neumann formula [34],

$$M_{ij} = \frac{\mu_0}{4\pi} \oint_C \oint_{C_j} \frac{s_i \cdot s_j}{|d|} \quad (51)$$

The infinitesimal positions  $s_i$  and  $s_j$  in (51) are derived under the assumption that the magnetic field is evenly distributed, more concentrated toward the center of the loop than in other places, and in a mostly linear distribution. In this form, the loop wire is considered to be contained of coaxial circular filaments [31], illustrated in Fig.2.13.

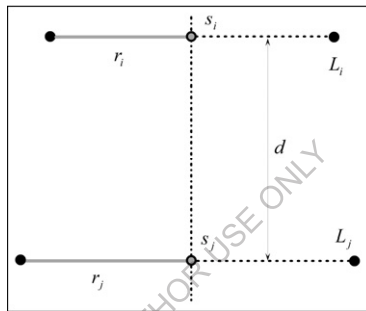


Fig.2.13. Coil properties describing (51).

Mutual inductance is exclusively a property of the coupling of the self-inductance between coils  $L_i$  and  $L_j$ . The magnetic flux intercepted by one coil is analogous to a unit of current flowing in the other [35], the mutual inductance of the  $i^{th}$  and  $j^{th}$  elements and the integration over the surface  $S_\theta$  show the mutual inductance can also be represented as,

$$M_{ij} = \frac{\iint_{S_j} \mathbf{B} \cdot \vec{n} dS}{I_{L_i}}, \quad (52)$$

where  $\mathbf{B}$  is the flux intercepted by the receiver coil,  $I_{L_i}$  is the current passing through the first coil,  $\mathbf{n} = (n_x, n_y, n_z)$  is the unit surface normal

vector, and  $dS$  is an infinitesimal area element of the local appearance of  $S_\theta$  as  $S_j$ . It is possible to transform the surface integral in (52) into a simpler line integral by using the magnetic vector potential,

$$\mathbf{B} = \nabla \times \mathbf{A}, \quad (53)$$

together with Stokes theorem, which states that a surface integral of the curl of a field equals the closed line integral over the rim of the surface,

$$M_{ij} = \frac{\int \int (\nabla \times \mathbf{A}) \cdot \mathbf{n} dS}{I_{L_i}} = \frac{\oint \mathbf{A} \cdot \mathbf{t} dl}{I_{L_i}}, \quad (54)$$

where  $\mathbf{t} = (t_x, t_y, t_z)$  is the unit tangent vector of the curve  $S_\theta$  and  $dl$  is an infinitesimal line element. The mutual inductance, then, depends upon the parameters  $\frac{r_i}{r_j}, \frac{d}{r_j}$ , and its proportionality to the radii, as,

$$M_{ij} = \mu_0 \sqrt{r_i r_j} \frac{2}{\alpha} \left[ \left( 1 - \frac{\alpha^2}{2} \right) K(\alpha) - E(\alpha) \right], \quad (55)$$

where  $K(\alpha)$  and  $E(\alpha)$  are elliptic integrals and  $\alpha$  is obtained by,

$$\alpha = \sqrt{\frac{4r_i r_j}{(r_i + r_j)^2 + d^2}}. \quad (56)$$

Using the table of formulas in [31] to find the value where,

$$M_{ij} = \alpha \sqrt{r_i r_j} = \alpha r_j \sqrt{\frac{r_i}{r_j}} (\mu\text{H}), \quad (57)$$

where  $\alpha$  is determined as depending on the variable,

$$u^2 = \frac{\left(1 - \frac{r_i}{r_j}\right)^2 + \frac{d^2}{r_j^2}}{\left(1 + \frac{r_i}{r_j}\right)^2 + \frac{d^2}{r_j^2}}, \quad (58)$$

from (53). A calculation was performed in *Circuit calculator* for the mutual inductance  $M_{ij}$  based on (57) and (58) from the specifications listed in Table 2.1,

$$\begin{aligned} u^2 &= 0.5, \\ M_{ij} &= 0.0042558 \mu\text{H}, \end{aligned} \quad (59)$$

where the result is used to calculate the discrete value of

$$\kappa_{ij} = 0.002346. \quad (60)$$

Table 2.1. Loop coils theoretical specification.

Coil	$L_i$	$L_j$
Coil radius (mm)	30	30
Wire radius (mm)	0.4	0.4
Wire length (cm)	65	65
Number of turns	3.5	3
Leg length (cm)	3	3
Number of legs	3	2
Loop inductance ( $\mu\text{H}$ )	2.0306	1.4918
Total inductance ( $\mu\text{H}$ )	2.1207	1.5519
Resonance frequency (Hz)	345607.761	404004.671
Differential frequency (Hz)		58396.910
System frequency (Hz)		374806.212
Differential system frequency (Hz)		433203.126
Wavelength (m)		692.037

The coupling strength between resonators is described by the coupling coefficient. Besides what has already been described as methods for calculating the coupling strength, another method [36] is to consider the bandwidth of the transmission, as,

$$\text{bandwidth} = \frac{2(f_i - f_j)}{f_i - f_j}, \quad (61)$$

where  $f_i$  and  $f_j$  are the split resonance frequencies of the resonators, which are most effective using a narrow bandwidth. In the sense of the arrangement illustrated in Fig.2.35, there is shown a separation of the resonators into their current and magnetic components. To maintain cohesion in the beam of energy exchanged between  $L_i$  and  $L_j$ , insights into the *why* the coupling is so significant to magnetic resonant power transmission are important to ascertain. A novel approach [37] called the perturbation method, strives to glean insights about those components which most affect the overall coupling. The following equation, modified,

$$\kappa_{ij} = \frac{\int_{L_i}^{} \mu H_0^+ \cdot H_0^* dV - \int_{L_i}^{} \epsilon E_0 \cdot H_0^- dV}{\int_{L_j}^{} \epsilon |E_0|^2 dV}, \quad (62)$$

implies that the motivation to understanding the coupling coefficient is where  $E_0^-$  makes the strongest contribution toward the intensity of  $H_0^+$  and what circuital components would support the transfer. It also suggests that increasing the amount of magnetic field at the loop would result in additional improvements. In its most basic sense, answering these subtle questions takes time and experience and they are addressed as motivations in this work; they will irrevocably remain a most important topic of future research. However, the author can identify that it is the *contribution of potential magnetic vector decomposition on the interface*, which is of greatest importance to understand. The description of the interface is that of the loop is in situ with free-space. The transmission loop and the “amount

of magnetic lines” crossing the receiving loop is a typical description of a radiated magnetic field and its effect on distant objects. An example is shown in Fig.2.14.

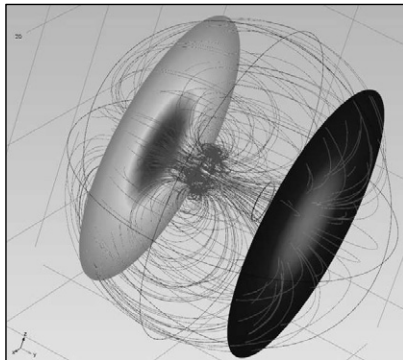


Fig.2.14. Magnetic coupling of low- $\kappa$  modes of distant resonators in space and time.

As noted in [24, 38], distance does not affect modal coupling, rather, spatial extensions in the  $z$  direction relate more closely to the transport of electrical power due mutual inductance, expressed in the  $\mathbf{E}$  and  $\mathbf{H}$  fields. With such effects, broadcast power is subject to attenuation over the impedance of free-space if the potential is assumed to contribute minimally to the fields. Nevertheless, it is important to keep in mind that the boundary does not describe and is independent of the sinusoid as well as its wave function. Therefore, the presence of the antenna and the presence of physical free-space constitute the entirety of the signal. If one considers the argument that the waveform is unique from its conductor—in the manner of induction described by Faraday as well as the original equations of Maxwell—the disturbance and the displacement open the door to questions of what in free-space is allowing the equilibrium of the forces of the currents driving radiation and its influence between antenna at distances greater than those described for the skin-effect. To model the relative

position and motion of the energy in terms of the exchange of photons, the path and intensity is described by the density of magnetic lines, illustrated in Fig.2.14.

The antenna, by the nature of its size, geometry, and symmetry couples the magnetic component of the energy on the coil-wire surface to an interface [29]. Under closer examination and consistent with the circuit architecture, the presence of the impressed wave is wholly due to the properties of the inductor  $L_i, L_j$  with the potential of free-space  $\mathbf{A}$  given its impedance  $Z_0$ . The magnetic loop, at a ratio to its quarter wavelength, contains the effects of a full ac cycle impressed on it by the incident wave in terms of transmission or reception.

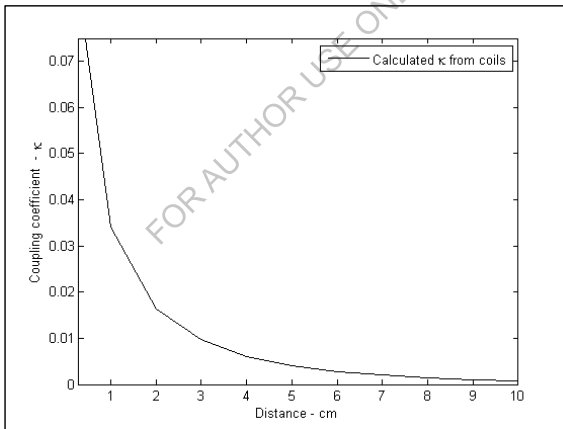


Fig.2.15. Theoretical coupling coefficient over a distance given (45).

The data in Fig.2.15 is derived from the calculation of coupling, shown in (45) in context of antenna as a function of transmitted power, in the manner of free-space interpretation of [48, 52, 61]. The result is the value of  $\kappa_{ij}$  attenuated by free-space. As is shown, the solution of this type of description suggests that a different analytical tool is required to show the

mechanisms responsible for energy transmission. As the purpose of the arrangement is to transport energy efficiently, the numerical solution of the circuit power is intended to measure the quantity of energy stored between the resonators and the dissipated power at the receiver available to a load. Therefore, coupled-modes in space describe the distribution of an energized field while coupled-modes in time yield the rate at which energy is transported.

### 2.1.2 Coupled-mode power

The energy stored and dissipated between two or more coupled objects describes a power distribution system. While the pursuit of a wired analog is desirable to some applications [10], for the purposes here, it is more effective to consider the coupling in terms of energy transport by a virtual waveguide. It is argued by the author that this particular methodology will yield greater insights not only about the model under investigation, but also about the environment where the model is operating. Energy transfer is an observable result in the context of forces moving charges. In the driven case, one can quantify forces due to amplification. In more subtle cases, the distribution of forces on charges is described by the Lorentz-Fitzgerald transformation [39, 40] used in special relativity and the source of Minkowski light cones and other innovative spatial geometries with moving forces [41, 42].

The Larmor force transfers energy between the field and charges. The power  $F \cdot v$  of the force equation is  $q\mathbf{E} \cdot \mathbf{v}$ , thus the power received by the electric charges per unit of volume is  $\mathbf{E} \cdot \mathbf{J}$ . Charge carriers convert power at the receiver from the local electromagnetic field into other forms of energy, including the kinetic energy of particles. Conversely,  $\mathbf{E} \cdot \mathbf{J}$  can be

negative, in which case there is a transfer of energy from the charge carriers to the field. One process is as a time-reversal of the other. Therefore, it is preferred to retain the family-time solution of Maxwell's equations to the motion of the sources and changes in the field that are reticent. The geometry of a circular loop is such that the radiation takes the pattern of a hyperbolic function, a transmitter of a primary loop in an exchange of energy with a primary loop of a receiver in a theoretical context is shown in Fig.2.7.

In terms of the total magnetic intensity,  $\mathbf{H}$ , is comprised of the projection of force  $\bar{\mathbf{H}}$ , and the flux density  $B_0 = \mu_0 H_0$  emitted between antenna. Solving  $\nabla \times \mathbf{v}_{ij}$  for all desired measurement points of  $H_0$  will indicate the amount of energy the field stored at the given point. To calculate this value reliably, it will require a fitted solution to Poynting's Theorem. It is desirable to express the energy as a property of the electric field and current density and compare this with the value of  $\nabla \times \mathbf{v}_{ij}$  for an arbitrarily-given  $H_0$ . The quantity  $\mathbf{E} \cdot \mathbf{J}$  is expressed in terms of the electromagnetic fields by taking the dot product of the current density into  $-\mathbf{E}$  on both sides of the Ampère-Maxwell equation,

$$-\mathbf{E} \cdot (\nabla \times \mathbf{H}) + \mu_0 \mathbf{H} \frac{\partial \mathbf{H}}{\partial t} + \epsilon_0 \mathbf{E} \cdot \frac{\partial \mathbf{E}}{\partial t} = -\mathbf{E} \cdot \mathbf{J}. \quad (63)$$

The identity,

$$\mathbf{E} \cdot (\nabla \times \mathbf{H}) = \mathbf{H} \cdot (\nabla \times \mathbf{E}) - (\nabla \cdot \mathbf{E}) \times \mathbf{H}, \quad (64)$$

and Faraday's law yield,

$$-\mathbf{E} \cdot (\nabla \times \mathbf{H}) = H_0 \cdot \frac{\partial \mathbf{H}_0}{\partial t} + (\nabla \cdot \mathbf{E}) \times \mathbf{H}. \quad (65)$$

The point where this occurs is at a potential value for equilibrium of the energy exchange between  $H_0$  and the current density at an arbitrary point,

$$(\nabla \cdot \mathbf{E}) \times \mathbf{H} + \frac{\partial}{\partial t} \frac{\epsilon_0 \mathbf{E}^2 + \mathbf{H}^2}{2} = -\mathbf{E} \cdot \mathbf{J}, \quad (66)$$

yields Poynting's theorem around that point.

$$\mathbf{S} = \mathbf{E} \times \mathbf{H}, \quad (67)$$

showing the density of power is emitted is a relative property of the antenna at the interface [107]. At any point in the volume, given the possible locations shown in Fig.2.7, the time-averaged energy stored is,

$$\frac{1}{2} \epsilon_0 (\mathbf{E}^2 + c^2 \mathbf{H}^2). \quad (68)$$

Equation (68), a derivation of the Poynting theorem, will show that a variation of energy in a given volume comes from power that is either delivered directly by sources or radiated across the surface—as flux flowing along a cavity or in this particular model, a virtual waveguide. The implication is that a perfect electrically-short loop antenna at a favorable ratio would have efficiency of radiation at maximum, indicating a related amount of power transfer and energy storage in the volume. The physical model is for the case of circular loops in §2.3.1. These cavities, while homogenous in free space, maintain a total internal reflection [83]. To sustain the state of equilibrium of the field, an opposing force is allowing the suspension. This implies a force-driving element, appearing in the circuit as the acceleration value of electrons flowing in the conductor of the

antenna. The observable behavior in the physical model will be discussed firstly from the point-of-view of the magnetic potential  $\mathbf{A}$  as  $\mathbf{B} = \nabla \times \mathbf{A}$ , then to the transition to circuital mathematical properties. Before this can be clearly stated, a discussion of how the metric of performance is derived in the model needs to be addressed.

### 2.1.3 Efficiency, quality, and loss

The fitness of the model is in terms of its overall efficiency, that is, by a comparison between the energy stored at the input to the energy dissipated including those in losses. The efficiency of the model is measured by the equation [43],

$$\eta_{ij} = \frac{\kappa_{ij}^2 Q_i Q_j}{1 + \kappa_{ij}^2 Q_i Q_j}, \quad (69)$$

where  $\eta_{ij}$  is dependent on the coupling coefficient  $\kappa_{ij}$ , but also by the qualities  $Q_i$  and  $Q_j$  of the coils  $L_i$  and  $L_j$ . The quality of a coil [44] is obtained,

$$Q_i = \frac{\omega_0 L_i}{R_i}, Q_j = \frac{\omega_0 L_j}{R_j}, \quad (70)$$

as a property of the energy stored in the angular frequency  $\omega_0$  the inductance  $L$ , and the free-space projection  $\bar{H}_0$  with the dissipation by the resistance  $R$  of the  $i^{th}$  and  $j^{th}$  coils. The quality factor is then determined by,

$$\frac{1}{Q_i} = \frac{1}{R_i} \sqrt{\frac{L_i}{C_i}} + \frac{1}{R_{pi}} \sqrt{\frac{L_i}{C_i}} = \frac{1}{Q_{R_i}} + \frac{1}{Q_{L_i}} \quad (71)$$

comprised of the inductance  $L$ , resistance  $R$ , and capacitance  $C$ , and of the  $i^{th}$  and  $j^{th}$  coil in the oscillator and receiver circuits. The scheme is defined so that the system is performing work, the unloaded quality  $Q_{L_i}$  is neglected. The quality factors then become,

$$Q_i = \frac{1}{R_i} \sqrt{\frac{L_i}{C_i}}, Q_j = R_j \sqrt{\frac{C_j}{L_j}}, \quad (72)$$

for both cases of a series and parallel configuration in an ideal circuit arrangement. The coils are arranged within their respective circuits as to maximize the amount of energy stored between the inductances and the capacitances. The maximum energy stored in  $L_{i,j}$  and  $C_{i,j}$  is,

$$\begin{aligned} u_{L_i} &= L_i I_0^2, u_{C_i} = C_i V_0^2, \\ u_{L_j} &= L_j I_R^2, u_{C_j} = C_j V_R^2, \end{aligned} \quad (73)$$

which is discussed in greater detail in §2.3.1. The loop can be treated as a standard oscillator in coupled mode defining (43)(44) as

$$a_i(t) = \sqrt{\frac{L_i}{2}} I_0(t). \quad (74)$$

It is well-understood that quality factor has a direct consequence upon the efficiency of an electrical transmission circuit. The remaining component relevant to the properties of coupled-modes is the losses in the system resulting from the materials used in the construction of the loops. Losses in the system are observed as dissipation of the energy stored. For the losses due to ohmic resistance [57],

$$R_{i,j} = \sqrt{\frac{\mu_0 \omega_0}{2\sigma_m}} \sum_{i=1}^{n_i} \sum_{j=1}^{n_j} \frac{\ell_{i,j}}{4\pi r_{i,j}}, \quad (75)$$

where  $\sigma_m$  is the conductivity of the material,  $n$  the number of turns,  $\ell$  the wire length of the coil, and  $r_{i,j}$  the wire radius of the  $i^{\text{th}}$  and  $j^{\text{th}}$  coils. The calculation of the quality factor and the losses for the system are shown in Table 2.2.

Table 2.2. Energy, quality, and loss specification.

Coil	TABLE 2.2 ENERGY, QUALITY, AND LOSS SPECIFICATION		
	$L_i$	$L_j$	$L_m$
Resonance frequency (Hz)	345607.761	404004.671	433203.126
Oscillator current (A)	1.25		
Oscillator voltage (V)	6.20		
Ohmic resistance ( $\Omega$ )	0.00593	0.00508	168820.035/cm
Energy storage ( $\mu\text{J}$ )	7.158	6.269	
Quality factor	776.583	775.472	3.225
Magnetic field $\mathbf{B}$ (T)	2.618E-05		
Scheme efficiency	0.7682		

Column  $L_m$  in Table 2.2 is provided for the object impressed on free-space as a function of the inductance and resistivity of the medium. Averaged, the potential efficiency is very high for the coupled-mode, although it will be shown in experiments that it is transformed solely on the properties of the material consisting the antenna. In *local* space, the efficiency is observed to be very high but it refers to the ability of the loop to transform the acceleration of electrons into photons, not including any quantum considerations. Efficiency of the transmission over distance is the linear decay of power over  $1/r$ . This is discussed in terms of radiated power of the antenna in §2.3.2. Energy storage in Table 2.2 is shown per cycle.

With these baseline criteria for the expected properties of the antenna as a function of the materials and geometry of the wire established, §2.2 will address the circuit model that can sustain the oscillations. The criteria is the

means by which differentiating models will be judged to be used in commonplace application, such as that in §2.4. The system under consideration is designed with compactness in mind and each component chosen for an expected level of performance. The purposeful choice of using the type of oscillator described herein is primarily for its simplicity and size.

#### 2.1.4 The magnetic potential

The magnetic vector decomposition is useful to describe the nature of the field object between the resonators as a result of the forces that shapes the object. The field model is centered around the assumption that the geometry can be understood from topological arguments of the forces in the region. The model uses the magnetic vector potential  $\mathbf{A} = (A_x, A_y, A_z)$  to construct a finite solution by casting a projection  $A_t$  as the dot product of the tangent vector and the magnetic potential, as,

$$A_t = A_{t_x} \cdot t_x + A_{t_y} \cdot t_y + A_{t_z} \cdot t_z. \quad (76)$$

(76) is the response of the potential to the disturbance of the wave. Its magnitude is relative to the energy stored in the field object and the forces at the interface. While not appearing inside the field, it occurs at the limit of the field at its boundary and is symmetrical along the space between coupled-mode objects. The field has dispersion dependent on the geometry of the antenna; the transmitter and receiver placed at separations in all three Cartesian directions. The unity of the potential in context with the field object is observable under measurement of an unpowered antenna and is extant at the nulls to the left and right minor lobes. Modal magnetic resonance coupling is more effective at describing magnitudes of magnetic

flux density in terms of the potential, one such is description is in terms of displacement currents.

The antenna loop carries a complex current,

$$I(t) = I \cos \omega t, \quad (77)$$

which is confined to the loop near its surface—the surface of the conductor consisting of Litz wire. The vector potential from the loop is expressed as,

$$\mathbf{A}(r) = \frac{\mu_0 \mathbf{I}}{4\pi} \oint_{\ell} \frac{e^{-jkr'}}{r'} dl', \quad (78)$$

where  $\mathbf{I} = I \cos \omega t$ . To simplify the appearance of the harmonic current in the following equations, it is expressed as

$$\mathbf{I} = \mathbf{u}_\gamma. \quad (79)$$

By inspection of (78), the evaluation of the potential depends of the location where  $dl'$  is being observed. Expansion of the exponential form,

$$e^{-jkr'} = e^{-jkr} e^{jk(r-r')} \approx e^{-jkr} [1 - jk(r'-r)], \quad (80)$$

is similar to the approximation of the electric dipole [20]. (78) is transformed to,

$$\mathbf{A}(r) = \frac{\mu_0 I}{4\pi} e^{-jkr} \left[ (1 + jkr) \oint_{\ell} \frac{dl'}{\rho'} - jk \oint_{\ell} dl' \right] \mathbf{u}_\gamma. \quad (81)$$

For the purposes here, the second integral in (81) is zero since all it indicates is to continue moving the observation around the circle to the starting point of integration. Therefore, evaluation of the first integral in (81) yields, by vector identity [45],

$$\oint_{\ell} b dl' = \int_{\Delta s} (\mathbf{u}_n \times \nabla b) \cdot ds, \quad (82)$$

to convert to a surface integral. The scalar  $b$  is equal to the inverse of the amplitude  $\frac{1}{r'}$ , the unit vector  $\mathbf{u}_n = \mathbf{u}_z$ , since the loop is wholly in the  $x-y$  plane and projecting along  $z$ . This results the vector to be decomposed into,

$$\begin{aligned} \oint_{\ell} \frac{dl'}{r'} &= \int_{\Delta s} \left( \mathbf{u}_z \times \nabla \frac{1}{r'} \right) \cdot \mathbf{u}_{\gamma} ds, \\ &= - \int_{\Delta s} \left( \mathbf{u}_z \times \nabla \frac{\mathbf{u}_{r'}}{(r')^2} \right) \cdot \mathbf{u}_{\gamma} ds, \end{aligned} \quad (83)$$

where the surface integral yields the factor  $\pi a^2$ . Because it is expected by geometric inspection the shape be homogenous and elliptical, the result requires representation to be in spherical coordinates. Taking the vector relation,

$$\mathbf{u}_z \times \mathbf{u}_r = \sin \theta \mathbf{u}_{\gamma}, \quad (84)$$

gives,

$$\oint_{\ell} \frac{dl'}{r'} = \frac{\pi a^2}{r^2} \sin \theta. \quad (85)$$

Using (84) in (81) and evaluating reveals the interaction of the vector potential with the field object. This is,

$$\mathbf{A}(\mathbf{r}) \approx j \frac{\mu_0 (I \pi a^2) \kappa}{4\pi} \frac{e^{-jkr}}{r} \sin \theta \mathbf{u}_{\gamma}. \quad (86)$$

(86) suggests there are observable effects at the boundary between the field object and the potential. The result was simulated and is shown in Fig.2.16.

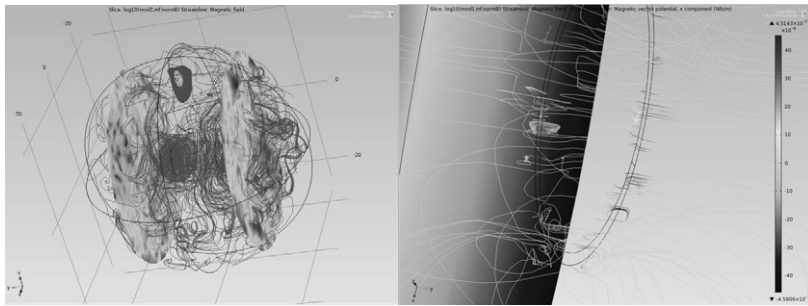


Fig.2.16. (a) The vector potential in the magnetic field, (b) the potential component on the loop interface.

The simulation shows that the electromagnetic potential is enmeshed in the field, but also is in motion at the boundary between the field and free-space following the  $x-y$  plane of the loops. What is interesting is that motion is closely connected to the interfacing of the loop and the medium and that it occurs in differential degrees of magnitude. What is *most* interesting is that if the potential can influence the line integral at the interface. If it can significantly move it away from zero, it would show a second coupled mode, or a “recoupling” inside the boundary.

Two questions asked are: is the potential,  $\mathbf{A}$ , a component of the entirely contained within the magnetic intensity  $\mathbf{H}$ , else a coupling to  $\mathbf{B}$ ? Is it a property of the medium inferring a transfer of force between  $\mathbf{B}$  and  $\mathbf{A}$ ? The use of the Maxwell displacement current  $\mathbf{D}$  is the form of the displacement because of the forces between antenna and a field object [46], as,

$$\mathbf{B} = \nabla \times \mathbf{A} = \frac{\mu_0}{4\pi} \int \frac{j \times r}{r^3} d\nu + \frac{\mu_0}{4\pi} \int \frac{(\partial \mathbf{D}/\partial t) \times r}{r^3} d\nu. \quad (87)$$

The sequence of solutions to find the potential, in terms of a circuit, is difficult when trying to decompose the potential vector on the interface to quantify the dependence of the potential on coupling; this is especially difficult when there is no definition, outside of the impedance, of free-space. There is free-space in the sense of that on a planet, free-space in the sense of the “vacuum” of outer space, and the contention that there is dark matter filling the apparently empty space. Can there be a unification [26, 47, 49] by using the Minkowski cones and time dilation of Einstein’s special theory? Are electromagnetic forces and the charges that populate them strictly dependent on the quantum effects, i.e., the duality of the electron [48] and its esoteric properties? Can wave-particle duality be expressed in such energized structures at atmospheric pressure and temperature? The author contends this provides sufficient material to support the notion of free-space waveguides, constructed by this scheme, and energy can be transmitted across them. It could very well indicate evidence of properties only visible in the quantum universe, are also available to the macro world [49]. The model would then be described topologically as a waveguide field [50],  $\text{WG} \rightarrow \text{F}$ , and the primary contributor to the closure of currents in an open circuit across free-space.

A substantive claim presented in this work is a degree of independence of the magnetic field from its electric counterpart in terms of force and attraction—described in terms of the magnetic potential at the interface of the antenna. It is most observable under particular conditions in the antenna where the radius of the antenna is expressed as a ratio,  $\mathfrak{R}$ , of the loop circumference to its wavelength as an exponential function, shown in (42), whose **B** field takes the form of (21) and (22), with the additive component  $\cos(\theta)$ . The interaction of the magnetic potential at the interface yields a

true conduction current, described by (4) and (7). Geometrically, the displacement field creating the conduction current extends from the center of the loop to form a hyperbolic plane along the  $z$  and  $-z$  directions. An illustration is shown in Fig.2.17.

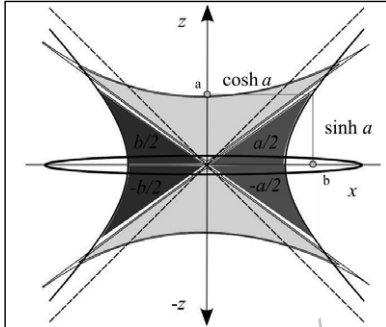


Fig.2.17. A single loop projecting a magnetic field.

The presence of the field in free-space emitted by a magnetic loop is obtainable by discrete trigonometric functions, given its projection [30]. The effective area, where forces deform the isotropy into a discernible shape, transforms into a composite of sufficient flux density providing the appearance of a closed surface. The equilibrium of the area is dependent upon the magnetic energy contained within and where the boundary is discerned. Although in fact the boundary is indeterminate at extreme positions along the curvature of field propagation, where the received power approaches zero is such a boundary. Description of this boundary is given by the infinitesimal of the magnetic field. The surrounding free-space is considered as a periodic locally-approximated waveguide [26, 107, 111] with implicit time-dependence  $e^{j\omega t}$ . The spatial equations (43) given their weak time dependence of amplitudes  $a_T$  and  $a_R$  (44), and coupled state (45), when equivalent to the relationship of the stored energy at resonance via conductance  $G$  and resistance  $R$  attenuating the transmission,

contributing simultaneously to a complex impedance  $Z_0$  and admittance  $Y_0$ , construes that the forces exchange energy in constructive and destructive interference patterns as a global oscillatory force representing the waveguide [26, 107, 111].

It is proposed that if a special circuit could accelerate electrons in an antenna, the emitted radiation could be controlled and directed by manipulating the presence of the magnetic component. An increase of  $\mathbf{B}$  will yield a greater mutual inductance (54), because of the extra “floating” induction at the interface. With the addition of metallic accretion discs, that is, discs forming a uniform conductive surface, lying in the  $x$ - $y$  plane and projecting along  $z$  so that a corona effect occurs in the gap between the disc and the inner loop surface. Such discs are aligned with their centers at the same point as the loop center to enhance conductivity at the interface, illustrated in Fig.2.18.

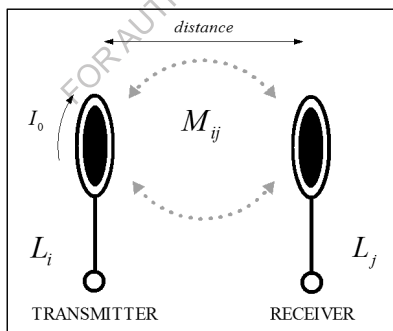


Fig.2.18. Two circular loops with accretion discs.

Under normal atmospheric pressures and temperatures, a magnetic field has a potential flux density which is evenly distributed, is concentrated toward the center of a loop rather than in other places, and can be modified to induce currents at a distance [107]. With respect to the loop described by

(124), the magnetic field in the  $x - y$  plane takes the following form at a distance,  $d$ , along the  $z$ -axis from the center of the loop, is,

$$B_z = 2\pi r_i \frac{r_i}{d} \frac{\mu_0 I_0}{4\pi d^2} = \frac{1}{2} \frac{\mu_0 I_0 r_i^2}{(d_B^2 + r_i^2)^{\frac{3}{2}}}, \quad (88)$$

in which  $d_{B_z}$ , is the ordinal field distance. When a current,  $I_0$ , is applied to the loop, the magnetic field lines extend from the center of the loop and form a curvature as a hyperbolic plane along the  $z$  and  $-z$  directions, as illustrated in Fig.2.17. The presence of the field in free-space emitted by a magnetic loop is obtainable by discrete trigonometric functions, given its projection. The effective area, where forces deform the isotropy into a discernible shape, transforms into a composite of sufficient flux density providing the appearance of a closed surface. The equilibrium of the area is dependent upon the magnetic energy contained within the area and where the boundary is discerned. Although the boundary is indeterminate at extreme positions along the curvature of field propagation, where the received power approaches zero is such a boundary. Description of the momentum of energy propagation is given by the infinitesimal of the magnetic field. Considering Fig.2.8, the geometry of the energy pattern emitted from a circular loop by its intensity in motion across free-space, displacing the space given its magnitude,  $\bar{\mathbf{H}} \cdot \delta \mathbf{B}_z$ , in both the positive and negative directions of  $z$ . The phenomenon of projection,  $\bar{\mathbf{H}}$ , is manifest as a shock wave from a transmission antenna where an acceleration force has been applied to electrons on its conductive interior. The length and intensity of the projection is due simultaneously to the geometry of the antenna and the power applied to it.

In Fig.2.8, the length of transmission along the  $z$ -axis is a component consisting of the projection field length  $d_{\bar{H}}$ , and the ordinal field distance  $d_{B_z}$ , given its radial size  $r_{B_r}$ , and the infinitesimal field  $\delta\mathbf{B}$ . The length of  $u$  is given by the persistence of amplitudes to the limit of their ambience, manifest as  $\mathbf{B}$  given in both directions of propagation in  $z$ . By calculating the angle  $\theta$  and integrating around the loop, one can determine the amount of energy present in  $\mathbf{B}$ . The magnetic flux density is dependent upon the current applied to the loop antenna. An increase of  $\mathbf{E}$  or  $\mathbf{B}$  will quasi-linearly increase the flux density of the field, given thermodynamic laws. The assumption is that an increased  $\mathbf{B}$  will yield an equal increased amount of  $\mathbf{E}$  in the model. The model offered here is a weakly-coupled, low  $\kappa$ , system at resonance behaving analogously to a locally-approximated transmission-line resonator [31, 111]. Under such conditions, the complex current and voltage operating on the loops take the form,

$$\begin{aligned} I(z) &= I_0 \cos\left(\frac{\pi z}{l}\right), \\ V(z) &= -jZ_0 I_0 \sin\left(\frac{\pi z}{l}\right), \end{aligned} \quad (89)$$

where  $I_0$  is the current in the short-circuit and  $l$  is the length of the attractive transmission path. The simple impedance,  $Z_0$ , is that of free-space,  $\sim 377\Omega$ . The average stored magnetic energy  $\langle W_m \rangle$  in the loop at angular frequency  $\omega_0$  is

$$\begin{aligned} \langle W_m \rangle_{\omega_0} &= \frac{1}{4} \int_0^l L |I_z|^2 dz = \frac{1}{4} L |I_0|^2 \int_0^l \cos^2\left(\frac{\pi z}{l}\right) dz \\ &= \frac{1}{8} L l |I_0|^2. \end{aligned} \quad (90)$$

The average stored electrical energy does not need to be calculated separately since the system is at resonance. i.e.,  $\langle W_e \rangle_{\omega_0} = \langle W_m \rangle_{\omega_0}$  as,

$$\langle W_{total} \rangle_{\omega_0} = \langle W_e + W_m \rangle_{\omega_0} = \langle 2W_m \rangle_{\omega_0} = \frac{1}{4} Ll |I_0|^2. \quad (91)$$

With the aforementioned implicit time-dependence  $e^{j\omega t}$ , uncoupled, has spatial dependences  $e^{-j\beta_1 z}$  and  $e^{-j\beta_2 z}$ ,  $\beta_1 \approx \beta_2$  are the propagation constants. For the geometry shown in Fig.2.2, Fig.2.8, Fig.2.9, and Fig.2.10 with a period  $\Lambda$ , the coupling coefficients  $\kappa_T$  (transmitter) and  $\kappa_R$  (receiver) take the form  $2\kappa_{TR} \cos(2\pi z/\Lambda)$ . Therefore, to a fitted version of (43), the spatial equations are,

$$\begin{aligned} \frac{d}{dz} a_T &= -j\beta_T a_T - j2\kappa_T \cos\left(\frac{2\pi z}{l}\right) a_R, \\ \frac{d}{dz} a_R &= -j\beta_R a_R - j2\kappa_R \cos\left(\frac{2\pi z}{l}\right) a_T, \end{aligned} \quad (92)$$

given a weak time dependence of the amplitudes  $a_T$  and  $a_R$  to resonance frequencies  $\omega_T$  and  $\omega_R$ , to a fitted version of (44),

$$\begin{aligned} \frac{d}{dt} a_T &= j\omega_T a_T + j\kappa_T a_R, \\ \frac{d}{dt} a_R &= j\omega_R a_R + j\kappa_R a_T, \end{aligned} \quad (93)$$

relative to the coupled state of the resonating elements  $L_T$  and  $L_R$ , from (45). The mutual inductance of the elements and the integration over the localized spherical surface  $S_j$  from Fig.2.2, fitted from (54) is therefore,

$$M_{TR} = \frac{\int \int (\nabla \times \mathbf{A}) \cdot \mathbf{n} dS}{I_{L_T}}, \quad (94)$$

proportional to the current of the opposing resonator  $I_{L_R}$  yielding the property that energy can be applied to the system to a maximum point that the waveguide can sustain. The dissipated power, while a property of the load present, is also a property of the power sustained in the magnetic field, as,

$$\begin{aligned} \langle p_d \rangle &= \frac{1}{2} R |I(z)|^2 + \frac{1}{2} G |V(z)|^2 \\ &= \frac{1}{2} R |I_0|^2 \int_0^l \cos^2\left(\frac{\pi z}{l}\right) dz + \frac{1}{2} G |V_0|^2 \int_0^l \cos^2\left(\frac{\pi z}{l}\right) dz, \end{aligned} \quad (95)$$

shown in (134) to be equivalent to the relationship of the stored energy at resonance. Once the electrons within the conductive material are accelerated, they subsequently radiate energy in a quantized form upon deceleration [5]. Reviewing Larmor's conjecture from (11), the energy emitted in the form of radiation from the charge  $q$  with acceleration  $a$  is given by,

$$\langle p_e \rangle = \frac{q^2 a^2}{6\pi\epsilon_0 c^3}, \quad (96)$$

where  $c$  is the speed of light. The emission of energy, in a dipolar form, is

$$\langle p_\gamma \rangle = \mu_0 \sin^2 \theta, \quad (97)$$

where  $\theta$  is the angle between the direction of acceleration and the emission. The radiation is polarized such that the emission field is parallel to the acceleration force on the electron. It is proposed that if a circuit could

accelerate electrons in an antenna, the emitted radiation could be controlled and directed by manipulating the presence of the magnetic component. An increase of  $\mathbf{B}$  would then yield a greater value of  $M_{ij}$  with the addition of metallic accretion discs.

The magnitude of projection at a distance from the loop is given by the quantities of  $\cosh a$  and  $\sinh a$ , shown in Fig.2.17, between the limit at the transient zone, at point ‘b’, and the center. Point ‘a’ is where the influence of the magnetic field is at a maximum, such that a second loop absorbs a maximum quantity of transmitted power yielded by the first loop. The power densities in the darker grey zones, labeled  $\pm a/2$  and  $\pm b/2$ , based on their orientation on the  $x$  and  $z$ -axis, are equal unless there is an azimuthal field present. The power density in these zones is dependent upon the current  $I_0$  applied to the loop. If a loop is set at a distance with a second loop of the same number of turns, loop radius, and wire diameter (to a reasonable degree of equal approximation) the field “lines” extend the hyperbolic plane from  $(x_0, y_0, z_0)$  to  $(x_1, y_1, z_1)$  with less curvature  $\theta$  than that observed in the case of a singular loop. The limit between the distance, given by  $(x_1 - x_0, y_1 - y_0, z_1 - z_0)$ , and the fall-off of the field in this scenario, given by  $1/r^2$ , is asserted due to the curvature of the propagation in the virtual waveguide and is not necessarily dependent upon the size of the loop.

The addition of a conductive media lying along the  $x-y$  plane, perpendicular to  $z$ , will contort the zones. If a flat metallic sheet is placed in the plane of a length and height greater than the diameter of the loops, then energy is absorbed on its surface. Contrastingly, the introduction of a

metal disc at the center of the receiving loop will increase the magnitude of **B**. The propensity of the discs to enhance the magnetic field has a greater influence on the receiver as opposed to the transmitter.

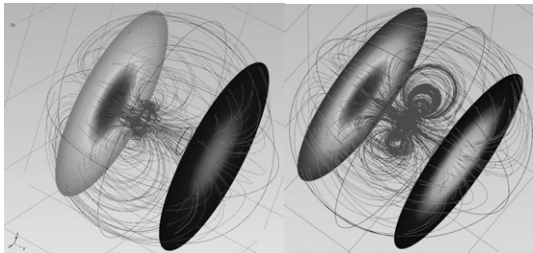


Fig.2.19. (a) Magnetic flux of loop antenna, (b) disc adds flux strength.

The magnetic loop, at a ratio to its quarter wavelength, contains the effects of a full alternating-current (ac) cycle impressed on it by an incident wave [30]. The rate of exchange of energized particles is then represented by the density of “magnetic lines”, illustrated on the left side of Fig.2.19. The right side of Fig.2.19 meanwhile shows the same loop system with an accretion disc added at the center of the transmission loop. The more attraction between the loops, so the more efficiently the energy is transferred. The lines in Fig.2.19a and Fig.2.19b show the magnetic flux density while the slices at the ends show magnetic field intensity at the loop at norm **B**. In the simulation, the number or “density” of field lines precludes a higher magnetic flux in the region while a shade from dark to light denotes greater intensity.

The strength of the magnetic field generated by the loop may be increased by adding turns  $n$  of conducting wire, instead of a single turn and increasing the length of the legs  $m$ . In terms of the experiments carried out in §2.4, loops were constructed where  $n = 3$  cm and  $m = 4$  cm. For the

calculation of the magnitude, it is more appropriate to consider the magnetic field in terms of  $\mathbf{H}$  where  $\mathbf{B} = \mu \mathbf{H}$ .

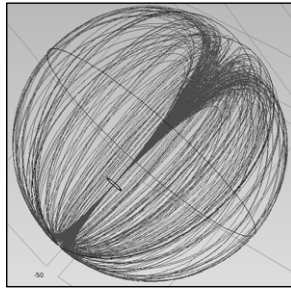


Fig.2.20. Propagating energy in  $\mathbf{B}$ .

A single disc is placed inside the receiving loop so that it lies on the  $x - y$  plane while its center lies along the  $z$ -axis, as shown in Fig.2.20, where the magnitude of  $\mathbf{B}$  is directed through its center. With the addition of the disc, distortions are present by imbalances in the field, where additional transformed energy,  $J_\phi$ , appears in the azimuthal field, shown in Fig.2.21 as,

$$J_\phi = f(r, \theta) \hat{\phi}. \quad (98)$$

A disc, approximated as a consecutive sequence of wire-turns in the form of a spiral where the width  $w$  between the winding arms approaches twice the wire radius, as,  $w \rightarrow 2a$ , has a surface radius of 12 mm. It is expected the disc will increase the magnitude of  $\mathbf{H}$  relative to its size with the addition of the new vector  $u$ . The azimuthal magnetic field is expressed as a second order phenomenon. An increase in energy in the field is observed by an increased conversion of electric current into  $\mathbf{H}$ .

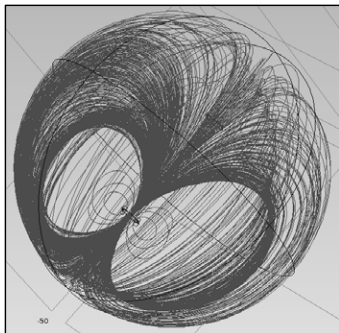


Fig.2.21. Density of azimuthal  $\mathbf{B}$  field.

As discussed earlier, distance does not directly affect modal coupling [24], rather, spatial extensions in the  $z$ -direction relate more closely to the transport of electrical power attenuated along its length. Therefore, broadcast power is subject to an attenuation rate dependent upon a value of impedance. The appearance of an azimuthal component when the disc is placed inside the loop is likely due to shearing effects, or imbalances in the equilibrium state of the magnetic field consisting the waveguide as it transforms from isotropy toward anisotropy in the  $x-y$  plane. Experimental work on this theory is presented in §2.4.2.

## 2.2 The circuit model

As it is desired that a transmission system transmit waves, the oscillator is considered to be the driving-force of the system. Without oscillations, waves would not propagate. For comparative purposes, if the antenna was charged with a non-oscillating current such as that provided by a direct current (dc) power supply, the receiver would not see the signal and magnetic energy statically emitted into space, given the area,  $dA$ , of the conductor. The aim of this section is to describe the construction of a circuit, which illustrates the diagrammatic representation of the source, the

oscillator, and the loops illustrated in Fig.2.1. The circuit model will also attempt to satisfy the mathematical descriptions of the previous sections while introduce a reconciliation of the circuit verses field model discontinuities [51] only in the confines of an agreement of the supposition of resonant circuit-as-antenna correlation. To satisfy these aims, a circuit which consists of a transmitter and a receiver is required consisting of a compact oscillator driving a magnetic-resonant loop antenna. The coupling of the source and oscillator objects are wholly responsible for the character of the manifest field between the antennas, as described in §2.1. The most immediate and obvious question is what kind of oscillator to use: compact, powerful, and the ability to impress the expected currents on the loop. Efficiency is important here as the transmission scheme has a criterion of fitness, taken into consideration when choosing the oscillator type.

In the early days of radio, numerous types of oscillators for signaling were based upon the spark-gap transmitter first used by Hertz [52, 53]. As the transmission of radio waves evolved from telegraphy into voice, increasingly the oscillator needed to be free from noise for broadcasting. As the spark-gap started to fall out of favor, sinusoidal oscillators able to contain modulation were proposed in the form of the regenerative circuit by Armstrong [54]. The universality of the scheme showed that any radio-frequency oscillator was a topology containing feedback. This topology could be modified to provide a controllable reduction in feedback loop coupling on the antenna circuit. If the method of coupling was to split the characteristic impedance of the circuit through an amplification stage, it functions as a combination of an oscillator and mixer, which converts the modulation directly to the baseband.

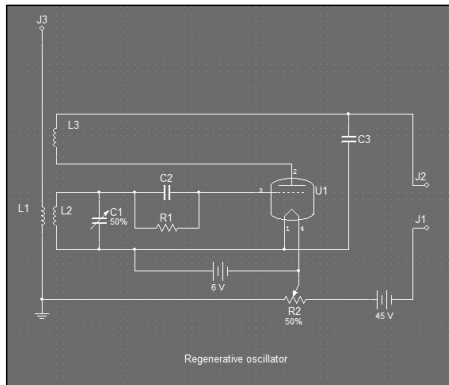


Fig.2.22. The regenerative oscillator.

Illustrated in Fig.2.22, the driving force of the vacuum tube U1 is carried across a pair of inductances, a coupling coil, L2, and tickler coil, L3, along with tuning capacitor, C1. The capacitor C2 serves to suppress leakage from the grid of U1, capacitor C3 for frequency bypass. The application of dc power to the triode amplifies the signal incoming to terminals J1 and J2 treating the beat frequency of the antenna and power impressed on it as if the entire package was a combination of source and oscillator amplifying the resonant frequency of the antenna. If the circuit is modified to split the antenna into two equal phases and the driving amplitude powering each  $180^\circ$  phase-shift, a circuit with twice as much applied power could be constructed. Such a circuit is the push-pull oscillator.

The push-pull oscillator is a type of electronic circuit that can drive both a positive and a negative current phase-shift into a load. Appearing in the early 1920s, later described in detail by Hoag [55], the model is a highly-efficient oscillator which contains a complementary pair of power-drivers, one dissipating or sinking current from the load to the negative power supply, and the other supplying or sourcing current to the load from a positive power supply over a center-tapped coil during a complete duty

cycle. Because of the high-efficiency and the simplicity of the model, it is ideal for wireless power transmission shown in Fig.2.1. Since the scheme is based on induction, the oscillator will have to be modified to also phase-shift the antenna inductance through the cycle.

An inductively-coupled push-pull oscillator is shown in Fig.2.23. When voltage is first applied by the dc source,  $V_1$ , the fluctuation of the voltage makes the grid of  $U_1$  positive and the grid of  $U_2$  negative. Because the current is lagging behind the voltage, it is expressed as changes in the plate current. The lag of the current is an important feature, which is directly captured in this type of oscillator, the dipole is created on the plate. The resonance between the inductance and capacitance in the plate circuit causes voltage changes on the plate, which feed through the plate to grid capacitance or by magnetic coupling between the two tank circuits, reverses the polarity of the grids. As this continues, the tank circuit impresses the voltage changes on the grids and current on the plates, so that oscillations are of an increasing magnitude. The magnitude rises to a limit imposed by the source voltage and energy dissipated evenly across the circuit given its symmetry. Eventually, the rise reaches a magnitude where the dipole breaks and energy is released.

### **2.2.1 The push-pull oscillator**

The push-pull oscillator is a balanced oscillator. This type of circuit is able to deliver larger outputs with less distortion than single-triode amplifiers. The output is a sinusoid relating the opposing forces of absorption and dissipation in the tank circuit created by the coupling of coils and capacitors across the amplifiers.

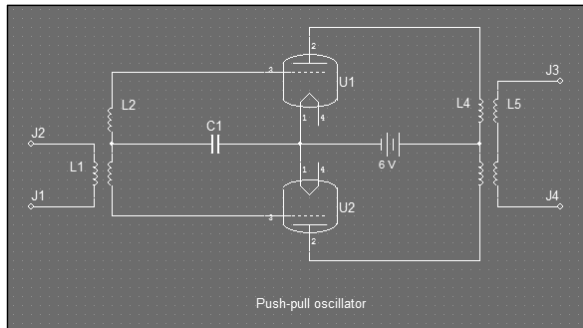


Fig.2.23. Inductively-coupled push-pull oscillator.

Because the oscillator in Fig.2.23 is suitable to drive the scheme, it is necessary to recast the circuit since the antiquity and power needs of the vacuum-tube triodes make recreating the circuit in its exact form impractical. What is more realistic is to replace U1 and U2 with something like a semiconductor triode, which has the ability to impress a high level of amplitude with fast switching speeds. Such an item very advantageous for this purpose is the n-MOSFET transistor. A field-effect transistor dependent upon high-speed, electric field switch-transitions, the n-MOSFET has coupled-modes. The mode relevant here is the triode mode or linear region, also known as the ohmic mode [56]. The architecture of an n-channel MOSFET is shown in Fig.2.24. A metal-oxide-semiconductor field-effect transistor has three terminals: the source, the gate, and the drain. In an n-MOSFET, both the source and the drain are n-type and the substrate between them is p-type. A thin layer of silicon dioxide insulates the gate and the p-type substrate. Due to this insulation, there is no gate current to either the source or the drain.

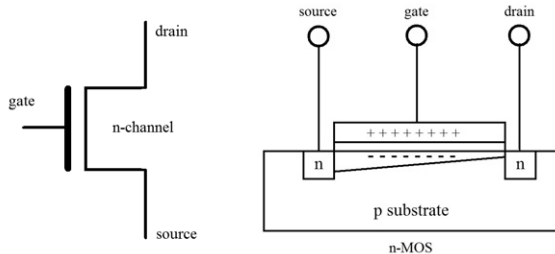


Fig.2.24. The n-channel MOSFET structure.

The n-MOSFET is equated with a voltage-controlled switch. When a sufficient voltage  $V_{GS}$  is applied between the gate and the source, the positive potential at the gate will induce enough electrons from the p-type substrate to form an electronic channel creating an inversion layer between the source and the drain, and a current  $I_{DS}$  is formed. The behavior of a n-MOSFET can be described by the function  $I_{DS} = f(V_{GS}, V_{DS})$  with a threshold voltage  $V_T$ . These properties can be taken advantage of in the wireless power scheme by placing the n-MOSFET in the circuit in such a way as to split oscillations into two groups: those of the transmission antenna and those between the pair, illustrated in Fig.2.25, and the steps through each phase, illustrated in Fig.2.26.

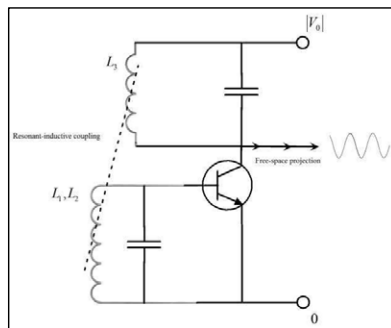


Fig.2.25. Schematic representation of accelerating electrons split across a tank circuit.

Fig.2.25 is intended to show how a single MOSFET in the application applies an acceleration force, as a property of the potential (voltage) and inductance where the oscillation is sustained in the antenna. The ability to phase-shift between each part of the cycle synchronizes with the shifting phases of the potential closing the circuit periodically and allowing energy to transfer. Free-space wave projection is possible when the synchronization is with any one of the rest-state potentials embedded in the phase. Although the specification of these potentials is outside the scope of this work, suffice to say the synchronization satisfies the presence of the antenna as analogous to coupled-modes. It is at the shifting between phases where interaction with the interface takes place. A deeper inspection of this behavior is given in §2.2.4.

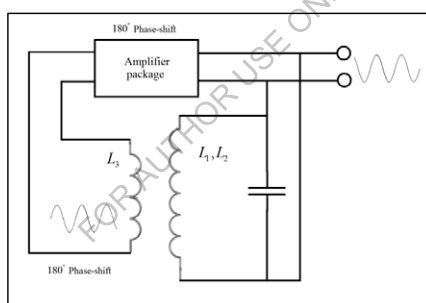


Fig.2.26. Phase-shift amplifier on coils.

As such, a power n-MOSFET is a suitable component to replace U1 and U2 of Fig.2.23. The arrangement of Fig.2.23 is altered to Fig.2.27:

- Coil L2 becomes the antenna, and is connected across the drain of Q1 and Q2 to split in half the antenna circuit including the feed from the power supply, polarity opposite,
- plate terminals U1 and U2 are tied together and connect to the negative feed from the power supply, and,

- coil L4 is the receiver antenna, shown in Fig.2.28.

A schematic of the revised oscillator to drive the circuit is illustrated in Fig.2.27.

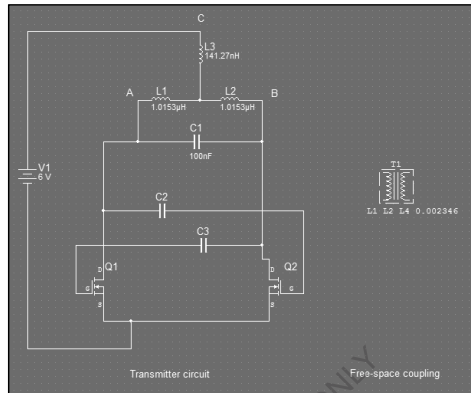


Fig.2.27. The transmission element with a coupled-mode.

This model contains only a simple description of the dipole but it is suspected such a description could go deeper, examined in §4. Regardless, the circuit will create and destroy its dipole in a cycle releasing its energy. Since destruction of the dipole is occurring by the current returning to the source in the form of feedback power from the antenna, excess energy will bleed off as heat. The component that emits the heat due to internal losses and feedback of energy coupling at the interface is the capacitor C1. At higher source levels, heating of Q1 occurs; heat-sinks for both Q1 and Q2 and a metalized capacitor will keep the circuit from burning out. The author strongly suggests future research be conducted on Joule heating in the circuit.

### 2.2.2 Simulation and construction of the circuit

Consider the circuit coupling diagram shown in Fig.2.28a.

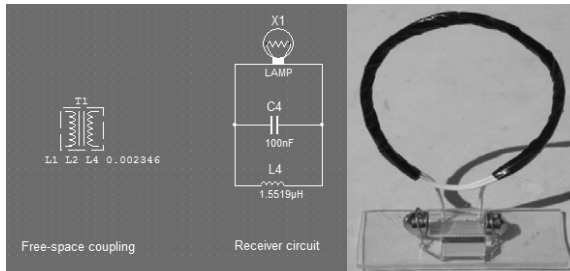


Fig.2.28. (a) The receiving element with a coupled-mode, (b) an example receiver.

Using a suitably constructed receiver, illustrated in Fig.2.28b, a simulation of the circuit is conducted. The driving function of the circuit in the simulation will be a pulse. Hertz proposes that a “ringer” is required to start the oscillator [52]. A pulse current  $I_{pulse}$  will be used in substitution of V1, shown in Fig.2.29. This is similar to the use of a spark-gap. One of the amplifiers must be shorted while power is applied in order to ring the resonator strongly enough for oscillations to be sustained. A momentary short is placed between the gate and the drain of Q1. The oscillator is self-sufficient requiring only phase offset amplifiers to sustain the oscillations through the cycles thereafter. This is an ideal representation of a kick-start because when the pulse current is adding energy, it forms a closed circuit. To simulate a momentary burst of energy to the oscillator, the settings of the pulse current are listed in Table 2.3.

Table 2.3. Simulation circuit properties.

TABLE 2.3 SIMULATION CIRCUIT PROPERTIES	
Property	Value
Initial value	0
Pulsed value (mA)	100
Time delay (ms)	10
Rise time ( $\mu$ s)	10
Fall time ( $\mu$ s)	10
Pulse width (ms)	1
Period (s)	1

The broadcasting model these settings are applied to is shown in Fig.2.29.

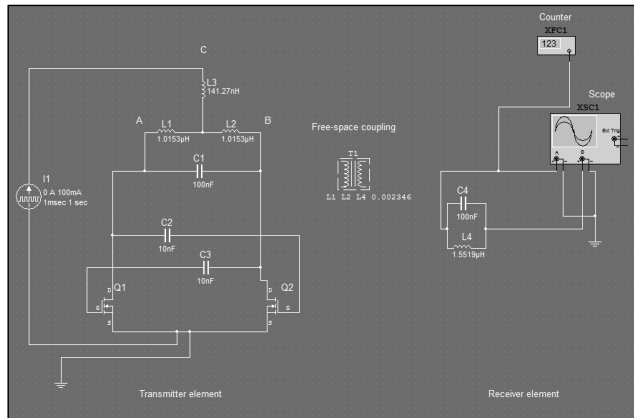


Fig.2.29. The broadcasting model for simulation.

The frequency counter reads 422 kHz; the signal at the oscilloscope, 2 volts per division on the  $y$ -scale, with a time base of  $200 \mu\text{s}$  per division on the  $x$ -scale is shown in Fig.2.30.

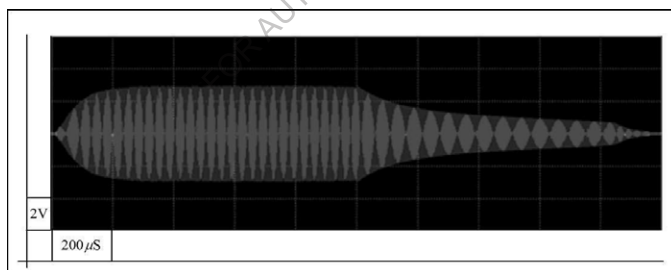


Fig.2.30. Simulated signal seen by the receiver.

The simulation refers to both the transmitter and receiver elements of the theoretical model first illustrated in Fig.2.1. As the simulation is taken in context to inductively-coupled elements based on circuital laws, the components consisting the broadcast model have the properties:

- Components L1, L2, L3, and C1 simulate the one resonator—the transmission antenna illustrated in detail in Fig.2.38; likewise, L4 and C2 simulate a second resonator, they are coupled across free-space at the calculated coupling coefficient from (45),
- Q1, Q2, C3, and C4 constitute the oscillator driven by voltage source V1,
- The system transmits energy given the theoretical predictions. Variation of the coupling coefficient  $\kappa_{ij}$  shows the various circuit responses, using the same  $x$  and  $y$ -scale divisions of Fig.2.30, shown in Note that in Fig.7.1, the  $x$  and  $y$ -scales for each waveform are  $200\mu\text{s}$  and 2 volts per division, respectively. (a)  $\kappa=0.002$ , (b)  $\kappa=0.004$ , (c)  $\kappa=0.008$ , (d)  $\kappa=0.010$ .
- in the Appendix.
- L3 contributes weakly to the inductance of the loop.

Component L3 is the positive connection to the amplifiers in the circuit, as shown in Fig.2.29. Since it is only a one-half turn on the loop, the inductance of L3 is much smaller than the inductance of the loop represented between components L1 and L2.

### 2.2.3 Equations of the circuit model

It is expected that a sinusoid is emitted from the transmission antenna with both a positive and negative group velocity outward along  $z$  from the loop surface lying in the  $x - y$  plane. Group velocity is defined as a group of amplitudes used to distinguish emanated waves in both positive and negative directions of  $z$ , projected by the antenna. If only one side is considered, then the efficiency is divided by the missing group waves at a complex velocity since it cannot be assumed that each photon is moving at a constant velocity throughout the projection. This assumption is because

the velocity is due to the magnitude of the force of acceleration on the electron in the conductor. The assumption is compatible with the consideration of the wave envelope, however, with a stochastic distribution of energies. Alignment of loop centers, or axial alignment, will yield the highest magnitude of energy transmitted in this arrangement. Performance in the circuit is ideal when node C is placed at the point one-half of the length of AB, referring to Fig.2.37. It would be interesting for future research if this wire placement differs in performance on the length. The cyclic quality,  $Q(t)$ , is relevant to describing the internal quality of the oscillator at any particular time  $t_0$  when,

$$Q(t) = \frac{\omega_0 L_e}{R_e} t_0. \quad (99)$$

(99) infers a complex set of amplitudes present across the field object. The effective quality factor  $Q_e$  along with the effective damping factor  $\zeta_e$  satisfies the traveling wave solution. These properties are based on the states of the oscillator for each instance of the antenna elements as,

$$\begin{aligned} & \sum_{m=1}^x Q_i, Q_j, Q_k, \dots, Q_m, \\ & \sum_{n=1}^x \zeta_i, \zeta_j, \zeta_k, \dots, \zeta_n, \end{aligned} \quad (100)$$

for each of the antenna elements  $i, j, k, \dots, n$ . The states describe behavior of the system when there are small changes in  $R_e$ , given (72), shown in Table 2.4.

Table 2.4. Oscillator state by  $Q$  and  $\zeta$ .

Oscillator state	$Q$	$\zeta$
underdamped	$Q_e > 0.5$	$\zeta_e < 1$
critically damped	$Q_e = 0.5$	$\zeta_e = 1$
overdamped	$Q_e < 0.5$	$\zeta_e > 1$

Depending on the values of the effective damping  $\zeta_e$  and the effective quality factor  $Q_e$  in both the antenna and the oscillator, the emitted waveform will be one of the three types. The meaning represented in the different states of oscillation is due to the displacement of a wave in space given its periodic motion. In order to satisfy periodicity, the oscillator must be elastic—in the sense of returning precisely to its original configuration after deformation: this requires a known position of equilibrium and a counter force which restores equilibrium. The oscillator must be able to produce a sustained single frequency on a source object with a tolerance small enough that an object designed to absorb the oscillations will do so if it has approximately the same parameters. The antenna will comprise the vibrator while the oscillator will provide synchronous amplitude.

In the traveling wave case for radiative energy emitted from the coupled antenna, the solution is given by the wave equation, transformed from (5) using (9),

$$\frac{\partial^2 u}{\partial x^2} + \frac{\partial^2 u}{\partial y^2} = \frac{1}{v^2} \frac{\partial^2 u}{\partial t^2}, \quad (101)$$

where  $v$  is the phase velocity. As the wave propagates in both the  $+z$  and  $-z$  directions—positive and negative group velocity—the description of

the transverse motion  $\frac{2\pi v}{\lambda} = 2\pi f = \omega$ , where  $v = f\lambda$  transforms the description to,

$$\begin{aligned}y(x,t) &= A \sin \frac{2\pi}{\lambda}(x - vt) \\v_y(x,t) &= \frac{dy}{dt} = \omega A \cos \frac{2\pi}{\lambda}(x - vt) \\a_y(x,t) &= \frac{d^2y}{dt^2} = -\omega^2 y = -\omega^2 A \sin \frac{2\pi}{\lambda}(x - vt).\end{aligned}\quad (102)$$

The following equivalent parametric forms of the wave solution of (102) are,

$$\begin{aligned}y(x,t) &= A \sin(kx - \omega t), \\y(x,t) &= A \sin \frac{2\pi}{\lambda}(x - vt), \\y(x,t) &= A \sin 2\pi \left( \frac{x}{\lambda} - \frac{t}{T} \right).\end{aligned}\quad (103)$$

The determination of the velocity,  $v$ , and its inhibition,  $\bar{v}$ , is dependent upon the properties of the medium in tandem with the coupled inductance which forms an approximation given the wave relationship. The parameters are shown in Table 2.5.

Table 2.5. Oscillator traveling wave parameters.

Coil	TABLE 2.5 OSCILLATOR TRAVELING WAVE PARAMETERS		
	$L_i$	$L_j$	$L_s$
Resonance frequency (Hz)	345607.761	404004.671	433203.126
Wavelength (m)	867.436	742.052	692.037
Quarter wavelength (m)	216.859	185.543	173.00925
Wave period ( $\mu s$ )	2.893	2.475	2.308
Wave number	0.0072	0.0085	0.0091
Quarter-wave velocity (m/s)	7.4948153e07	7.4960238e07	7.4948147e07

Particular to the wireless power case, discussed in greater detail in §2.2.4, the traveling wave emitted by the antenna is a function of the amplitude generated in the oscillator and confined to one plane in space and varying sinusoidally in both space and time is expressed in combinations of,

$$\begin{aligned} y &= A \sin(kx - \omega t), \\ y &= A \cos(kx - \omega t), \end{aligned} \quad (104)$$

and of the complex form,

$$y = Ae^{i(kx - \omega t)}. \quad (105)$$

As an Euler identity, the form takes,

$$e^{i\theta} = \cos \theta + i \sin \theta. \quad (106)$$

Alterations to the circuit would affect strong changes to its state. The transmission circuit is a series circuit and the addition of  $R_e$  would make  $Q_e$  smaller. The receiving circuit is arranged in parallel so that changes in  $R_e$  will make  $Q_e$  larger.

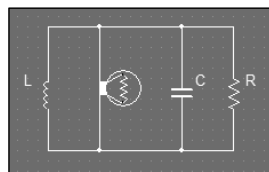


Fig.2.31. Simplified circuit diagram.

From these theoretical discussions, a circuit is constructed based on the schematic used in the simulation to a real model. The transmission circuit including the antenna discussed in §2.3.1, is shown in Fig.2.32. Measured with a frequency counter, the broadcasting frequency is  $f_0 = 428$  kHz. It is

expected that if the dipole could be preserved after each cycle, discussed in §4, that efficiency would increase as well as the potential at the boundary.

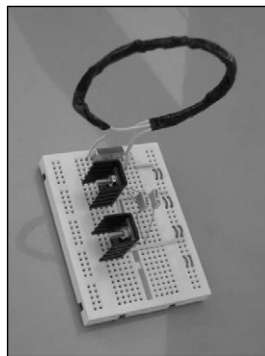


Fig.2.32. The constructed oscillator.

The next section addresses the details of the propagation model proposed in this section.

#### 2.2.4 The circuit model with acceleration

To review, the circuit illustrated in Fig.2.27 is a push-pull oscillator driven by n-MOSFET power transistors Q1 in  $\pi$  and Q2 in  $\pi$ , each part in  $2\pi$  applying force in quantities of voltage yielding a magnitude of acceleration to electrons relative to the current at an atomic structure on a conductor. In a dynamic context, the combination of the transmission antenna with its capacitor and the relationship between it and the n-MOSFET power transistors Q1, Q2, results in a synchronous oscillation between charges in the circuit and charges in the conductor. The pattern of this behavior is illustrated in Fig.2.33.

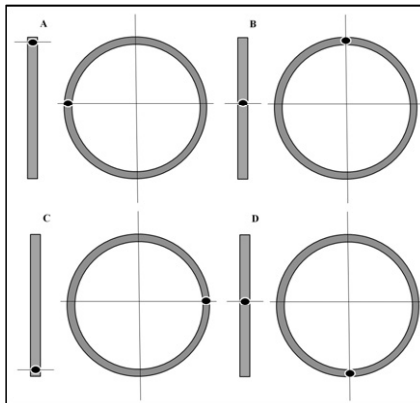


Fig.2.33. Representation of oscillator cycle circulating charges in the antenna conductor.

Each movement through the circle is marked at points  $\pi/2$ . At the start of the cycle, A of Fig.2.33, one transistor is responsible for the acceleration of charges moving them through  $\pi$ , B and C of Fig.2.33. For the end of the cycle, the other transistor accelerates the charges through the remainder of the loop, D and A, through  $\pi$ , returning the cycle to its starting point. The system of equations for this arrangement begins around the use of an inductor and capacitor placed in parallel relative to each other—a combination of inductive and capacitive discharge. Based on Kirchhoff's circuital laws, the relationship between these elements is,

$$-\frac{q}{C} - L \frac{di}{dt} = 0. \quad (107)$$

Representing the current,  $i$ , as  $i = dq/dt$ ,

$$L \frac{d^2q}{dt^2} + \frac{q}{C} = 0, \quad (108)$$

and the angular frequency,  $\omega$ , as  $\omega = \frac{1}{\sqrt{LC}}$ , (108) is transformed to,

$$\frac{d^2q}{dt^2} + \omega^2 q = 0, \quad (109)$$

which takes the form of the equation for a mass on a string,

$$m \frac{d^2x}{dt^2} + kx = 0. \quad (110)$$

In terms of a real circuit, the value of resistance, regardless of the size, is included as,

$$L \frac{dq^2}{dt^2} + R \frac{dq}{dt} + \frac{q}{C} = 0, \quad (111)$$

yields a second-order system,

$$\frac{d^2q}{dt^2} + 2\zeta\alpha_0 \frac{dq}{dt} + \alpha_0^2 q = 0, \quad (112)$$

where the force coefficient,  $F$ , is the sum of the amplitudes,

$$F = A_+ \cos(\omega t) + A_- \sin(\omega t), \quad (113)$$

governed by polynomials expressed by the oscillator,

$$2x^2 - 2x + 1, \quad 2x^2 + 2x + 1, \quad (114)$$

where the  $2x$  component is for the first cycle in  $\pi$  and  $-2x$  for the second cycle of  $\pi$ , illustrated in Fig.2.33. The force following from the sum of amplitudes of the under-damped system at the damping ratio of  $0 \leq \zeta < 1$  sustains oscillations to a transient solution,  $q_{ts}$ ,

$$q_{ts} = e^{-\zeta t} \left[ c_1 \cos(\sqrt{1-\zeta^2} \omega_0 t) + c_2 \sin(\sqrt{1-\zeta^2} \omega_0 t) \right], \quad (115)$$

which converges to a steady-state solution of the form,

$$q_s(t) = A e^{i(\omega t + \phi)}, \quad (116)$$

where its derivatives are

$$\begin{aligned} \frac{d^2 q_s}{dt^2} &= -\omega^2 A e^{i(\omega t + \phi)}, \\ \frac{dq_s}{dt} &= i\omega A e^{i(\omega t + \phi)}, \\ q_s &= A e^{i(\omega t + \phi)}. \end{aligned} \quad (117)$$

The amount of magnetic force, as a density of linked flux-lines, influences the density of the energy transported on the waveguide, in this case, of free-space. At the characteristic angular frequency,  $\omega_0$ , energy flows in both directions, e.g., from transmitter to receiver in the case of acceleration by transistors, and from receiver to transmitter in the case of reflection, while also subject to a projection,  $\bar{\mathbf{H}}$ , derived from Maxwell's vorticity and represented as a force, in the form of dynamic elasticity [117]. Following Larmor's conjecture, if the coordinates of the space where the equations are operating include potential energy, a material framework per unit volume is a force,

$$\begin{pmatrix} u \frac{dF}{dx} + v \frac{dG}{dx} + w \frac{dH}{dx}, \\ u \frac{dF}{dy} + v \frac{dG}{dy} + w \frac{dH}{dy}, \\ u \frac{dF}{dz} + v \frac{dG}{dz} + w \frac{dH}{dz} \end{pmatrix}, \quad (118)$$

and a couple,

$$(vH - wH, wF - uH, uG - vF), \quad (119)$$

from a rotational virtual displacement of the elements. In the case of the Ampère-Maxwell, there should simply be a force at right angles to the current,

$$(vc - wb, wa - uc, ub - va), \quad (120)$$

forming the special axes of coordinates,

$$\left\{ -w \left( \frac{dF}{dz} - \frac{dH}{dx} \right), w \left( \frac{dH}{dy} - \frac{dG}{dz} \right), 0 \right\}. \quad (121)$$

Larmor argues such a forcive differs from Ampère-Maxwell by

$$\begin{aligned} & \text{a force } \left( u \frac{dF}{dz}, v \frac{dG}{dz}, w \frac{dH}{dz} \right), \\ & \text{and a couple } (-wG, wF, 0), \end{aligned} \quad (122)$$

constrained to an equivalency of forces acting on the ends of each linear current element, equal at each end to  $(wF, wG, wH)$  per unit of cross-section, positive and the front and negative at the rear. Therefore, the internal stresses are homeostatic for each circuital current and do not disturb the resultant force on the conductor due to the presence of the field.

### 2.3 The propagation model

The propagation model consists of the transportation of energy across free-space by a pair of tuned circuits, symmetric and set a distance apart, when one of the circuits is electrically charged by electron acceleration. In

practice, this means an electric current will be induced in any distant circuit where the magnetic flux intersects with an appropriate conductor in the path of the oscillations. The placement of the resonant objects in the scheme will be in the path based on the projections of their antenna, coupled to their resonant circuits. The quarter-wavelength magnetic loop antenna is a useful device to transmit significant quantities of electrical current at reasonable efficiency. For brevity, this is a fundamental artifact of the scheme presented in this work. The complete range of behavior available is exclusively due to the interface between a set of electrical charges and an ambient structure of free-space at normal temperatures and pressures, for the purposes here of atmospheric air with characteristic impedance.

The mathematical components needed to describe the problem at hand are currents in the conductive media and currents in the dielectric. If the medium inside the waveguide is homogenous and isotropic and if the surface impedance at the boundary is zero, the method of separating variables obtains a set of normal, uncoupled modes of propagation. Any irregularity or discontinuity in the waveguide provides a coupling between some, or all, modes of propagation [23], transported on a transmission element whose radius is smaller than the dielectric space, whose waveguide is sufficiently infinite, to impose ideal planetary electrical characteristics.

A necessarily narrowband antenna with steep nulls is required to allow the power to transmit in the signal while rejecting spurious noise and other transient phenomena the magnetic fields could be subject to, including solar radiation. The quarter-wavelength magnetic loop antenna has very sharp nulls at right angles to the plane of the loop. These nulls can be very useful for suppressing radio interference. A rotation of the loop will reduce

noise. Because the nulls are sharp, small changes in antenna orientation can make a large change in signal or noise received from the direction of the nulls allowing the interference to bleed into the field. The nulls are sharpest on the smallest loops at a perimeter approximately  $0.05\lambda$  which linearly increases to  $0.1\lambda$  at the periphery [29].

The propagation model, for reasons stated in the previous sections, and in detail in §2.1, is concerned primarily with small antenna sizes with a high efficiency. In the proposed model, the loop size is the most critical property. If coil loop is wound at a specific ratio of circumference to wavelength, it is equivalent to conductor connected to an electrically-short transmission line with coupled modes [24, 30, 107]. To maximize the emission of radiation, the magnetic loop should be at a ratio of its circumference to its quarter wavelength. Such a magnetic loop will be shown to have the ideal ratio, in terms of maximum transmission efficiency, is when this ratio falls on an exponential scale, shown in (42). Consider a circuit consisting of a single loop of insulated wire wound in such a way as to create a circular loop of a few turns. This loop and its capacitor become one-half of a resonant circuit forming a transmitter  $T_x$ . The length of this wire loop,  $\ell_t$ , is then duplicated to construct a similar loop of identical characteristics,  $\ell_r$ , along with a capacitor forming the second half of a resonant circuit forming a receiver  $R_x$ .

A current applied to this circuit induces an electrical field in the self-inductance of loop  $\ell_t$ , creating a magnetic field which is coupled at the interface. By placing a load in parallel to the voltage gap in loop, magnetic energy is drawn into the gap and then converted into electrical current. Inclusive in the loop is a voltage gap of width  $w$  no greater than the loop

radius, so that  $w < r$ . The coil  $\ell_t$  is positioned in such a way that the  $x - y$  plane forms the loop surface and the  $z$ -axis the trajectory out from the loop in the directions of the group velocity of the radiation—positively for right-handed, negatively for left-handed. This relationship is illustrated in Fig.2.34. The chosen frequency computes (48) to be between 412 and 526 kHz.

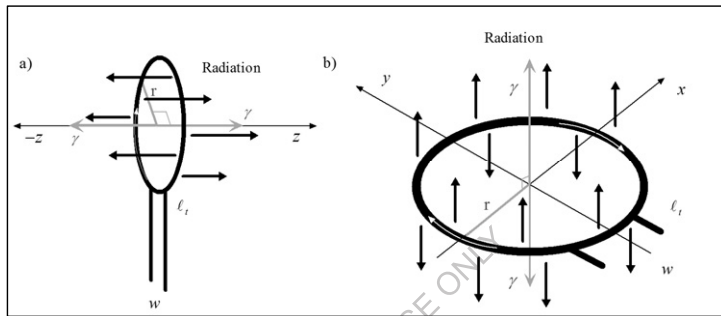


Fig.2.34. Radiation emissions of a magnetic loop antenna.

The antenna loop is excited by the acceleration of electrons on its curvature, driven by the current  $I_0$  from the amplifiers in the circuit. The positive group velocity emits radiation in the form  $H_0^+$ , the negative group velocity emits radiation in the form  $H_0^-$ , and  $\gamma_\theta$ , the quantized energy due exclusively to photons, illustrated in Fig.2.35.

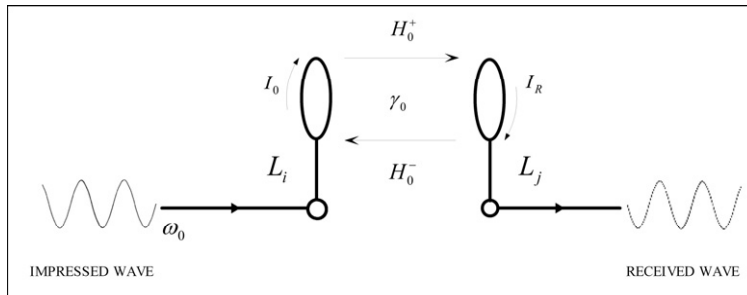


Fig.2.35. Wave propagation for the modal coupling scheme of wireless power transfer.

An assumption of symmetry will reveal the model of magnetic waves, or currents, in the form of photons of a given angular frequency  $\omega_0$  flow positively at a given coordinate  $(\gamma_\theta, H_0^+)$  from coils  $\ell_i \rightarrow \ell_r$  and negatively at  $(-\gamma_\theta, H_0^-)$  from coils  $\ell_r \leftarrow \ell_i$  with an efficiency  $\eta$ . From the circuital point of view, antennas appear as a resistance,  $R_r$ , called radiation resistance. It is not related to any resistance in the antenna itself, rather, a resistance coupled from space to the antenna terminals. Active radiation raises the ambient temperature of  $R_r$ . This temperature is equivalent across the circuit because the temperature of the distant antenna (respectively from the transmitter) can only see its symmetric analogue due to the nature of inductive coupling in that the photons extant in the magnetic field only react with like or other resonant objects [30, 57]. Under such conditions  $R_r$  is quantified by the region of space inside the loop as a function of the virtual transmission line linking the antenna to the distant region, shown in Fig.2.36.

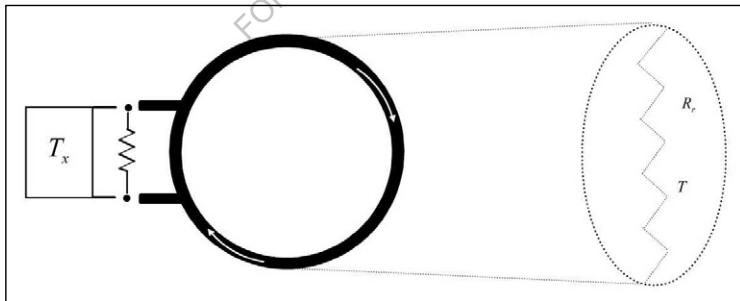


Fig.2.36. Schematic representation of a virtual transmission line of an antenna to a region of space.

The loop will operate using a single-band transmission with regard to the antenna impedance, directivity, and gain. The antenna analysis is essentially equivalent to that for a curved dipole and projected magnetic

field given (22). The computation of the antenna will target electrically small loop antennas in the normal and axial mode of operation. Radial mode is an advanced topic. Multiple modes are exhibited in §2.4. Following the discussion of the circuit properties in §2.2, and the schematic shown in Fig.2.27, the transmission antenna coil must be designed to conform to the shifting phase of the amplifiers. Following Larmor's theorem, discussed in §1.1 and §2.1.2, it is ideal if an electrical force can be applied to a conductor in such a way as to accelerate electrons between one half of the conductor and the other, similar to a wire treated as a dipole. The movement is treated as the phase. Phase is defined as representing movement along the arc of the antenna through divisions  $2\pi$  through the circle's circumference where the radius  $r$  is the magnitude of the electric field,  $E_\phi$  and  $v$ , a component of velocity of the shifting phase representing the velocity of the electrons. A schematic representation is shown in Fig.2.37.

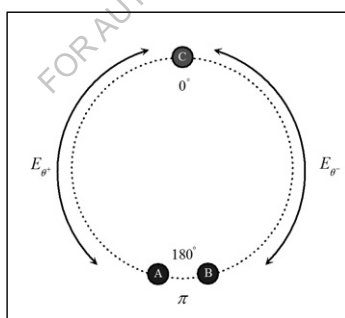


Fig.2.37. Angular motion of the oscillator transition phase.

The acceleration forces move through  $\pi$  on the loop, shifting direction between components L1 (A) and L3 (C), and L2 (B) and L3 (C) which are negative and positive voltages respectively. Theoretically, the force contained in the current accelerates the electrons through one phase of  $\pi$

then switches direction through the other phase of  $\pi$ . At each switch in direction, the electrons in the conductor decelerate and release their energy in the form of photons along the direction of the magnetic field, discussed in detail in §2.2.4.

The material of the coil should sustain the angular velocity of the currents,  $\omega_0$ , oscillating through integer multiples of  $\pi$ . Copper is sufficient while other materials could substantially alter the reactance. An insulated length of wire,  $\ell$ , given by A, B, is wound into a loop of a chosen specification. It has a break cut into its insulation at the midpoint in the loop, where  $C = \frac{1}{2}\ell$ , and a third wire follows the loop forming an extra number of turns,  $n = 0.5$ , and an extra standing length, or leg, illustrated in Fig.2.38.

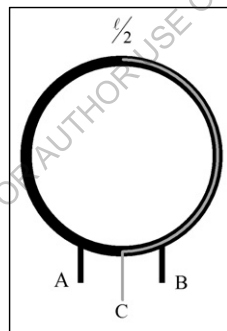


Fig.2.38. The transmitter coil.

The transmission antenna is now a three terminal coil, antenna (A, C, B) corresponds to (L1, L3, L2) respectively, with (L1, L3, L2) behaving as an oscillator when connected directly to an amplifier. Terminals A (L1) and B (L2) are connected across a capacitor to the corresponding drains of two n-MOSFETs whose sources are connected to the negative terminal of the power supply. Terminal C (L3) is connected to the positive terminal of the power supply.

A generalizable computation, the method of moments, will be fitted to solve the problem of the circular loop antenna as a function of the scattering of the field emitted by the transmitter. This general solution is solved using the software package *Matlab* and files from [58]. Properties of the loop antenna can then be put into the program *Circuit calculator* to render the theoretical values. The computational structures will be these scripts, their purpose is listed in Table 2.6.

Table 2.6. Computational elements from mesh to field solutions.

TABLE 2.6 COMPUTATIONAL ELEMENTS FROM MESH TO FIELD SOLUTIONS				
Problem class	Input	RWG-element file	Output	Purpose
Circuit	magneticLoopMesh.mat	rwg1.m	geoMesh.mat	Creates RWG edge elements.
	geoMesh.mat	rwg2.m	rwgGeoMesh.mat	Creates RWG edge elements.
	rwgGeoMesh.mat	rwg3.m	impedance.mat	Computes the impedance.
	rwgGeoMesh.mat	rwg4.m		Determines excitation voltage and solves MoM equations.
	impedance.mat		current.mat	
	rwgGeoMesh.mat	rwg5.m	Plot	Determines and visualizes surface currents.
Field	rwgGeoMesh.mat	efield1.m		Computes the radiated field on a ring with center $P$ .
	current.mat		Parameters	
	rwgGeoMesh.mat	efield2.m		Computes the radiated/scattered field.
	current.mat		gainPower.mat	
	sphere.mat			Displays the 2D radiation pattern in a polar plot.
	rwgGeoMesh.mat	efield3.m	Plot	
	current.mat			
	gainPower.mat			

Each of the element files were compiled against the mesh files created in each progressive step. The antenna was solved for and its properties computed. These theoretical results and comparison to the measured results will be discussed in the next sections.

### 2.3.1 The receiving antenna

A receiving antenna may be viewed as any metal object that scatters an incident electromagnetic field from a transmitting antenna which propagates a single-band signal. Because of scattering, an electric current appears on the antenna's surface. That current in turn creates a corresponding electric field. If a capacitor is attached to the free ends of the loop, as shown in Fig.2.39b, a voltage difference appears at the terminals.

The terminal voltage constitutes the received signal, power is extracted through the voltage and fed to an incandescent lamp, shown in Fig.2.28b. Analytically speaking, it is ideal if the scheme could be addressed as a surface current distribution over the antenna in terms of a three-dimensional oval surface using its edges as the propagation of the magnetic field expected in a Boltzmann distribution. The description here will be for a two-dimensional flat surface antenna.

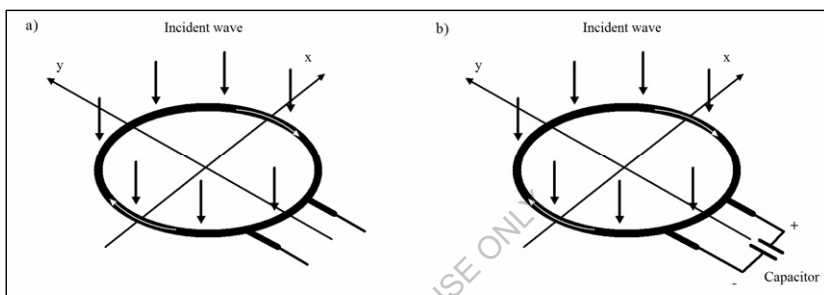


Fig.2.39. (a) Schematic of the receiving loop antenna. (b) Loop antenna connected to a capacitor at the voltage gap. The white arrows are surface currents.

Considering solely the viewpoint of energy transfer, an antenna in receiving mode collects electromagnetic energy over a specific area, shown in Fig.2.39a, extracts the captured power while both absorbing and reflecting the energy back into free-space, behaving like a signal repeater. The specifications of the coils, as illustrated in Fig.2.1, are shown in Table 2.7.

Table 2.7. Transmission and receiving coils physical specification.

TABLE 2.7 TRANSMISSION AND RECEIVING COILS PHYSICAL SPECIFICATION				
Coil	Coil radius (mm)	Wire radius (mm)	Wire length (mm)	Number of turns
$L_i$	30	0.4	650	3
$L_j$	30	0.4	650	3

The method of moments is solved for the antenna surface using Rao-Wilton-Glisson (RWG) edge elements [60]. A short discussion of the detail of the RWG algorithm is required to understand how the edge elements are used to approximate the field solution [65]. The surface of an insulated metal loop antenna divided into separate triangles as shown in Fig.2.40a. Each pair of triangles, having a common edge, constitutes a corresponding edge element, shown in Fig.2.40b. One of the triangles has a plus sign and the other a minus sign indicating the direction of the current. A vector basis function,

$$f(\mathbf{r}) = \begin{cases} \left( \frac{l}{2A^+} \right) \rho^+(\mathbf{r}), & \mathbf{r} \text{ in } T^+ \\ \left( \frac{l}{2A^-} \right) \rho^-(\mathbf{r}), & \mathbf{r} \text{ in } T^- \\ 0, & \text{otherwise,} \end{cases} \quad (123)$$

is assigned to each edge element where  $l$  is the edge length and  $A^\pm$  is the area of triangle  $T^\pm$ . Vector  $\rho^+$  connects the free vertex of the plus triangle to the observation point  $\mathbf{r}$ , shown in Fig.2.40b. Vector  $\rho^-$  connects the observation point to the free vertex of the minus triangle [59]. The vectorized surface electric current on the antenna surface, shown in Fig.2.40a, is a sum of the contributions over all edge elements with unknown coefficients. These coefficients are found from the moment equation (123). The surface current density on a surface  $S_\theta$  of a perfectly conducting structure is given by an expansion into RWG basis functions over  $m$  edge elements. The moment equations are a system of linear equations with the impedance  $\mathbf{Z}$ . The basis function of the edge element corresponds to a small but finite electric dipole of length  $d = |\mathbf{r}^{c-} - \mathbf{r}^{c+}|$

shown in Fig.2.40b and [20]. Fig.2.40c denotes the curvature at the center of triangle  $T^\pm$  for the division of a loop antenna structure into elementary electric dipoles, shown in Fig.2.40d.

The approximation here is similar approach to describe the currents according to Maxwell's equations [60] in terms of those specified at in §1.1. The current density,  $\mathbf{J}$ , and the antenna impedance  $\mathbf{Z}$  is represented on surface  $S_\theta$ . If  $S_\theta$  is open,  $\mathbf{J}$  is regarded as the vector sum of surface currents on opposite sides of  $S_\theta$ , as,

$$\mathbf{J} = \sum_{m=1}^M I_m \mathbf{f}_m, \mathbf{f}_m = \begin{cases} \left( \frac{l_m}{2A_m^+} \right) \rho_m^+(\mathbf{r}), & \mathbf{r} \text{ in } T^+ \\ \left( \frac{l}{2A_m^-} \right) \rho_m^-(\mathbf{r}), & \mathbf{r} \text{ in } T^- \\ 0, & \text{otherwise,} \end{cases} \quad (124)$$

where  $\mathbf{Z}$  expresses the vector voltage from expansion coefficients  $I_m$  forming the impedance moment  $\mathbf{Z} \cdot \mathbf{I} = \mathbf{V}$ . The antenna voltage is expressed by [59],

$$\mathbf{V}_m = I_m \left( \mathbf{E}_m^+ \cdot \frac{\rho_m^{c+}}{2} + \mathbf{E}_m^- \cdot \frac{\rho_m^{c-}}{2} \right), \mathbf{E}_m^\pm = \mathbf{E}^{inc}(\mathbf{r}_m^{c\pm}), m = 1, \dots, M, \quad (125)$$

where  $\mathbf{E}^{inc}$  is the electric field on an incident electromagnetic signal over the length,  $l_m$ , of the antenna. The voltage excitation vector is analogous to the circuit voltage. The surface electric current on the antenna surface is a sum of the contributions (124) over all edge elements.

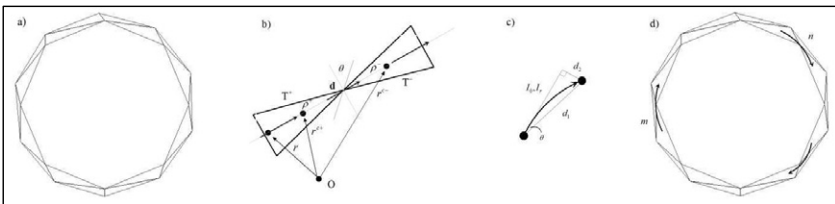


Fig.2.40. Modified schematic of RWG edge elements and dipole interpretation for curvature  $\theta$ .

The impedance  $\mathbf{Z}$  describes the interaction between neighboring elementary dipoles given over the length of the conductor. If edge elements  $m$  and  $n$  are dipoles, the element  $\mathbf{Z}_{mn}$  describes the contribution of dipole  $n$ , through the radiated field, to the electric current of dipole  $m$ . The size of  $\mathbf{Z}$  is equal to the number of edge elements. This contribution is calculated using the electrical field integral equation [61, 62].

The antenna was constructed and simulated using *Matlab* while theoretical equations were computed using the *Circuit calculator*. Using *Matlab* with the PDE toolbox, the surface mesh is designed by creating a model of the loop and creating RWG triangles. Visually, one can create the meshes based on a 2-D model approximation of a loop surface, shown in Fig.2.41a for 180 nodes and 288 triangles and Fig.2.41b for 648 nodes and 1152 triangles. A procedural description of how the simulation is generated is contained in Table 7.2.

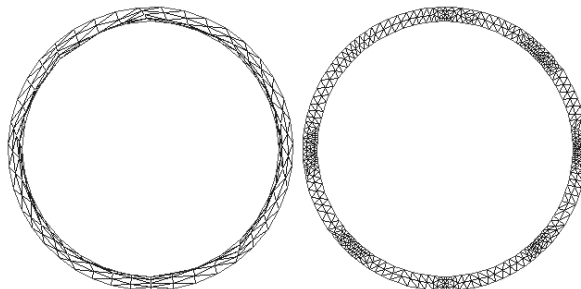


Fig.2.41. Two loop meshes: (a) 288 triangles and (b) 1152 triangles.

During the process of creating the mesh, checking the triangle quality will provide an average characteristic before continuing with the RWG analysis. The triangle quality of both meshes shown in Fig.2.42a while the expected current density, shown in Fig.2.42b, is confined to the inner edge of the loop. The RWG edge elements are more advantageous than the simple finite dipoles. In particular, they support a uniform axial electric current along a thin metal strip, approximating for curvature [63]. For help calculating in *Matlab* for the desired antenna characteristics from the constructed meshes, code from [64] will be used to perform the computations.

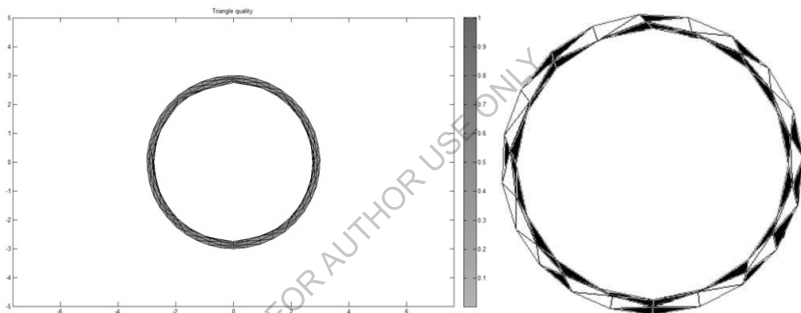


Fig.2.42. (a) Triangle quality of the loop mesh, (b) current density on the loop.

The .mat files containing the compiled mesh of the antenna structure are used as input to the edge generator `rwgl1.m` and to the rest of the code sequence listed in Table 2.6. The PDE tool is used created compiled mesh “magneticLoopMesh.mat” with 288 triangles.

Using the input characteristic antenna data:

- $412 \text{ kHz} \leq f_0 \leq 526 \text{ kHz}$ ,
- observation point: 50 centimeters on the  $z$ -axis,
- radiation sphere radius: 100 centimeters,

- feeding edge:  $[-1, 0, 0]$ , dipole,

resulted the sequence for output data is listed in Table 2.8.

Table 2.8. Matlab computed input characteristic antenna data.

Property	$L_i(ideal)$
Edges total	1656
Impedance ( $\Omega$ )	$0.000 + 0.493i$
Feed power (W)	$7.12e-11$
$I_0(A)$	1.25
$E_\theta$	$1.0e-05 *$ $-0.0007 + 0.0001i$ $0.1080 - 0.0239i$ 0
$H_\theta$	$1.0e-08 *$ 0 0
Poynting field $S_\theta$	$0.1039 - 0.2206i$ $1.0e-15 *$ 0.8249 0.0054 0
Stored energy (J)	$8.249e-12$
Total power (W)	$1.271e-10$
Gain (dBi)	2.4778
Radiation resistance	$6.1799e-11$

The computation of the model suggests that the structure of the radiation is exclusively a property of the geometry of the coil. A specific pattern of radiation emission is observable by showing intensity of projection field  $\bar{H}$ , out from the dipole at the center of the loop, shown in Fig.2.43.

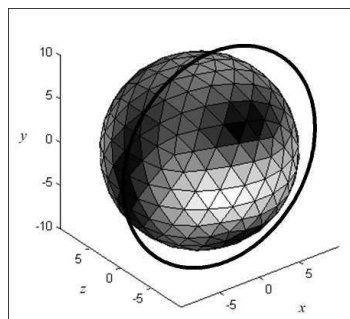


Fig.2.43. Directional power density of field on its approaching wave front, white shows higher intensity.

By examination of Fig.2.43, the field emanating from the loop antenna, the whiter toward the center of the loop is the plane of projection, relative to the loop around the sphere. The power signature is due to the dipole releasing energy and the forces upon the electrons in the conductor. The height of displacement along the  $y$ -axis is its beam width. It is interesting to now describe the computations which determined the emitted power and radiation resistance of the field given the distance between the antenna based on [29].

### 2.3.2 Radiated power

In terms of the circuit model of the physical antenna, energy and power are computed using the C# program *Circuit calculator*. The voltage and current are related via the impedance of the loop. In the case of electrically-small loops, impedance is the series combination at the angular frequency,  $\omega_0$ , of the reactance of the external inductance,  $L_e$ , and radiation resistance  $R_r$ , and ohmic resistance,  $R_o$ , of the conductor,

$$Z_0 = R_o + R_r + j\omega_0(L_e + L_i), \quad (126)$$

and terms operating on the loop have the forms,

$$\begin{aligned} I(z) &= I_0 \cos\left(\frac{\pi z}{\ell}\right), \\ V(z) &= -jZ_0 I_0 \sin\left(\frac{\pi z}{\ell}\right), \end{aligned} \quad (127)$$

where  $I_0$  is the current in the short-circuit at  $z=0$  and  $\ell$  is the length of the attractive transmission path. The average stored magnetic energy in the loop in its single mode at resonance is

$$\begin{aligned}
\langle W_m \rangle_{\omega_0} &= \frac{1}{4} \int_0^L L |I_z|^2 dz \\
&= \frac{1}{4} L |I_0|^2 \int_0^L \cos^2 \left( \frac{\pi z}{\ell} \right) dz \\
&= \frac{1}{8} L \ell |I_0|^2.
\end{aligned} \tag{128}$$

The average stored electrical energy does not need to be calculated separately since the system is at resonance,  $\langle W_e \rangle_{\omega_0} = \langle W_m \rangle_{\omega_0}$ , so,

$$\begin{aligned}
\langle W_{total} \rangle_{\omega_0} &= \langle W_e + W_m \rangle_{\omega_0} \\
&= \langle 2W_m \rangle_{\omega_0} = \frac{1}{4} L \ell |I_0|^2.
\end{aligned} \tag{129}$$

One interpretation to be drawn from the mathematics is that energy can be applied to the system to the point as the waveguide can sustain, a verification of the theory discussed earlier. This reveals the contention that the potential of free-space is expected to be very large given the radius of the coils. This is a very important feature which can be explored by this methodology.

The dissipated power, while a property of the load present, is also a property of the power sustained in the magnetic field. A resonant object will allow power to be seen at the receiver as,

$$\begin{aligned}
\langle p_d \rangle &= \frac{1}{2} R |I(z)|^2 + \frac{1}{2} G |V(z)|^2 \\
&= \frac{1}{2} R |I_0|^2 \int_0^L \cos^2 \left( \frac{\pi z}{\ell} \right) dz \\
&\quad + \frac{1}{2} G |V_0|^2 \int_0^L \cos^2 \left( \frac{\pi z}{\ell} \right) dz.
\end{aligned} \tag{130}$$

Its impedance yields the stored energy at resonance within the transmitted wave. For a non-isotropic radiator if the emitted power is  $P_{rad}W$  at a distance  $d$  from the source, the magnitude of the Poynting vector, in power per unit area, is

$$P_t = \frac{P_{rad}}{4\pi d^2}. \quad (131)$$

The radiated power  $P_{rad}$  is replaced by  $P_t G_t$ , where  $P_t$  is the power delivered to the transmitter antenna by the amplifying switches in the circuit and  $G_t$  is the transmitter antenna gain. The electric field intensity, the result of active coupling, at the antenna interface is

$$E_\theta = \sqrt{Z_0 P_t}, \quad (132)$$

where  $Z_0$  is the impedance of free-space (37). At a relatively large distance from a non-isotropic radiator, the electric field intensity, or the simple magnitude of the disturbance, is

$$I_{E_\theta} = \sqrt{120\pi \cdot \frac{P_t G_t}{4\pi d^2}} = \frac{\sqrt{30 P_t G_t}}{d} \text{ V/m.} \quad (133)$$

If the electric field intensity and power at the receiving antenna are  $E_{rec}$  and  $P_{rec}$ , respectively, the maximum power able to perform work intercepted by the receiver is

$$P_r = \frac{\lambda^2}{4\pi} \cdot P_{rec}. \quad (134)$$

For a non-isotropic antenna of receiver power gain,  $G_r$ , and given (130), the received power is,

$$P_r = \frac{\lambda^2}{4\pi} \cdot P_{rec} G_r = \frac{\lambda^2}{4\pi} \cdot \frac{E_{rec}^2}{Z_0} \cdot G_r = \left( \frac{E_{rec}\lambda}{2\pi} \right)^2 \cdot \frac{G_r}{120}. \quad (135)$$

The average radiated power can be considered lost as far as the source oscillator is considered, therefore, the antenna behaves similar to a resistor as dissipating power from the source. The radiation resistance  $R_r$  is defined as an average quantity,

$$R_r = \frac{I_0^2}{2} \frac{1}{P}, \quad (136)$$

where  $I_0$  is the input current to the transmitter coil, see Fig.2.1 and Fig.2.35. This is implying that the Ampère unit here is representative of a force. Modifying (136), assuming a uniform current restricted to a Boltzmann distribution,

$$R_r = 20\pi^2 (ka)^4, \quad (137)$$

where  $ka = 2\pi a/\lambda$ . Solving for radiation resistance of the antenna,

$$R_r = \frac{I_0^2}{2} = 10\beta^4 A^2 I_0^2, \quad (138)$$

where  $I_0$  is the peak amplitude applied to the antenna terminals. The ratio of separation between the coils and the geometric mean of the transmitter and receiver coil radii  $r_{\bar{j}} = \sqrt{r_t r_j}$  will be the measure of this maximum gradient along the length away from the coil along the z-axis, illustrated in Fig.2.44.

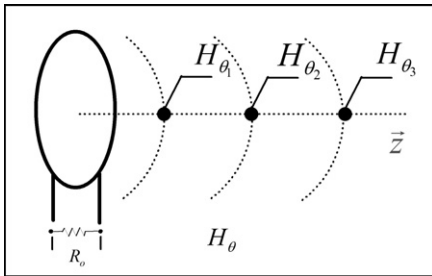


Fig.2.44. Projection of magnetic currents with highest potential coupling points  $H_\theta$ .

In the space containing the energy, the intensity of the magnetic field can be known in advance given the distance between the coils and the radius of the primary coil. In a multiple-turn Litz-wound coil of  $n$  turns with radius  $r_i$ , the magnetic field strength along  $z$  from the center of the coil along the axis can be written as [65],

$$H(z, r_i) = \frac{\mu_0 I \cdot n \cdot r_i^2}{2\sqrt{(r_i^2 + z^2)^3}}. \quad (139)$$

Differentiating with respect to  $r_i$  shows that for  $r_i = z\sqrt{2}$ ,  $H_\theta$  will be maximized [66]. The ratio implies a geometry of the emitted fields, to explore this, it is relevant to discuss mapping the field to determine where energy is stored in greatest quantities and in what forms. The ambience of the field emission, or flux, is described as a direct consequence of the circuit's electrical properties. It will be shown that for an antenna of a given loop ratio, the flux as well as the intensity are calculated to be maximum in terms of the exchange of energy between the transmitter and the receiver. As discussed in §2.1.2, the amount of power transmitted is closely related to the coupling between the loop coils. The potential

coupling, where  $\psi H_\theta = \psi H_\phi$ , shifts the further the distance away as a measure of coordinates along it.

### 2.3.3 Field emissions

Results from the simulation show the emission pattern is a function of the antenna geometry, as illustrated in Fig.2.45.

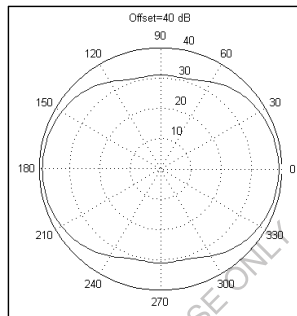


Fig.2.45. Average power-over-space antenna radiation pattern looking into the coil.

The result of the computational pattern agrees with what is expected, given [30], and illustrates that the pattern is a beam of a particular width. It is now relevant to create a set of experiments, given in the simulation resulting from the theoretical framework, where this beam pattern is confirmed and shown in what magnitude given a distance away from its source. There will be two areas of illustration and discussion:

1. At distances where distance is less than the radius of the coils,  
 $d < r$ , and,
2. at distances where the distance is greater than or equal to the  
radius of the coils,  $d \geq r$ .

It was postulated if the broadcast area of power transmission could be extended along the  $x - y$  plane. During research on the antenna consisting

of a coil loop in the form of a Litz winding, the question is: what if the Litz winding is “unwound” and lying flat on the plane? Would the power transmission be equally spread out? Tests of the emissions of the antenna was found to be of the same uniformity for that of a single Litz winding. This is not terrible surprising since [31] discusses in detail that the entire *length* of a conductor determines its self-inductance. So, if an antenna of a particular design is used to transmit power over a given area, one can replicate the antennas and overlap them in the manner of a daisy where their connections are chained together, else, unwrap a single loop and spread it out over the same area. Creativity in configurations aside, it is an interesting topic to perform a detailed map of the energy distribution in the field in terms of the forces over areas, discussed in §2.3.4 and §4.3.

### 2.3.4 Energy derived by forces over areas

The parameters of energy derived by forces via electron acceleration over a given area is described by Maxwell’s notion of vorticity, expressed at right angles to the magnetic field,  $\mathbf{B}$ .

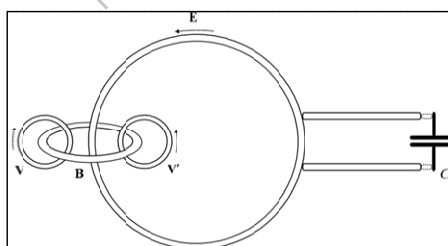


Fig.2.46. Maxwell’s vortices at the interface of a loop.

The circulation of energy through the rings, illustrated in Fig.2.46, expressed for the energy in the field,  $U_\phi$ , in terms of vortex filaments,

$$U_\phi = \frac{1}{2} \sum \iint \sigma_1 \sigma_2 r^{-1} \cos \varepsilon ds_1 ds_2, \quad (140)$$

is a potential distribution of energy of all filaments since they are constrained by an identical forcive. Thus, when using the coordinate system in (118) and ignoring internal stress of any kinetic components, the distribution holds since the electric velocity is not generalized, particular to the forcive at the aperture over the area of the antenna. It is therefore possible to calculate the energy contained in the field using a complete elliptic integral at the aperture, if it is considered continuous and statistically complete in the local neighborhood. It is of the first kind,

$$K(m) = \int_0^{\pi/2} \frac{dt}{\sqrt{1 - m \sin^2(t)}}, \quad (141)$$

where  $m = m - m_1$  using the approximation  $P(x) - \log x Q(x)$ , and  $K(0) = \pi/2$  for the first rotational velocity, illustrated in Fig.2.33, and of the second kind,

$$E(m) = \int_0^{\pi/2} \sqrt{1 - m \sin^2(t)} dt \quad (142)$$

using the approximation  $P(x) - x \log x Q(x)$ . Displacement of the field in directions away from the aperture yield the virtual waveguide in terms of forces. The strength between these forces, expressed as resonant linking, referring to Fig.2.19 and determined by classical methods [9, 21, 24, 26, 45, 52, 66], yields a simple relationship of a coupling coefficient  $\kappa_{ij}$  between magnetically-resonant coils from (45).

Therefore, the energy present in a given circular loop can be spread out over a larger area with the same broadcast power present. The caveat is that a receiving antenna, in order to consume the entirety of the potential at the interface, must be not only of the same wire length, but also have a similar unfolded structure. If a Litz wound coil is brought to couple with an area antenna, it would still resonate since it has similar parameters, but would only absorb partially given its area, determined by the basic geometric formula  $A = \pi r^2$ . For more loops, the area would be an integer multiple including partial loops.

## 2.4 The circuit experiments

Five distinct sets of experiments were performed with the circuit and antenna model described throughout §2. These groups of experiments are:

1. Using a single transmitting and receiving coil,
2. using a single transmitting and receiving coil, using a conductive disc at the center of one or both coils, and,
3. using a pair of transmitting and receiving coils.

Of each of the experiments, different sets of properties are manipulated to shape an understanding of the behavior of the arrangement, given the theoretical implications in the model.

### 2.4.1 Measured power at a distance with a single loop transmitter and receiver

The first experiment was to test the theoretical framework, the simulation, and circuit model, shown in Fig.2.1. Some assumptions are the use of off-the-shelf rubber-insulated copper wire of fairly high quality to apply as much optimization as possible. If optimization is kept in mind during

experimentation, it is but a linear increase of power transmission with more deliberately made materials, such a niobium-tin, a topic of future research. A diagram of the circuit is shown in Fig.2.47.

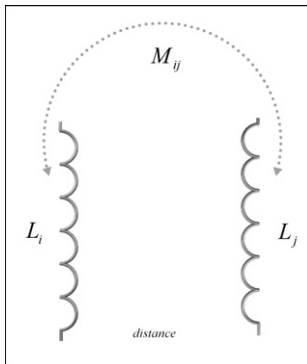


Fig.2.47. Diagram of the circuit for a single coupled-mode.

Using the coil specification listed in Table 2.7, with single transmitting and receiving Litz wire antennas including legs, shown in Fig.2.38 and Fig.2.39, of number— $i = 3$  and  $j = 2$ —of two centimeters of the total inductances  $L_i, L_j$ , at a transmission distance varied between contact and six centimeters, experiments were conducted to test the properties of the coils and energy transfer given the theoretical framework. The calculated specification is listed in Table 2.9.

Table 2.9. Experimental coils calculated electrical specification I.

EXPERIMENTAL COILS CALCULATED ELECTRICAL SPECIFICATION I				
Coil	Wire radius (mm)	Inductance ( $\mu\text{H}$ )	Mutual Inductance ( $\mu\text{H}$ )	Coupling coefficient ( $\kappa_{ij}$ )
$L_i$	0.4	1.547	0.02489	0.0162
$L_j$	0.4	1.529	0.02489	0.0174

Capacitance  $C_i, C_j$  is set to as equal as possible, at a value of 100 nF. With an input at the oscillator of 4.5 volts and 1500 mA from an external dc supply, power measurements were taken by measuring the voltage and

current present at the receiver at steps between close-proximity of the coils and distances to six centimeters. The results of power measurements at a distance are shown in Fig.2.48.

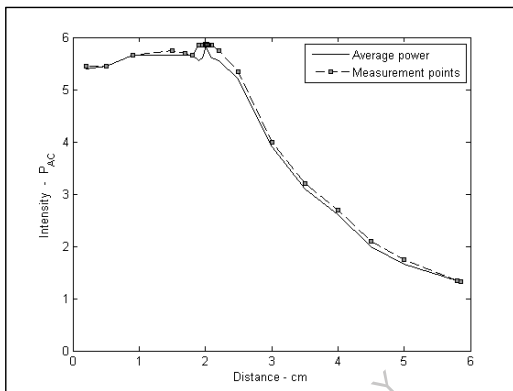


Fig.2.48. Power over distance showing the projection field  $\bar{\mathbf{H}}$ , where  $C_i \approx C_j$ .

It is apparent there is an area, as described in the theory, of a projection where the energy is nearly constant across the increasing distance. At the end of the projection, which contains a peak value, transmission power over distance falls off linearly, as,  $1/r^2$ . The pattern is present when the capacitor value used with the transmitter coil is nearly equal,  $C_i \approx C_j$ . It is expected that the projection would be less intense the more each half of the circuit drifts away from resonance with the other.

A second set of experiments were conducted to test the power over a distance of 100 centimeters. The results of power measurements at a longer distance are shown in Fig.2.49.

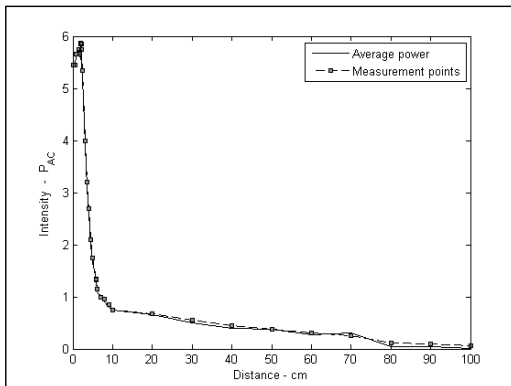


Fig.2.49. Power transmission over a longer distance.

The behavior illustrated in Fig.2.49 is, while after the projection there is a falloff of  $\frac{1}{r^2}$ , near to the point of distance of ten centimeters, falloff transitions to a rate of  $\frac{1}{r}$  and is continuous until the noise floor of the environment. A suggestion for future research is to obtain a more exacting set of data could be obtained by using a spectrum analyzer with an attenuator to prevent overloading at distances less than six centimeters.

A third set of experiments were conducted using a thicker wire to see if performance could be improved. It is expected that a higher amount of power would be observed at each measurement point from the previous set of experiments. The coil properties are listed in Table 2.10.

Table 2.10. Experimental coils calculated electrical specification II.

Coil	EXPERIMENTAL COILS CALCULATED ELECTRICAL SPECIFICATION II			
	Wire radius (mm)	Inductance ( $\mu\text{H}$ )	Mutual Inductance ( $\mu\text{H}$ )	Coupling coefficient ( $\kappa_{ij}$ )
$L_i$	0.5	1.469	0.02489	0.0170
$L_j$	0.5	1.451	0.02489	0.0181

It was observed during experiments that the coupling coefficient increases with a thicker wire, while the mutual inductance between the coils stays the

same. Two conditions were applied to the experiment: one where the capacitor at the transmitter and receiver are equal, and one where the capacitors are not equal. The results of power measurements of a thicker wire at a distance are shown in Fig.2.50.

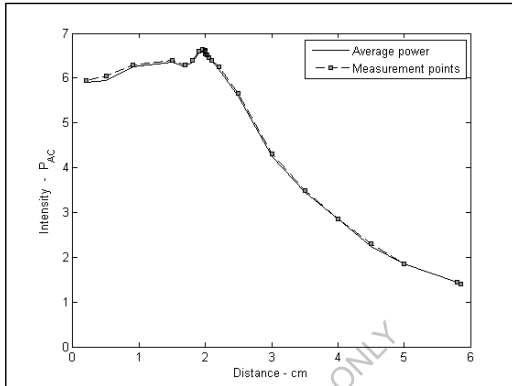


Fig.2.50. The power over distance using a thicker antenna wire.

It is confirmed that the assumption of more power transmitted per quotient of distance increases. It is also noted that the power seems, for lack of a more precise word, “smoother” using the thicker piece of wire. There is a property of conductor thickness given electron acceleration at the antenna which is an interesting point to study in future research. It is expected a similar behavior, expect a greater level of power delivery in the same manner as Fig.2.50 will manifest over the length of 100 centimeters as in the previous set of experiments.

A fourth set of experiments were conducted changing the value of the capacitor between the transmitter and the receiver, component C1 of Fig.2.27 and C4 Fig.2.28 respectively. In the previous set of experiments, the value of capacitors was set to be as equal as possible, given the limitations of the components and the laboratory measurement equipment

with differences no greater than 50 pF. In this set of experiments, the value of the capacitance at the receiver was reduced incrementally to zero, or no capacitor present. The result of measurements over the distance is shown in Fig.2.51. Between the cases when  $C_i \approx C_j$  and  $C_i > C_j$ , a contrastingly different behavior is observed. It is hypothesized that the reason for this behavior is the synchronous nature of the inductance and capacitance discharges are more strongly present in the  $C_i \approx C_j$  case. From data in the experiments, it is expected that the projection,  $\bar{H}$ , is more intense the more narrow the drift in circuit resonance between the two halves. The amount of received power is due more strongly to the inductive component than the capacitive component, in this model given credence by lamp intensity even if no capacitor is used at the receiver.

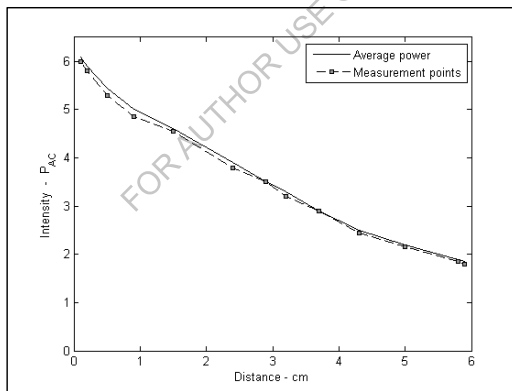


Fig.2.51. The power intensity over distance showing linear falloff, where  $C_i > C_j$ .

A fifth set of experiments were conducted when  $C_i \approx C_j$  using a non-uniform Litz loop winding. At the measurement points given in the previous experiments, energy is still transmitted, although with a far less intensity, calculated to be at about 22% of either set of experiments using the different wire thicknesses. The projection field,  $\bar{H}$ , is also present. It is

noted that the energy reception is tied more directly to the total wire length of the receiving antenna than that of the geometry of the loop. In the case when  $C_i \approx C_j$ , the energy contained in the projection,  $\bar{\mathbf{H}}$ , as well as the area of the transmission where falloff is at a rate of  $1/r^2$ , is due to the incident  $\bar{E}_1$  and reflected  $\bar{E}'_1$  waves, as,

$$\bar{E}_1 e^{j(\omega t - k_0 z)}, \bar{E}'_1 e^{j(\omega t + k_0 z)}, \quad (143)$$

where  $k_0$  is the vacuum wave number. The calculated value is shown in Table 2.5. There are points in the field where there is constructive and destructive interference in the beam inferring a polarization in the plane-waves. These fields are transverse and only the tangential components exist at the boundary plane where  $z=0$ . (143) represents the electric field present at the incident and reflected waves constructive interference. The determination of the strength of the electric field at the coil winding is dependent upon the current at the Litz winding,

$$I_{E_\theta} = I_0 \sin \frac{\sin^2(\beta)}{\beta^2} \frac{\sin^2(n\partial)}{\sin^2(\partial)}, \quad (144)$$

where,

$$\beta_{E_\theta} = \frac{\pi \sin \theta}{\lambda}, \quad \partial = \frac{\pi d \sin \theta}{\theta}. \quad (145)$$

The quantity  $I_{E_\theta}$  is the electric field intensity on the wire,  $d$  is the diameter, and  $\theta$  is the index of refraction. The profile of the antenna and the pattern of the transmission energy are illustrated in Fig.2.52.

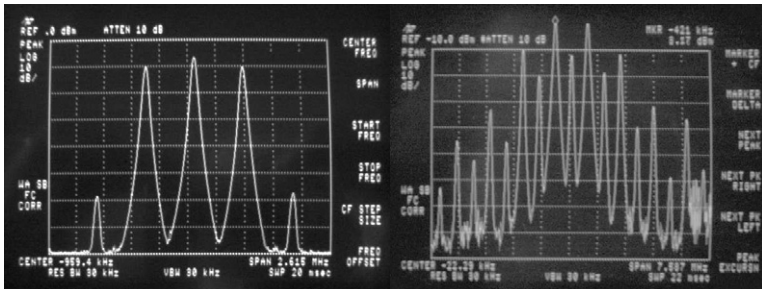


Fig.2.52. Radiation pattern observed at the receiver.

The plot to the left of Fig.2.52 shows the radiation pattern observed from the receiver. The plot to the right of Fig.2.52 shows a higher resolution bandwidth. Following the theoretical discussion of the expected beaming pattern in §2.3.3, the radiation pattern of Fig.2.52 is observed where  $r$ , proportional to the field intensity, is approaching maximum at a distance from the transmitter. The pattern has its main-lobe maximum in the  $z$  direction ( $\theta=0$ ) with minor lobes to the left and the right in other directions. Between the lobes are nulls in the directions of zero or minimum radiation.

The radiation pattern with respect to the field intensity and polarization requires three features: the  $\theta$  component of the electric field  $E_\theta(\theta,\phi)(V\ m^{-1})$ , the  $\phi$  component of the electric field  $E_\phi(\theta,\phi)(V\ m^{-1})$ , and the phases of these fields as functions of the angles  $\theta$  and  $\phi$  or  $\delta_\theta(\theta,\phi)$  and  $\delta_\phi(\theta,\phi)$ . Dividing a field component by its maximum value will reveal a normalized field pattern, a dimensionless number with a maximum value of unity. The normalized field pattern for the  $\theta$  component of the electric field is

$$E_\theta(\theta, \phi)_N = \frac{E_\theta(\theta, \phi)}{E_\theta(\theta, \phi)_{\max}}. \quad (146)$$

At distances relative to the size of the antenna and small compared to the wavelength, the field pattern is expressed in terms of power per unit area, or the Poynting vector  $S(\theta, \phi)$ . Normalizing the power with respect to its maximum value, as in the electric field example, yields a normalized power pattern as a function of angle, which is a dimensionless number, with a maximum value of unity. The normalized power pattern is,

$$P_n(\theta, \phi) = \frac{S(\theta, \phi)}{S(\theta, \phi)_{\max}}, \quad (147)$$

where  $S(\theta, \phi)$ , the Poynting vector, equals

$$\frac{E_\theta^2(\theta, \phi) + E_\phi^2(\theta, \phi)}{Z_0} \text{ W m}^{-2}, \quad (148)$$

expressed in rectangular coordinates on a decibel scale,

$$\text{dB} = 10 \log_{10} P_n(\theta, \phi), \quad (149)$$

shown in Fig.2.52. The efficiency of the transmitted power in the primary mode is given by the ratio of its total beam area,  $\Omega_A$ , consisting of the main-lobe area,  $\Omega_M$ , plus the minor-lobe area  $\Omega_m$ . The ratio of the main beam area is the beam efficiency,

$$\eta_M = \frac{\Omega_M}{\Omega_A}, \quad (150)$$

while the ratio of the minor-lobe area to the total beam area is the stray factor,

$$\xi_M = \frac{\Omega_m}{\Omega_A}, \quad (151)$$

with a total efficiency of,

$$\eta_M + \xi_M = 1. \quad (152)$$

In experiments conducted in this section, this value is shown to be 0.768. The calculated values of the radiated power characteristics for the antenna are listed in Table 2.11. These were calculated in the *Circuit calculator* software.

Table 2.11. Calculated antenna characteristics based on [29].

Property	TABLE 2.11 CALCULATED ANTENNA CHARACTERISTICS BASED ON [30]	
		$L_i(\text{lossy})$
$I_0(\text{A})$		1.25
$E_0(\text{A/m})$		1.572e-04
$H_0(\text{T})$		4.170e-07
Poynting field		8.249e-16
Directivity (dBi)		1.76
Gain (dBi)		2.10
Radiation resistance ( $\Omega$ )		1.1396e-11
Radiation efficiency factor		2.62e-10
Depth of penetration (m)		1.22e07

The operational circuit including the antenna powering a lamp a distance is shown in Fig.2.53. The field shows a continuous flow of energy from transmitter to receiver on spatial and temporal vectors. Conception of the energy in the field was a combination of the current at the surface of the antenna and the density of propagated energy across free-space. Directional finding [67] is possible in the scheme but was not explored in depth. Information transfer, although not directly examined is also possible by means of the same circuitry, given the sinusoidal nature of the power

transmission. Additions to the amplifier circuit would however be required where a modulation signal is introduced to the carrier. Modifications to the receiver would however also be required. For simplicity, the wave is understood as a characteristic of its potential power, given the circuital characteristics already discussed.



Fig.2.53. Prototypical wireless-power oscillator demonstrating the theoretical model.

The radiation pattern as a function of the field emission is observable directly as a property of geometry, and match the simulated pattern shown in Fig.2.45. Organic material does not destructively interfere with the transmission. A suggestion for future research is to use metal plates to create eddy currents induced by a changing magnetic field to leverage the signal to a human connection, such as the coupling of the nervous system to an external computer via magnetic coupling including modulation as an information carrier.

This section discussed a single loop power-scenario exclusively, primary coil to primary coil coupling of a single mode. Introduction of methods to enhance the magnetic field culminating at the center of the loop, following observations from experiments, are proposed in the next section.

## **2.4.2 Measured power at a distance with an enhanced magnetic field at the potential**

This section proposes a method to enhance the magnetic fields in an inductive-coupled, resonant-link model which realizes an improvement in power received at a distance.

The theoretical description of the improvement utilizes a single mode of propagation [24], an isotropic waveguide transformed anisotropically by the motion of a magnetic field between a transmitting and receiving element, which results from an acceleration force present in the electric field at the source. Isotropy in this case implies that changes to the magnetic field are present equally in both the  $x-y$  and  $z$  planes. The working definition of radiation emitted in a locally-approximated isotropic waveguide is an exchange of discretized energy whose velocity is attenuated by a characteristic resistive quality of displacement in the media. Such resistance is also due to the magnetic field density and coupling errors expressed by drift of the resonance frequency, or resonant-link, between the elements. The exchange of electromagnetic forces increases anisotropy and forms the waveguide into a shape with a particular curvature, yielding a state of equilibrium where currents are observed flowing from the transmitter to perform a quantity of work at the receiver.

A goal is to examine a technique of increasing the real-valued flux density and bind the curvature of propagating charges across a circuit consisting of two loops operating at a typified resonance frequency. It is proposed that if the flexion of curvature is reduced in the waveguide by the introduction of conducting discs, then the received power is increased over longer distances. The results reveal details of the theoretical framework underpinning the hypothesis that wireless energy transfer in coupled-modes

is also dependent upon the state and order of the magnetic field. Theoretical and experimental setup is shown in Fig.2.18.

Four sets of experiments were performed: a straight forward power transmission without discs, transmission with one disc in the transmitting loop, transmission with one disc in the receiving loop, and finally with one disc in both the transmitting and receiving loops simultaneously. The experiment consisted of a circuit of two loops driven to a frequency of 450 kHz at a power level of 4.5 volts and 1.1 amperes, similar to that from the experiments conducted in the previous sections.

In order to show the prediction of an increase in received energy due to the addition of a metal disc, a position is determined so that movements away demonstrate the reduction in electrical potential and power linearly as  $\frac{1}{r^2}$ , affecting the matrix by introducing a vector  $u$ . The relative difference between two loops with a radius of 3 cm, at a potential of 4.0 volts yields power measured using a spectrum analyzer of 11.26dBm at a calculated value of  $460\Omega$ , although it is anticipated that it could be a much higher load impedance [30], given its angular frequency  $\omega_0$ .

By moving the receiver away from the transmitter, so the less likely it is to intersect with the hyperbolic field, illustrated in Fig.2.17, given the curvature of the field established by coupling. The addition of the disc increases  $\mathbf{H}$ , or, reduces the curvature of the hyperbolic function where more field lines will intersect with it, shown in Fig.2.19. During the experiment, the electric field was measured by a probe and exhibited as a function of the loop antenna lying in the  $x - y$  plane and calculated in Joules. The magnetic field was measured by a Hall probe and exhibited as a function of its projection along the  $z$ -axis and calculated in Teslas with the

dominant azimuthal magnetic field—neglecting contributions of minor azimuthal fields—in Teslas at a pressure of one atmosphere and a temperature of 20C.

Table 2.12. Calculated quantities in the projected magnetic field.

Experiment	CALCULATED QUANTITIES IN THE PROJECTED-PROPAGATING MAGNETIC FIELD $\bar{\mathbf{H}} \cdot \delta\mathbf{B}_z$ .	
	E-field ( $\vec{x}, \vec{y}, J$ )	B-field ( $\vec{z}, T$ )
A: Loops sans disc	$(2.0 \cdot 10^{-6} + 0.02i, -2.77 \cdot 10^{-8} - 0.002i)$	$(5.0 \cdot 10^{-7} - 0.067i)$
B: Transmitter disc	$(1.62 \cdot 10^{-6} + 0.32i, -2.52 \cdot 10^{-6} - 0.3452i)$	$(2.0 \cdot 10^{-7} - 0.024i)$
C: Receiver disc	$(2.48 \cdot 10^{-6} + 0.02i, -3.21 \cdot 10^{-6} - 0.038i)$	$(8.76 \cdot 10^{-5} - 0.002i)$
D: Loops with discs	$(2.82 \cdot 10^{-6} + 0.02i, -3.45 \cdot 10^{-6} - 0.367i)$	$(7.48 \cdot 10^{-5} - 0.042i)$

Table 2.13. Calculated quantities in the projected magnetic field.

Experiment	CALCULATED QUANTITIES IN THE PROJECTED-PROPAGATING MAGNETIC FIELD $\bar{\mathbf{H}} \cdot \delta\mathbf{B}_z$ .	
	Dominant azimuthal B-field (T)	Impedance ( $\Omega$ )
A: Loops sans disc	$(1.62 \cdot 10^{-6} - 0.856i @ 45^\circ)$	$376 + 9.7165i$
B: Transmitter disc	$(3.2 \cdot 10^{-7} - 0.148i @ 62^\circ)$	$376 + 9.7165i$
C: Receiver disc	$(8.06 \cdot 10^{-6} - 0.856i @ 62^\circ)$	$376 + 9.7165i$
D: Loops with discs	$(9.895 \cdot 10^{-5} - 0.856i @ 87^\circ)$	$376 + 9.7165i$

Examination of the results contained in Tables 2.12 and 2.13 show that an increase in magnetic field yields an increase in quantized energy density. Lensing was not considered in the experiment, only how energy transformation was more efficient using the discs. A hypothesis for the increased efficiency is that a conversion of energy projected from the loop is taking place at a length closer to the receiver when it contains a disc. The incident waves, whose magnitude is nearer to where the power is being measured, are more efficiently converted into electric current. Given the geometric patterns of Fig.2.8 and Fig.2.17 of  $\mathbf{B}$  at the point where  $\delta\mathbf{B}$  makes a stronger contribution, field momentum is hyperbolic in its distribution on a circularly perfect antenna surface and the concentration of energy is confined to the area inside the loop along its transmission axes. Hence, it is more illustrative given the experimental setup, to calculate field decay over a distance following  $\bar{\mathbf{H}}$  as converging to a point at the center of

the receiver. Impedance is calculated given the power measured and that available to the spectrum analyzer—a range between 50 and  $600\Omega$ .

Table 2.14. Experimental quantities of the magnetic loop antenna.

Experiment	Distance (cm)	Potential (V)	Power (dBm)	Impedance ( $\Omega$ )
A: Loops sans disc	3.0	4.00	11.26	460
B: Transmitter disc	3.0	3.65	12.69	520
C: Receiver disc	3.0	4.45	16.06	260
D: Loops with discs	3.0	4.28	15.88	340

The results listed in Table 2.14 show equivalent values in terms of the equipment measuring the fields. The observation point was considered to be at the center of the loop, where the coordinate  $(0, 0, 0)$  was found. Any movements in the point of observation involved trajectories along the  $z$ -axis, although deflections in the  $x - y$  plane were also possible. In the case of the projection  $\bar{\mathbf{H}}$ , the magnetic field experiences minimum decay.

#### 2.4.3 The circuit experiment performed in human proximity

One scenario for the utilization of wireless power is a form where the circuit is attached to the human body. This method can transmit currents to subcutaneous implants, directly coupling to electrically-charged tissues such as neurons, and for powering miniature machines and components wirelessly connecting the human nervous system to a machine. Power delivery for biomedical implants is a major consideration in their design for both measurement and stimulation. When performed by a wireless technique, transmission efficiency is critically important not only because of the costs associated with any losses but also because of the nature of those losses, e.g. excessive heat can be uncomfortable for the individual involved. In this section a method and means of wireless power transmission suitable for biomedical implants is both discussed and

experimentally evaluated. The procedure initiated is comparable in size and simplicity to those methods already employed; however, some of Tesla's fundamental ideas have been incorporated in order to obtain a significant improvement in efficiency.

Implantable biomedical devices have, particularly in recent years, received much attention with regard to their application for a variety of uses involving both stimulation and monitoring. In direct contrast to wearable monitoring healthcare systems [68], one of the key issues for implanted devices is the satisfactory provision of power on an ongoing basis. For short term experimentation it is quite possible for sufficient transcutaneous power to be provided, a good example of this being in the three-month implantation testing of the Utah Array [69]. For long-term implantation however power needs can vary considerably [70, 71].

Implants such as the Utah Array have in fact been used for a variety of applications, including an alternative sensory input and neural control of prostheses as well as a new means of communication [72]. Transcutaneous power delivery for any long-term deployment will however always carry with it the chance of infection for the recipient as well as the possibility of mechanical leveraging. Clearly an onboard/on chip power pick up device that avoids transcutaneous power supply is an attractive alternative which will most likely result in more widespread use of the technology [73]. Some devices, which require several millamps of stimulating current, such as those used in the deep brain stimulating electrodes for the treatment of Parkinson Disease, need full battery implantation [74]. This technique then suffers from the requirement of periodic battery replacement. On the other hand, it is possible to consider energy harvesting within the body. This

approach is however still in its infancy and its practical usefulness is yet to be fully realized [75].

Wireless power delivery offers the advantages that it reduces the risks (particularly due to infection) associated with either battery replacement surgery or a transcutaneous supply. Inductive coupling can be employed for such power transfer, but the efficiency of transfer is sensitively-dependent upon coil dimensions and the distance between transmitter and receiver. Resultant efficiencies for biomedical implants are, as a result, generally very low [76], particularly so in a practical, working environment. The most attractive scheme is arguably therefore coupling between magnetically resonant objects [77].

While the idea of wireless power has been explored extensively in the literature with several competing power delivery techniques being considered, the most directly relevant are those in which power is not directed, but rather is absorbed [78, 79]. In essence, the required load or draw-down current is determined by the operational constraints and not by the beaming method employed. This feature allows magnetic currents to exist in a passive mode, i.e., the energy does not persist in the environment continuously but rather is tapped into on-demand. As a consequence of this, less energy is consumed to drive the circuits. What is made apparent here is the small size and relatively few components required in the method described as compared to the relatively large and efficient amount of power transmitted.

The transmission frequency selected for the system is 450 kHz, due primarily to the fact that no adverse biological effects have thus far been reported at this frequency [33]. Nevertheless, in the scheme of

magnetic resonance for power transmission, it has already been determined that the transmission does not interact with off-resonant objects [30]. Contrary to the purposes of other implementations [80, 81, 82, 83, 84], of specific interest here is to question whether a scheme could be accomplished using small coils of a few turns driven by a simple amplification circuit. The goal of this exercise is therefore to establish a driving circuit with a minimum amount of components, thereby reducing device complexity.

As a physical demonstration of the operating characteristics of the method described, a set requirement is to maintain a sufficiently high-powered signal reliably powering a lamp and motor. The reasoning being that if the technique can function well in terms of such external requirements, it will certainly perform adequately in the case of an implant specification. In this regard, it has not been the goal to deliver power at the sort of distances reported on in such as [81, 82] where efficiencies of 40%, rather by those appearing in earlier sections. The target, therefore, is transmission over relatively short distances of a few centimeters [85], with a high efficiency of transmission of over 75%.

An overriding aim is to overcome power supply issues, eminently apparent in the study of biomedical implants, by realizing a wireless scheme which is sufficiently powerful such that an implant can reliably receive its power remotely. Hence, direction of power transmission as well as the size of technology involved has been important in this study. The concept of wireless power transfer has been illustrated in the literature as a viable method to transport electrical current between distant points [23, 77, 85, 86, 87, 88]. The extension of this method herein maintains a significant amount of useful power transmitted at intensities of less than 15 volts in which,

across a volume of air, magnetic waves are exchanged between two or more coupled resonators.

Consider an extension of the circuit discussed in the previous sections, that multiple receivers can be fed from one common transmitter, thereby opening up the potential to power mobile platforms. A theoretical configuration of the circuit in such an implementation is a single fixed-position transmitter  $t$  delivering energy to distant receivers  $r$  and  $s$ . The receivers are grouped into two categories:

1. ac mode: lighting an incandescent lamp, and,
2. dc mode: turning a motor.

Either of the receivers  $r$  or  $s$  is a lamp or a motor which become synonymous and interchangeable where required. The experimentally-tested configuration of this method is illustrated in Fig.2.54 and Fig.2.55.

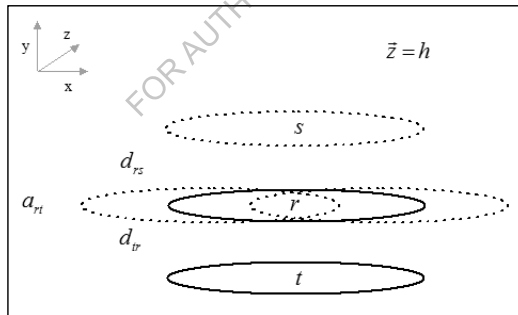


Fig.2.54. Experimentally-tested orientation of multiple receivers  $r$  and  $s$  with reference to each position at the transmitter  $t$  when there is no angle of rotation away from axial alignment  
 $a_{rt} = 0$ . The standing height of all coils are equal.

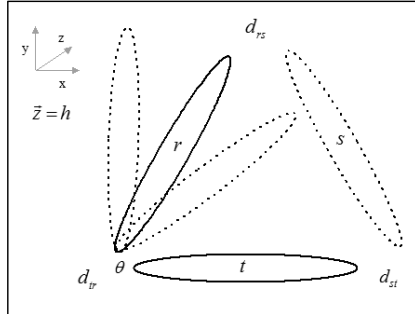


Fig.2.55. Experimentally tested orientation of multiple receivers  $r$  and  $s$ , through with an angle of rotation  $\theta$  away from axial alignment, with reference to each position at the transmitter  $t$ .  
The standing height of all coils is equal.

When using two or more receivers, the quality,  $Q_t, Q_r, Q_s$ , will be additive to the solution for each receiver from the perspective of the entire efficiency calculation. If interaction between the receivers is considered in the case of efficiency,  $\eta$ , modifying (69) then gives

$$\eta_{i,j,k,\dots,n} = \frac{(\kappa_{ij}^2 Q_i Q_j)(\kappa_{jk}^2 Q_j Q_k)(\kappa_{kl}^2 Q_k Q_l)}{\left[ (1 + \kappa_{ij}^2 Q_i Q_j)(1 + \kappa_{kl}^2 Q_k Q_l) + \kappa_{jk}^2 Q_j Q_k \right] \left[ 1 + \kappa_{jk}^2 Q_j Q_k + \kappa_{kl}^2 Q_k Q_l \right]}, \quad (153)$$

where it is desirable to consider the interaction of the magnetic fields each of the elements: transmitter, receiver one, receiver two, or more operating on each other. If the consideration is that the operation is limited to between transmitter and receiver one, receiver two exclusively and not interested in the coupling between each receiver but noticing the increase in  $\kappa$ , then the efficiency is given [44] by,

$$\eta_{i,j,k,\dots,n} = \frac{1}{\left[ 1 + \frac{1}{\kappa_{ij}^2} \left( \frac{1}{Q_i} + \frac{1}{R_i} \right) \left( \frac{1}{Q_j} + \frac{1}{R_j} \right) \left( \frac{1}{Q_k} + \frac{1}{R_k} \right) \right] \left[ \left( 1 + \frac{R_j}{Q_j} \right) \left( 1 + \frac{R_k}{Q_k} \right) \right]}, \quad (154)$$

where the loaded qualities,  $Q_i, Q_j$  are a property of the capacitances  $C_i, C_j$ , resistances  $R_i, R_j$ , and inductances  $L_i, L_j$  of the circuits containing the coils are defined in (72).

#### 2.4.3.1 Coupled-power delineation

The physical properties of the circuit constructed for the experiments in this section are shown in Table 2.7.

The experiment is designed to answer three questions:

1. What are suitable geometric positions for the coils in order to deliver power to sufficiently drive a ten-gram motor at six volts, with an operating torque of 3400 gram-centimeters?
2. What are suitable geometric positions in order to deliver power to sufficiently drive a twelve-watt incandescent lamp?
3. What is the consequence in terms of power availability and draw down of adding multiple receivers?

The quantities of measurement required are:

- Intensity by voltage present in the receiver, in the case of dc mode, from a minimum to maximum position,
- intensity by photometric intensity of a lamp, in the case of ac mode, from a minimum to maximum position.

Each receiver is constructed to test in one of two modes:

- ac mode, receiver  $r$  contains a capacitor and a lamp,
- dc mode, receiver  $s$  contains a capacitor, a full-wave rectifier bridge and a dc motor,

- with the insistence that each mode can be used separately or combined.

For one of the ac modes, a resistor is added in parallel to increase the  $Q$  value. For all dc modes, converting the radio-frequency signal to direct current is accomplished using germanium diodes as a bridge rectifier to ensure a minimum voltage drop. The behavior of the current at the receiver is contrastingly different between the ac and dc modes. The maximum effective transmission distance is seven centimeters in ac mode while in dc mode it is ten centimeters. The next section describes the operational freedom of the receivers utilizing the modes.

#### **2.4.3.2 ac mode**

Since this mode is the same as the one discussed in §2.1, §2.2, and §2.3, its performance illustrated in Fig.2.48, is the same. When using one ac mode, signal performance of a receiver  $r$  is maximum when its distance  $d_r$  from  $t$  is two centimeters and its axial difference  $a_r$  is no greater than three centimeters to the left or to the right of  $t$ , as illustrated in Fig.2.54. The maximum distance for the receiver when the lamp is absorbing enough power to remain lit is observed to be six centimeters.

When using two ac modes, meaning the use of two receivers in ac mode—essentially two lamps operating simultaneously, signal performance of one receiver  $r$ , while comparable to one ac mode, consumed power relevant to its proximity with  $t$ , as expected, but is attenuated by a distant receiver  $s$ . In experiments the maximum distance when the lamps were absorbing enough power to remain lit is observed to be six centimeters. However, by lining up  $r$  and  $s$  with minimum axial displacement, the currents constructively

interfere creating a solenoid-like structure. This method extends the range of useful induced current to ten centimeters.

When using one ac mode and rotating at an angle  $\theta$ , as illustrated in Fig.2.55, ideal signal performance of a receiver  $r$  is observed when  $\theta$  is between 40 and 90 degrees from  $t$ . In this range, the power falls off and remains steady until  $\theta = 90^\circ$ . At a distance  $d_r$ ,  $\theta = 60^\circ$ , the lamp is at peak brightness within 1.5 centimeters, movement along the axial length reduces the signal to its minimum at three centimeters. However, movement along the trajectory of  $\theta$  reduces the signal to a minimum at two centimeters. Exactly the same behavior is observed for receiver  $s$ . This observation suggests that the field object created in the free-space between the elements consists of a finite spatial geometry symmetric along its axial length. When using two ac modes and rotating at an angle  $\theta$ , signal performance of the receiver  $r$ , while comparable to one ac mode, it is found that for segments of its rotation through  $\theta$  energy is exchanged between the two receivers.

When introducing a third and fourth ac mode, e.g., adding a third and fourth receiver, the geometric positioning of the intensity of the magnetic field object remains constant and, relevant to the position of the other receivers, more energy is absorbed in the area of the projection,  $\bar{\mathbf{H}}$ .

#### 2.4.3.3 dc mode

When experimenting with one dc mode, using a germanium rectifier bridge, signal performance of a receiver  $r$  is maximum when the distance  $d_r$  is at its minimum proximity to  $t$  and the axial difference  $a_r$  is no greater than 1/3 of the radius to the left or to the right of  $t$ , as shown in Fig.2.54. Performance over distance is shown in Fig.2.56.

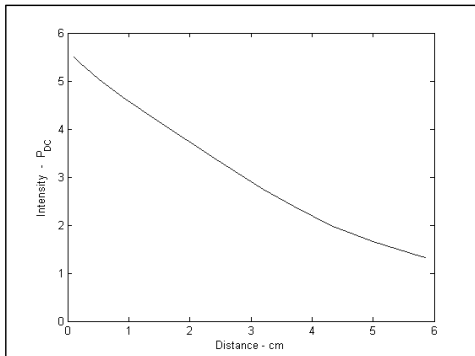


Fig.2.56. The dc power intensity seen by the receiving antenna with axial alignment.

In the first experiment, motor performance at the receiver is qualified by sufficient torque to drive a weighted wheel and is maximum when the receiving coil is closest to  $t$ , with the power falling off smoothly to a distance of four centimeters. When the motor is not loaded by a weighted wheel, it exhibited a similar performance to a distance of nine centimeters.

The second experiment involved using two dc modes, meaning the use of two receivers in dc mode—essentially two motors operating simultaneously, with a germanium rectifier bridge. The behavior using two modes is comparable to one dc mode in terms of power consumption relevant to proximity with  $t$ , as expected, but the effects of the distant receiver attenuated the power delivered at  $s$ . The maximum distance, when there is found to be enough power to drive a loaded motor, is nine centimeters. By arranging  $r$  and  $s$  with minimum axial displacement, the currents were in a state of constructive interference, creating a solenoid-like structure. In this way, sufficient power to drive a motor with a weighted wheel is extended to a distance of twelve centimeters. When using one dc mode and rotating at an angle  $\theta$ , as illustrated in Fig.2.55, signal performance of receiver  $r$  when  $\theta$  is between 40 and 90 degrees from  $t$ . In

this range, the power falls off and remains steady until  $\theta = 90^\circ$ . When using two dc modes and rotating at an angle  $\theta$ , signal performance of the receiver  $r$ , while comparable to one dc mode, exhibited segments in its rotation through  $\theta$  where energy is exchanged between the two receivers.

When using one ac and one dc mode, signal performance of the receivers is found to be comparable in each characteristic performance based on experimental observations. The exchange of energy is homogenous in that it is more or less evenly distributed by the position of the receiver relevant to its multiple based on the total energy input at the circuit amplifiers. By increasing power to the source, higher intensity currents are available to each receiver.

While demonstrating the transmitter generates magnetic waves which can pass through walls and does not interact with off-resonant objects such as humans or animals, there are reasons where it is undesirable to exchange energy with a circuit which shares characteristic properties of the resonant circuit. In such cases, shielding of a resonant object is possible by enclosing the machine in thin metallic foil. It is observed the magnetic field cannot penetrate such a substance and it induces currents in the form of eddy currents. Such an arrangement is ideal for the transfer of electrical current from the circuit through the surface of the skin, discussed in §5.1.1.

#### **2.4.4 Optimization of the circuit**

On examination of (72), and discussed in §2.2, it is theoretically possible to affect the quality factor of the coil by adding resistance to the receiver circuit. This is achievable particularly when using high-wattage resistors at low quantities of resistance. For example, adding a  $500\Omega$  resistor in parallel with the load raises the quality factor of the circuit causing the lamp to

yield a slightly brighter luminescence. Adding series resistance improves the efficiency of the circuit, to a limit [81]. By increasing the length of wire after the rectifier circuit, the useful range of the dc signal is extended to twelve centimeters.

In all experiments, the maximum power applied to the driving amplifier circuit was twelve volts. At this level, there is found to be significant heating of the transmitter's capacitor. Changing the input voltage alters the output voltage, i.e., there is no storage of magnetic energy in the magnetic field. Any increase or decrease in the supplied power does not alter the locations where the coils achieve a maximum or minimum in their resonance coupling, rather it increases or decreases respectively the available power at those locations while extending the maximum distance in dc mode.

In the case of two coils, of a radius of three centimeters set six centimeters apart, a measured power transfer efficiency of 76.82% is achieved. This compares favorably with the 82% reported in [77] and the 80% reported in [43]. It is worth adding that it compares even more favorably with the 45% reported in [85]. It is also apparent that the same method of power delivery, as tested in experiments, can also be employed in the case of multiple receivers. With the addition of additional receivers, the transfer efficiency remains at a minimum of 82% while dividing the power, based on the position of the receivers relative to the transmitter. This implies that the method introduced here could be useful to power several measurement and/or stimulating points within one body, without significant power degradation, from one single external transmission source.

Power issues faced by [89] deal with system consisting of modes—active and sleep—and are concerned with power consumption of a circuitry at random intervals, such as when a vibration triggers the piezoelectric response to generate voltages and currents. Regarding [90], the notion of beacon-delimited, ultra-low body network is comparable to the research detailed in this section by the overlapping of two common themes:

1. sending power for medical implants or body monitoring apparatus,
2. sending information at an appreciable data rate, however, the current research only acknowledges the apparatus has the *ability* to transmit data given the waveform is a steady-state sinusoid.

Because of the importance of the subject area, a body of research both theoretical and experimental has appeared, particularly in the last decade, on this topic. As a result the attempt is to make it clear how this work compares favorably with that of others in terms of the results obtained. It is important to also give an indication of how these improvements have been achieved through original differences in the fundamental design. It must be realized that the basic ideas underlying the differences have been gleaned by returning to some of the fundamental work of Tesla, Larmor, and Poynting, stemming from the original Maxwell equations. As such it is made clear in this section that the geometry of the magnetically coupled coils employed was not “standard”, rather, exhibited differences to that used in other work [77, 78, 79, 84, 87, 91]. Here is a list of differences.

Firstly, the antenna makes use of a Litz winding, not wound in any particular orientation. This same approach is used in [77], but not so in [43, 85]. Secondly, the radius of the receiver and transmitter coils in

experiments are the same (three centimeters), others meanwhile use one radius for the transmitter and another for the receiver [43, 78, 79, 91]. On top of this there are very few turns on both coils, where  $n = 3$ , and no use of a secondary coil. This is in direct contrast to [77, 85]. Also diverging with previous work, the prototype used an analog oscillator, integrated with the loops, i.e., the inductor and capacitor formed a resonant circuit. It also used plain, circular loops, whereas [43, 71, 76] all use flat coils while [77] uses a staggered arrangement. In this way, the loops consume the entire ac cycle. The prototype also broadcast a lower resonant frequency, or longest wavelength, than that in previous research.

Overall, the key to the approach is simplicity. The model used, by quite some way, the fewest number of components (13 in total for the oscillator) and yet generated a clean sinusoidal waveform at 450 kHz. The receiver contains only three components. By contrast, in [43] the authors employed a noisy digital driver, which also required supplemental circuitry. The operational circuit including the antenna powering multiple lamps a distance in approximated rotations away from axial alignment, discussed here, is shown in Fig.2.57.

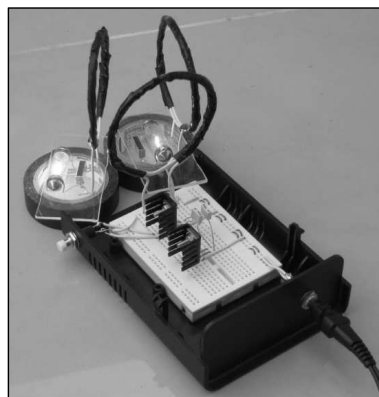


Fig.2.57. Operational oscillator powering multiple lamps.

Experimental results show that significant improvements in terms of power transfer efficiency are achieved by directly connecting the circuit to an amplifier circuit instead of excitation being achieved from an external sinusoidal source. The measured results were found to be in very good agreement with the theoretical models. The next step clearly will need to involve tests involving actual biological tissue for medical device purposes, discussed briefly in §5.1.1. Although, by analyzing results from previous comparable studies [44, 77], it is not anticipated that there will be any issues of significance, nevertheless such a study is a necessity before actual practical application of the procedure can be placed in situ.

It was found that the efficiency of the energy transfer system can be improved by increasing the quality factor of the coils. The power transfer system achieves at least four times more efficiency and power density in watts per centimeter, given its small size, compared to prior inductive-link schemes. The reasons behind the improved results, as reported in this work, are not particularly due to the antenna type or quality factor of the coils, as one might expect. The nature of the loop antenna has been thoroughly investigated in the literature. Rather, it is a property of the oscillator driving the system under resonance. In the design, the oscillator frequency is designed such that the loop is small and the radiation non-toxic in human proximity. It is suggested that it is actually beneficial to the electrical cells of the body.

The discussion in this chapter centered around a single coupled-mode with several experiments to prove the theory. Given the utility of the concept, it is interesting to supplement the discussion with an addition of a second coupled-mode given an alternative circuit arrangement.

### 3 Two coupled-modes without projection

The last chapter discussed the theoretical implications and framework of a single coupled-mode magnetic resonant transmission including experimental evidence confirming the proposed theory. This chapter will extend the work by adding a second coupled-mode to the arrangement. The concept of two coupled-modes will be discussed and illustrated in terms of a recreated model of Tesla's circuit described in his 1900 patent *A System of Transmission of Electrical Energy*, notably, the arrangement of four tuned circuits exhibited as two concentric spirals.

Three contributions are proposed in this chapter:

1. An analysis of the two coupled-mode model of wireless power transmission and constructing a circuit;
2. comparing the performance of the circuit with the those described one in the literature, [10]; and,
3. introducing an innovation wherein modification of the circuit links its model with the field model, in stronger support of the model, particularly the concept of the contiguous (virtual homogenous) waveguide of free-space described in in §2.

Tesla presented a model of wireless power transmission that he claimed in U.S. Patent #645,546 could be used to send wireless signals to anywhere on the planet. A drawing of his setup is shown in Fig.3.1.

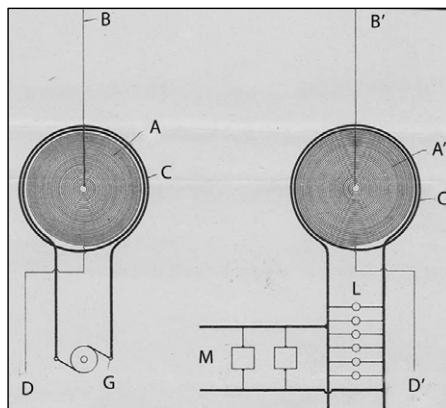


Fig.3.1. Tesla's wireless power model.

The Tesla circuit comprises four tuned circuits: a transmission and receiving pair of circular coils each containing a thick-wire primary of a few turns and a thin-wire secondary of many turns. Illustrated in Fig.3.1, (C) represents the primary coil (A) the secondary coil, (B) one free end of the secondary coil, and (D) the other free end of the secondary coil of the transmitter. For the receiver, these identical components are labeled with primes so as to distinguish the transmission side from the receiver side of the complete circuit.

The circuit windings, sensitively dependent upon the position of the coils relative to each other, perform ideally when the distance between the primary and secondary winding is no greater than the thickness of the primary, similar to the transformer effect at close proximity. This ensures maximum current displacement in the outer winding of the secondary. When a constant current is maintained on the secondary, it is possible to enhance the characteristic of this coil. An innovative enhancement will be discussed later in this chapter which introduces a connection of a third coil with passive components such as capacitors and resistors between (B) and

(D), and between (B') and (D') used to manipulate the order of the magnetic field, compounding the power series, projecting away from the secondary coil [21, 26]. Applying a sinusoidal current (G) to the ends of the primary coil at the transmitter, the input current is observed at the ends of the primary coil at the receiver. The current can be utilized via a load represented as lamps (L) and motors (M) and observed on a spectrum analyzer when transmitting at low power levels or using attenuators.

The windings, constructed and oriented as described, each form one-half of a tuned circuit. By placing each half of the circuit at a distance greater than the radius of its secondary coils, the total circuit expresses cavity effects occurring along the trajectory of energy transfer. It is assumed the observed behavior and the emission of plane waves is uniformly present, though perhaps in different quantities, with circuits of different sizes but having the same relative geometry. It is a fairly trivial exercise to artificially create resonance cavities, magnetically-coupled wherein energy and information are transmitted bi-directionally. These cavities, while homogenous in free-space, maintain a total internal reflection implying each individually or multiply-connected cavity is a holomorphic manifold [11]. It demonstrates that at the extreme limit of mid-field transfer, the transmitter and receiver can be placed at separations in all three Cartesian directions and can be designed in such a manner as to be a planetary transmitter, which is not unlike Tesla's original description [103, 113].

Considering the radius of the secondary coil and the length of the conductor consisting the spiral, a peak-transmission frequency is established when both halves of the circuit are built to exacting specifications yet wound in the opposite directions, which, for the purposes herein, is  $27.50 \text{ MHz} \pm 5\%$ . By applying an external sinusoidal steady-

state signal to the primary coil (C) at (G), the identical signal is observed at the primary coil (C') at (L) and (M) without drift or distortion. It is clear the circuit has a complex symmetry. By applying external sinusoids to either half—at the transmitter or receiver—the signal is observed at the other half. Experiments have shown that, in general, the higher degree of symmetry in the circuit, the greater the resonance and the better the performance.

The two pairs of self-resonant coils allow the transportation of quantities of energy at significant distances comparable to the sizes of the windings involved. Rather than the use of large coils relative to the distance of transmission which rely on fixed coil qualities, small coils are used with a tuning apparatus which controls the tuned state of the resonator cavity through ordered magnetic fields.

### 3.1 The theoretical model

The efficiency,  $\eta$ , is a measure of performance of a circuit to catalog the success of this particular experimental design, though sharing global characteristics with the other experiments discussed in this work. It is expressed as a fractional quantity,

$$\eta = \frac{\text{Useful power output}}{\text{Total power input}}. \quad (155)$$

Another measure of performance is the energy stored in the magnetic field  $H_0$  utilized for magnetic-resonant coupling. The circuit consists of an oscillator driving a loop of wire  $L_T$  coupled to a capacitor  $C_T$  and a resistor  $R_T$  at the circuit's resonance frequency  $\omega_0$  representing the transmitter. A second loop of wire  $L_R$  of equal radius coupled to a capacitor  $C_R$  and a resistor  $R_R$  connected to a light-bulb representing the receiver.  $L_T$  and  $L_R$

are placed at a distance apart from each other. The projection  $\bar{\mathbf{H}}$  is not seen in this model, as the energy is absorbed into the secondary coil. In terms of the properties of the radio-frequency waves transmitted by the circuit, the efficiency  $\eta$  is first given in terms of the degree of coupling between each half of the circuit as:

$$\eta = \frac{\kappa_{TR}^2 Q_T Q_R}{1 + \kappa_{TR}^2 Q_T Q_R} \quad (156)$$

where  $\kappa_{TR}$  is the coupling coefficient,  $Q_T, Q_R$  are the quality factor of the coils  $L_T$  and  $L_R$  driven at resonance frequency  $\omega_0$ . The criterion of efficiency in the scheme is parameterized by the coupling coefficient between the secondary coils in each half of the circuit and their quality factor yielding the energy stored. By creating a generic model of the means of transmission, it is possible to glean insights about the efficiency  $\eta$  of the scheme and how to improve it. Each part of the Tesla resonator is discussed in the following sections. It is advantageous to discern the system in terms of its geometry and construct the field model around it.

### 3.1.1.1 The transmitter coils

There are two sets of coils for each half of the circuit, they subsist of a pair of coupled circuits in the form of a spiral. The arrangement of the transmitter coils is shown in Fig.3.2. There is a primary coil of a few turns and a secondary coil of many turns. A tight coupling  $\kappa_{ab}$  between the primary's inductance  $L_a$  and the secondary's inductance  $L_b$ , suggests the capability to have a high mutual inductance  $M_{ab}$ , which greatly aids more power to be transmitted.

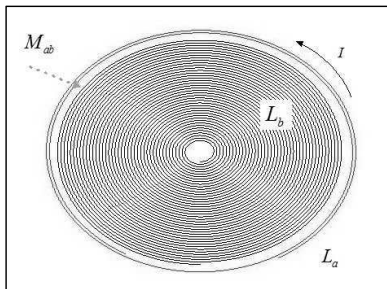


Fig.3.2. Transmitter coil package.

### 3.1.1.2 The receiver coils

Because of the symmetry a tight coupling  $\kappa_{cd}$  between the secondary's inductance  $L_c$  and the primary's inductance  $L_d$  is also observed yielding, again, a high mutual inductance  $M_{cd}$ . The arrangement of the receiver coils is shown in Fig.3.3. Note the sole difference is the direction of the winding. It is opposite to that of the transmitter.

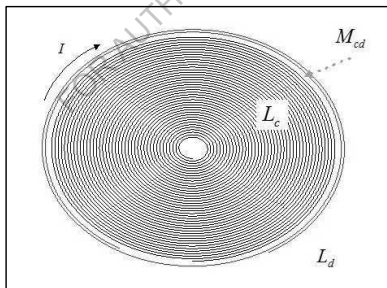


Fig.3.3. Receiver coil package.

The physical properties of the coils are shown in Table 3.1.

Table 3.1. Resonant coils physical specification.

TABLE 3.1  
RESONANT COILS PHYSICAL SPECIFICATION

Designation	Coil letter	Inner/Outer radius (mm)	Wire radius (mm)	Wire length (mm)	Number of turns
Tx Primary	a	40.5/51	1.30	700	1.80
Tx Secondary	b	10/40	0.384	5150	40
Rx Secondary	c	10/40	0.384	5150	40
Rx Primary	d	40.5/51	1.30	700	1.80

### 3.1.1.3 The coupling coefficient

The coupling coefficient  $\kappa_{bc}$ , mutual inductance  $M_{bc}$  between distant coils  $L_b$  and  $L_c$ , and the quality factors of all the coils are the significant physical properties in this arrangement. The mutual relationship and the coupling between each of the coils is illustrated in Fig.3.4. To understand the effectiveness of the scheme and the work done at a distance, the energy storage ability of the system is determined by coupling coefficients in transfer mode. The flow of the energy  $E_0$  in joules across the distance is determined by  $\kappa_{bc}$  between coils  $L_b$  and  $L_c$ ,  $\kappa_{ab}$  and  $\kappa_{cd}$  are relatively constant as the distance between coils  $L_a$  and  $L_b$ , and coils  $L_c$  and  $L_d$  do not move with respect to each other. If the resonance frequency  $\omega_0$  is kept constant, the inductances of coil  $L_a$  and coil  $L_d$  are small while the distances between coils  $L_a$  and  $L_d$ , coils  $L_a$  and  $L_c$ , and coils  $L_b$  and  $L_d$  are relatively large. Thus,  $\kappa_{ad}$ ,  $\kappa_{ac}$ , and  $\kappa_{bd}$  are relatively small and hence can be neglected. When a current  $I_0$  is applied to coil  $L_a$ , power flows from coils  $L_a$  to  $L_b$ ,  $L_b$  to  $L_c$ , and  $L_c$  to  $L_d$ .

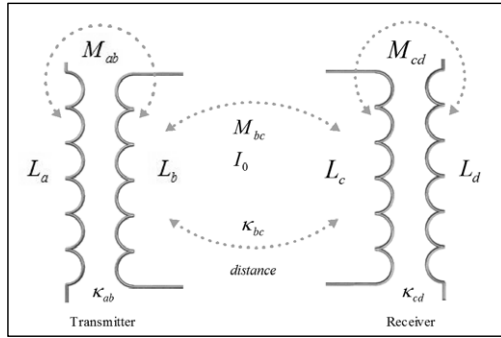


Fig.3.4. Schematic diagram of the circuit for two coupled-modes.

Referring to the scheme illustrated in Fig.3.4, the coupling coefficients between the significant magnetically-coupled coils, derived from (45), are

$$\kappa_{ab} = \frac{M_{ab}}{\sqrt{L_a L_b}}, \quad \kappa_{cd} = \frac{M_{cd}}{\sqrt{L_c L_d}}, \text{ and } \kappa_{bc} = \frac{M_{bc}}{\sqrt{L_b L_c}}, \quad (157)$$

where  $M_{ab}$ ,  $M_{cd}$ , and  $M_{bc}$  are the mutual inductances,  $L_a, L_b$  and  $L_c, L_d$  and  $L_b, L_c$  are the self-inductances of the coils. Since the coupling coefficient cannot be directly measured, it is necessary to calculate the inductances and the mutual inductance of the distant coils. For the coils  $L_a$  and  $L_d$ , the approximation for the inductance of a circular loop is

$$L_a \approx \mu_0 \mu_r n_a^2 r_a \left( \ln \frac{8r_a}{R_a} - 2 + Y \right), \quad L_d \approx \mu_0 \mu_r n_d^2 r_d \left( \ln \frac{8r_d}{R_d} - 2 + Y \right), \quad (158)$$

where  $r_a, r_d$  is the loop radius and  $R_a, R_d$  is the wire radius,  $n_a, n_d$  is the number of turns, and  $Y$  is the flow constant of the skin-effect of the emitted radiation. For the coils  $L_b$  and  $L_c$ , the approximation for the inductance of an air-core flat spiral coil [30] is

$$L_b \approx \mu_0 \mu_r \frac{r_b^2 n_b^2}{8r_b - 11(R_b + w_b)}, L_c \approx \mu_0 \mu_r \frac{r_c^2 n_c^2}{8r_c - 11(R_c + w_c)}, \quad (159)$$

where  $r_b, r_c$  is the loop radius and  $R_b, R_c$  is the wire radius,  $n_b, n_c$  is the number of turns, and  $w_b, w_c$  is the width between each turn of the windings.

Table 3.2 shows the calculated values for the coils.

Table 3.2. Resonant coils calculated electrical specification.

TABLE 3.2  
RESONANT COILS CALCULATED ELECTRICAL SPECIFICATION

Coil	Inductance ( $\mu\text{H}$ )	Mutual Inductance (between coils) ( $\mu\text{H}$ )	Coupling coefficient ( $\kappa$ )
a	0.78	0.340 (ab)	0.061
b	58.18	13.10 (bc)	0.225
c	58.18	13.10 (cb)	0.225
d	0.78	0.340 (cd)	0.061

### 3.1.1.4 Determination of mutual inductance in the model

The mutual inductance  $M_{bc}$  is calculated using the same methodology as (52),

$$M_{bc} = \frac{\int \int \mathbf{B} \cdot \vec{n} dS}{I_{L_b}}, \quad (160)$$

where  $L_c$  is the area of the receiver secondary coil,  $\mathbf{B}$  is the magnetic field,  $I_{L_b}$  is the current passing through the transmitter secondary coil and  $\vec{n}$  is the vector normal to the energy across free-space. In examining mutual inductance and the distance, the space between is filled with a radiated field object resulting from the exchange of energy and feedback between the coils, whose size and shape is dependent upon coil geometry. As such, it is expected the space to be a medium occupied by a charged field exhibiting an energy flow. An accurate calculation of mutual inductance depends on the assumption of energy distribution occupying the free-space between the

distant coils. It is assumed a Boltzmann distribution of the magnetic currents along the waveform limited at its boundary or other non-local positions, given Maxwell's notion of the potential. The model still however assumes a smooth boundary. Using these assumptions, the calculated coupling coefficients and inductances are also shown in Table 3.2. It is expected the space to be occupied by a hyperbolic-shaped field object in three dimensions saturated with charge and flow, illustrated in Fig.3.5. This field object is the consistence of the virtual waveguide discussed in Chapter 2 of this work.

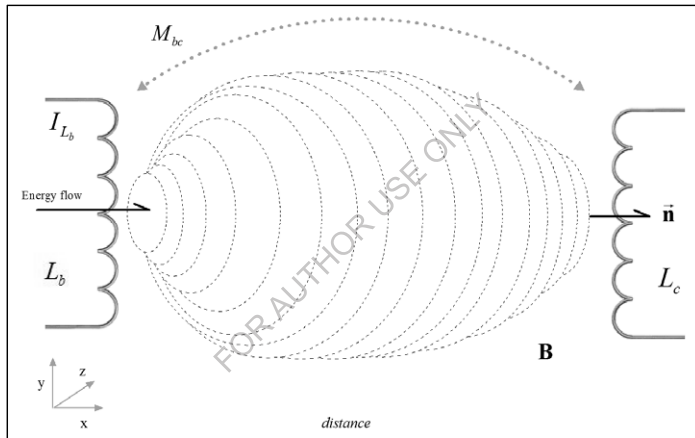


Fig.3.5. The virtual waveguide comprised of a coherent field in the model based on Fig.2.17.

### 3.1.1.5 On quality and loss

The quality factors of the coils loaded by a parallel circuit containing a capacitance,  $C_i$ , and a light bulb are calculated. Under such geometry, the quality factor is calculated the same manner for each of the four coils. In the scheme, the components of the circuit are in parallel with reference to each other between the transmitter and receiver secondary coils. The overall loaded qualities,  $Q_i$ , are defined via the relation,

$$Q_i = R_o \sqrt{\frac{C_i}{L_i}} + R_r \sqrt{\frac{C_i}{L_i}}, \quad (161)$$

where the quality  $Q_i$  represents the quality factor of the resonant circuit either due to ohmic resistance  $R_o$  and radiation resistance  $R_r$ . The losses are divided into the losses due to ohmic resistance,

$$R_o = \sqrt{\frac{\mu_0 \omega_0}{2\sigma}} \frac{\ell^2}{4\pi R}, \quad (162)$$

where  $\sigma$  is the conductivity of the material,  $\ell$  the wire length of the coil and  $R$  is the wire radius, and the losses due to radiation resistance,

$$R_r = \sqrt{\frac{\mu_0}{\epsilon_0}} \left[ \frac{\pi}{12} n^2 \left( \frac{\omega r}{c} \right)^4 + \frac{2}{3\pi^3} \left( \frac{wh}{c} \right)^2 \right], \quad (163)$$

where  $n$  is the number of turns of the coil and  $c$  is the speed of light. By examination of (161), increasing either the capacitance or circuit resistance will increase the quality factor of the coils. Given (156) a small increase of the quality factor of the coils will increase the amount of energy transported improving the effective efficiency. The power transfer efficiency of the four-coil system calculated from the quality factors and coupling coefficients from above is

$$\eta_{total} = \frac{(\kappa_{ab}^2 Q_a Q_b)(\kappa_{bc}^2 Q_b Q_c)(\kappa_{cd}^2 Q_c Q_d)}{[(1 + \kappa_{ab}^2 Q_a Q_b)(1 + \kappa_{cd}^2 Q_c Q_d) + \kappa_{bc}^2 Q_b Q_c][1 + \kappa_{bc}^2 Q_b Q_c + \kappa_{cd}^2 Q_c Q_d]}. \quad (164)$$

### 3.2 The propagation of magnetic currents

In order to satisfy the imposed conditions of the field model and in consideration of Fig.2.19, it is relevant to plot the magnetic field intensity

and the magnetic flux density of the magnetic currents emanating between the coils  $L_b$  and  $L_c$ , in this arrangement of two coupled-modes verses the single coupled-mode. It is insightful to map the fields between coils  $L_b$  and  $L_c$  when a source of one ampere is applied. Using *Comsol Multiphysics*, magnetic flux density and magnetic intensity between the distance coils is computed, shown in Fig.3.6.

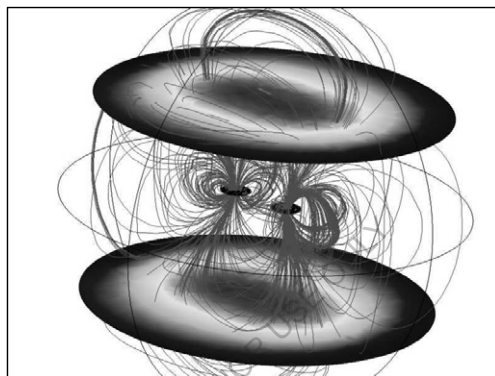


Fig.3.6. Magnetic field intensity and flux density between two secondary spiral coils.

To calculate the magnetic field strength at this distance from the coils, it is necessary to truncate the computational domain, because the finite element calculation requires a finite-sized mesh. The sphere,  $S$ , which serves as the computational boundary of the domain, has a radius of 80 centimeters. The plot displays a calculation of magnetic field strength (the ovals on top and bottom) and the magnetic flux density (the lines passing through and around the coils). The colors from light to dark show the increasing intensity of the magnetic field emitted by the coils, the peak strength (darkest color in the center) lies 1.5 times the radius of the coils. The minimum strength lies at 15 times the radius of the coils. The magnetic flux density (the field lines) extends the field intensity approximately 8 times the radius of the coils or halfway between the maximum and minimum

field strength. As shown in Fig.3.6, the magnetic field intensity is strong in the free space between the coils which suggest this geometry, given the strength of the fields to perform work at a reasonable efficiency, is suitable for transmitting electrical currents of sufficient magnitude.

It is also relevant to know if the model holds at distances at the extreme end of the mid-field region. Fig.3.7 is a plot of the same secondary coils  $L_b$  and  $L_c$  emitting a magnetic field at a distance of 75 centimeters, the boundary of the computation domain has a radius of 120 centimeters.

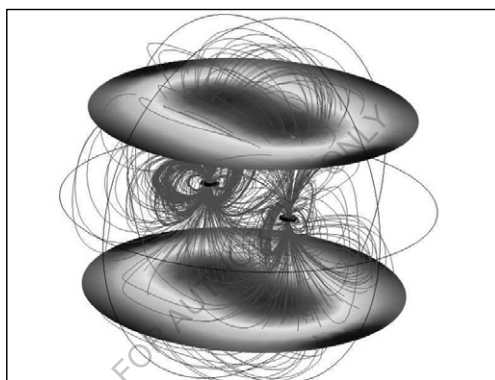


Fig.3.7. Magnetic field intensity and flux density at greater distance.

The intensity remains uniform across the distance. The limit at the boundary is obtained by the computation of the fields and the assumptions about free-space, given the discussions in the previous chapters. Continuing along this line of logic, a method appears to extend the limit for mid-range transfer. The innovation is the addition of a conical coil allowing the magnetization of the coils to be manipulated. The polarization of the fields across the space is such that it magnifies a magnetic monopole in the region which allows the stronger transmission of  $H_\phi$ . By manipulating this magnetization, the field can be tuned with the introduction of passive

components. The additional forces on the magnetic field from the conical coil constructively interferes with the magnetic field lying on the spiral coil given the two coils are sharing the same electrical field and electric potential. By adding capacitive and resistive components across both coils  $L_b$  and  $L_c$  quality and coupling-coefficient values are directly accessed, altering the orders of the magnetic field [21, 26]. The third coil arrangement is shown in Fig.3.8.

Adding a third conical coil of radius  $r_e$  at a distance of ten centimeters along the  $z$ -axis of the secondary coil and connecting at terminal (B), the free end of the secondary coil, increases the value of  $L_b$  linearly. The value of  $\mathbf{H}$  is also increased, it is given the length of wire  $\ell_e$  contained on the curvature,  $\theta_e$ , of the conic. An approximate averaging of  $\mathbf{H}$  is achieved by setting the conic angle  $\theta_e = \pi/6$  along a length where  $r_e \leq r_b$  which yields a significant increase or connection to the magnetic potential  $A_\mu$ . An increase of  $H_\phi$  is observed by applying the force upon the dipole residing at the center of the secondary coil. Only a few experiments touched upon this behavior, it is a strongly recommended topic of future research.

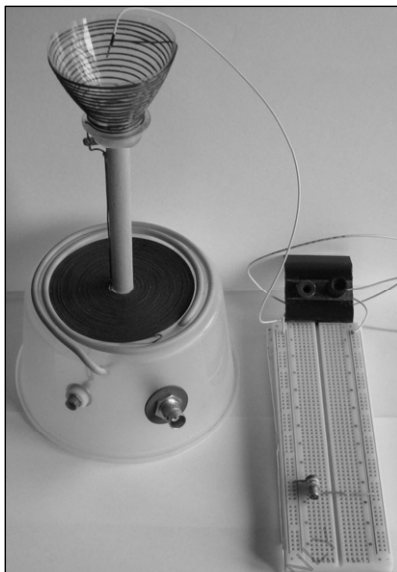


Fig.3.8. Receiver package and third coil. Component breadboard shown.

### 3.3 The circuit experiment

A reconstruction of the Tesla resonator, illustrated in Fig.3.1, was built with the physical specifications shown in Table 3.1. The inductances were measured on a Hewlett-Packard hp4192A into  $50 \Omega$ , shown in Table 3.3. The first test was to plot the results of applying a steady-state sinusoidal source at the peak resonance frequency of 27.50 MHz and chart the measured differential power between input and output. The efficiency,  $\eta$ , as a function of the distance between the coils is shown in Fig.3.9.

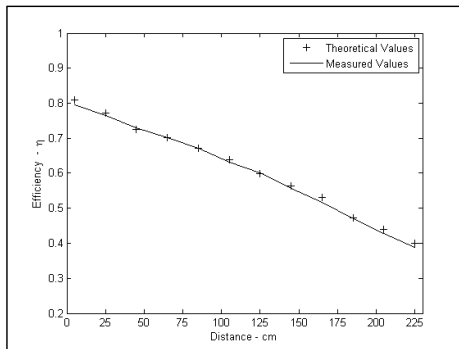


Fig.3.9. The efficiency of the Tesla resonator over a distance.

To understand how this model performed against a comparative wireless power system, results were contrasted with [10]. Although containing a different orientation and geometry, due to similar sources of prior art sufficient shared fundamentals exist. The significant difference, however, is the Tesla resonator can be placed without regard to position or orientation between the transmitter and receiver unlike the necessity of axial alignment in [10]. Fig.3.10 shows a contrast of the two schemes.

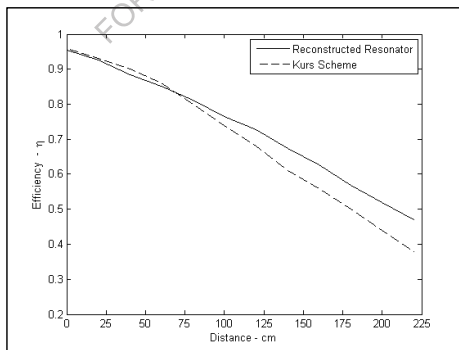


Fig.3.10. Comparison of the Tesla resonator with Kurs [10].

The reconstructed Tesla resonator, in its original form without modification, performs better with secondary coils of more winds yielding

more magnetic field properties. Considering magnetic resonance coupling schemes studied in this chapter insist a higher magnitude of magnetic flux density as directly translating into greater efficiency over mid-field distances, the observation of a linear relationship in force to energy density of the magnetic field is not surprising.

Table 3.3. Resonant coils measured electrical specification.

Coil	RESONANT COILS MEASURED ELECTRICAL SPECIFICATION			
	Inductance ( $\mu\text{H}$ )	Capacitance (nF)	Resistance ( $\Omega$ )	Quality factor (Q)
a	1.15	870	2.00	96.6
b	62.40	16	1.88	182.3
c	61.68	16	1.81	180.4
d	1.17	886	0.55	97.3

The second test was to add passive components to verify if, as according to (161), the quality factor of the scheme could be improved. By doing so, the efficiency shown in (164) is improved. Capacitors added in parallel to the transmission coil, while resistors added in parallel to the receiver coil would show an improved efficiency in the transmission. Such direct connections between the circuit and the field are aided by the addition of the third coil inductively coupled to the transmission field. Values of added or subtracted capacitance and resistance affected admittance and circuit impedance by altering the phase of the energy at the distant secondary coil. A series of five tests were conducted adding capacitance and resistance as value-based parameters to coils  $L_b$  and  $L_c$  coupled through  $L_e$ .

As illustrated in Fig.3.11, the coupling coefficient  $\kappa_{bc}$  can be affected by not only reducing the losses, but also affecting the quality factor by adding values of capacitance and resistance. Tuning the resonant frequency to the peak magnetic flux density of the circuit would further improve performance.

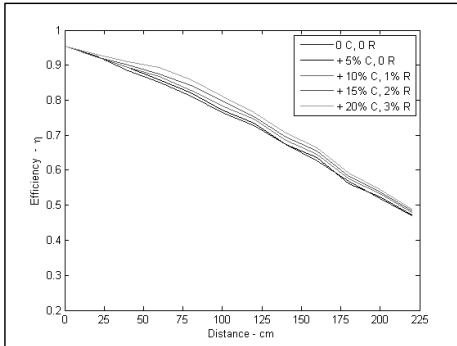


Fig.3.11. The efficiency of the Tesla resonator with enhanced quality factor.

This implies the cavity is contiguous and has a property inherent to it, suspended inside free-space. Following the theoretical framework of two coupled-modes, the experimental reconstruction of Tesla's signaling apparatus from his 1900 patent *A System of Transmission of Electrical Energy*, illustrated in Fig.3.1, is also examined in terms contrasted with other attempts claiming a Tesla wireless power system. In [10] the author concerned himself with Tesla's 1914 patent *Apparatus for Transmitting Electrical Energy* focusing primarily on the transmission of electrical currents given large coil loops of a few turns. Here, the attempt is to demonstrate an alternative approach using coils significantly smaller yet achieving better results for efficiency. One striking difference is that the geometry and orientation of the Tesla resonator examined in this chapter does not rely on an axial alignment of the coils; rather, the transmitter-receiver pair can be placed liberally at a distance relative to each other without any significant additional losses. According to [10], the limit of this type of transfer is 8 times the diameter of the coils, the electrical intensity between the coils diminishing at a rate  $\frac{1}{r^2}$ . Experimental results have indicated a greater link in the magnetic field density appears at the

secondary coils in this resonator-coupled model. The extreme distance measured in the experiment was four meters.

The third test was to discern if the reconstructed resonator could be modified to increase energy transmission and intensity of the magnetic fields in the magnetic-resonant model. What became immediately apparent was by adding passive component circuitry, the field object behaved as a cavity not unlike a transmission-line resonator. The sharing of those basic characteristics in our model gives a wireless transmission-line resonator. More research on this formalism is suggested. It has been observed that the resonator's performance is sensitively dependent upon its impedance, as expected. The signal generator used during experiments outputs into  $50 \Omega$ , impedance at the receiver was measured to be  $58 \Omega$ . Tuning the resonator, it is possible to more closely match the impedance of the circuit allowing more of the power seen at the source to be dissipated in the load. From this approach, by adding and subtracting impedance, efficiencies over longer distances are dramatically improved. Although, not directly addressed in the experiments in this chapter, the appearance of standing waves in the resonator suggests a possible explanation of voltage magnification lending credence to Tesla's description of velocity-inhibition.

The idea of velocity-inhibition is related to the Larmor concept of acceleration, used here in this work, and described in §1.1. What is further interesting is that Tesla first described a method of antipodes [110, 112, 113], or positions on the planet where it would be ideal to place transmitters for world wireless transmission. The addition of a third coil on the  $z$ -axis allowed the manipulation of the variables manifesting the magnetic fields at the secondary spiral coils yielding an improvement in performance. The presence of the coil  $L_e$  in the field along the trajectory

couples, through a higher-order magnetic field [26], to the transmission circuit of  $L_b$  and  $L_c$ , shown when there is and not a connection at (B) and (B'). Based upon this observation, it is of great interest in future experiments to investigate what access there is to the magnetic potential  $\mathbf{A}_\mu$ .

### 3.4 Observations of behaviors present in the circuit of two coupled-modes

The method here details mid-field wireless power transmission by means of low-frequency radiating waves, as opposed to either near-field inductive direct coupling or far-field microwave transmission. The proposal is a type of wireless power transmission based on the notion of a transmission-line resonator without any physical containment other than the fields themselves. It suggests that the existence of a pair of tuned circuits of a four-coil arrangement, as illustrated in Fig.3.1, or a two-coil arrangement illustrated in Fig.2.1, exhibits such possibilities when measuring unpowered outputs at both the receiver as well as the transmitter—a cavity presence is visible whether external power is applied or not. The observations lead to an implication of a resonator cavity with characteristic peaks in the frequency spectrum which go unchanged regardless of the distance between transmitter and receiver. It is this uniqueness that makes the circuit worthy of deeper study. Power efficiencies are respectable, being significantly higher than those previously reported for mid-field regions, without the need for the extremely large directed antenna. A detailed and quantitative analysis of the effect of external, non-resonant objects on the transmission circuit is compatible here as it is with the method discussed in the other parts of the work.

It is worth noting that the power transfer is not affected if humans or various everyday objects, both large and small, are placed between the receiver and transmitter. This includes cases where objects completely obstruct the line of sight or lie within a few centimeters of the coils. While the transmission frequency is somewhat outside that deemed safe for human exposure [19, 20, 34], coupling is only possible if a receiver contains a coil symmetric to the transmitter, but oppositely wound. It is suspected the radio-frequency fields react weakly with off-resonant objects.

During the course of conducting experiments, voltage magnifications were observed when applying resistances to the receiving circuit. Magnifications as much as 50 times were observed which manifest themselves as current spikes reflecting back across the resonator. Although noted, they were not directly analyzed during the investigation for this chapter. Nevertheless, it is apparent that Tesla's resonator has properties which appear either unrealized or under-investigated as such, although they were partially sketched out in Tesla's works and their interpretations [13, 14, 18, 25, 58, 79, 80, 81, 83, 84, 86, 89, 90, 103, 112, 113, 114, 121, 122]. It is therefore suggested that a detailed body of research be conducted on this topic. Tuning techniques and strategies, field-order coupling are also considered very fruitful paths.

While the results presented in this chapter are of interest in themselves, they also throw up a number of intriguing questions which need to be researched. For example, in terms of performance over distance, how important are the shape and directional settings of the windings and the amount of power drawn by the load with regard to the transmission efficiency? What remains consistent is that an improvement of quality leads directly to an improvement of performance not only at the distances

shown in the figures, but also at greater distances, as expected. Given the appearance of more complex wave patterns in the transmission, it is hypothesized the magnetic fields of the first-order are, at least in part, with the Schumann resonance [110]. This is supported by experiments conducted with the third coil present in both the transmission and receiving coils, introducing a third coupled-mode.

Compared to the single coupled-mode model from the previous chapter, this model shares many of the characteristics of the former. Coupling between close-proximity coils, where the distance is much smaller than the radius, resembles the commonly-understood transformer model. Coupling between distant coils, such as the coupling between each secondary coil, resembles the theoretical framework of the previous chapter in several ways. First, intersection of flux lines is deemphasized and the notion of the virtual homogenous waveguide is strengthened. Contrarily, it is also conceptually correct to consider the intersection of flux lines as the linking force constituting the structure of the waveguide. Second, although the oscillator in this case is not tightly integrated into the primary coil antenna and the circuit responds more to ringing than acceleration, it is distinctly apparent that the projection field,  $\bar{\mathbf{H}}$ , from the previous chapter is present because of the fact that the third coil experiences a magnitude of energy along the  $z$ -axis. Third, the enhanced magnetic field magnitude, again experienced by the third coil, is supported by the work of §2.4.2. The theory is further extended in this chapter by the concept of the ordered magnetic field—zero and first order—following from the theoretical discussions in [21, 26]. The demonstration of physical evidence of the first order magnetic field is a very powerful claim and deserves serious consideration in future research.

This chapter discussed two coupled-modes by illustrating a reconstruction of a Tesla system of wireless power, contrasted to the single coupled-mode of the previous chapter. The utility of the schemes illustrated in both chapters present many possibilities for the future of efficient wireless energy transfer in an industrial capacity.

#### 4 The dipole concept and accelerated electrons in matter

The dipole and the magnetic potential are fundamental concepts describing the motion and forces of separation of electric charges on an antenna. During Hertz' research, it was discovered some peculiar effects occur in certain antennas [16, 29, 75, 92] such as the circular loop. This chapter will discuss the dipole concept and introduce a modified model under acceleration [116]. It is interesting to examine the motions of separation of two charges from the viewpoint of de Broglie waves [48] as well as the description by Bohm [95]. The model presented here is an attempt to redraw the depiction of the dipole based on experimental evidence. The motivation for this chapter is suggestive of different behavior in the dipole than expected, an elasticity pronounced strongly in the projection,  $\bar{\mathbf{H}}$ , and that it can be preserved, e.g., not destroyed once it is returned to the power supply.

It is orthodoxy in electrical engineering and a basic tenet of physics, that work is done in electrical systems by the separation of charges and the release of energy when those same charges come back together with a feedback oscillation along the trajectory. Conservation laws dictate that the work done to separate charges is equal to the energy that is observed, subtended by losses in the system. While this understanding is convenient to finding solutions in common problems and has shown to be a rather

useful tool, in itself, portends the electron representing the charge, given Lorentz, is independent of the space where it is located. If the notion that charges exist because of matter is true, the separation of charges in the conductor projects energy onto the interface where they lie. The interface has an interesting feature in that the lag of current from voltage allows the dipole to sustain long enough for the energy to release when it is destroyed. The potential energy in the duration of time of the existence of the dipole is a window to see how the charges project themselves as waves simultaneously [93].

What is to be considered here is that the separation of charges by an electrical force results the electric dipole and the magnetic dipole to exist simultaneously at right angles to each other and that magnetic charge (if it were to exist) is a result of the potential energy of the magnetic moment. It is hypothesized that the coexisting charges, forces, and distribution of energies lie within a manifold, which describes a contiguous set of particles and energies in Minkowski space that produce radiant energies. This has been discussed in previous chapters as a field object. A magnetic dipole is the limit of either a closed loop of electric current or a pair of poles as the dimensions of the source are reduced to zero while keeping the magnetic moment constant. It is a magnetic analogue of the electric dipole. The magnetic monopole, the magnetic analogue to the electric charge, has not yet been proven [97]. The magnetic field around any magnetic source looks increasingly like the field of a magnetic dipole as the distance from the source increases. A new analogy is proposed combining the particle and wave attributes of the separation of charges [16, 48, 95]. The attention on this detail is due to a quandary of the electron having a magnetic dipole moment, that the electron's magnetic moment is not due to a current loop,

but is instead an intrinsic property of the electron [94, 95], the electron has not been observed to have an electric dipole moment [96].

If it is logical to accept the concept of the dipole as well as the manner in which it is manifest in antenna, one can also assume that space-time and its curvature, in the Minkowski sense, is not uniform in the presence of charges relative to their polarized opposites and do not exist as analogous points on a grid. While this assumption is not surprising, the crux is how often are particles of opposite electrical magnitude localized enough so that the force performing the work does not have to “reach” so far as to construct the dipole infeasible? An unhelpful answer would obviously be derived from probability and statistics but does not yield a proper explanation since the abstractions are completely arbitrary. As such, a possible explanation is proffered: that the charges exist as a property of free-space as they exist as a property of the material consisting the charges.

#### 4.1 Basic assumptions

Because of the assumption that a transverse wave is a disturbance, the disturbance contained around the charge is analogous when work is conducted on them, analogous to a quantum interpretation [49]. Such an analogue would allow the selection of charges of equal magnitude yet opposite charge and polarization based on the phase wherein a force is applied to separate them into gauge groups habituating Cartesian zones. The charges are still random in the statistical sense, yet drawn into suspension by simple forces of attraction and repulsion, constrained to perform work. The magnetic field of a dipole is calculated at the limit of a current loop split into two phases, a pair of charges as the source shrinks to a point while keeping the magnetic moment,  $\mathbf{m}$ , constant [97]. For a

current loop, this limit is most easily derived from the vector potential. Outside of the source region, this potential is

$$\mathbf{A}(\mathbf{r}) = \frac{\mu_0}{4\pi} \frac{\mathbf{m} \times \mathbf{r}}{r^3}, \quad (165)$$

and the magnetic flux density is

$$\mathbf{B}(\mathbf{r}) = \nabla \times \mathbf{A} = \frac{\mu_0}{4\pi} \left( \frac{3\mathbf{r}(\mathbf{m} \cdot \mathbf{r})}{r^5} - \frac{\mathbf{m}}{r^3} \right). \quad (166)$$

The scalar potential from the monopole limit is

$$\varphi(\mathbf{r}) = \frac{\mathbf{m} \cdot \mathbf{r}}{4\pi r^3}, \quad (167)$$

and the magnetic field strength at a point charge is

$$\mathbf{H}(\mathbf{r}) = -\nabla \varphi = \frac{1}{4\pi} \left( \frac{3\mathbf{r}(\mathbf{m} \cdot \mathbf{r})}{r^5} - \frac{\mathbf{m}}{r^3} \right) = \frac{\mathbf{B}}{\mu_0}. \quad (168)$$

The magnetic field is assumed symmetric under rotations about the axis of the magnetic moment  $\mathbf{m}$ .

## 4.2 Point-charge representation and forces under separation

Fig.4.1 shows a point-charge emitting a field into free-space, illustrating the axial and lateral emission of energy: electrical for an electric point-charge, magnetic for a magnetic point-charge.

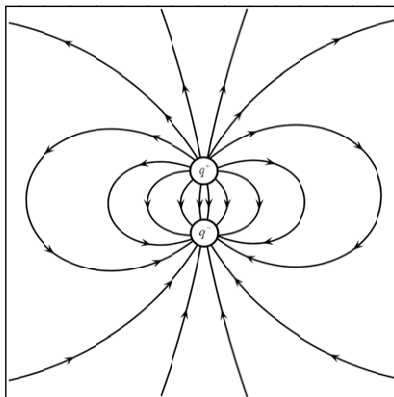


Fig.4.1. Point-charge dipole under separation.

While the pattern of the field emission is uniform over the axes of propagation, the depiction implies the point-charge is not moving, e.g., not subject to any force. Since the Hertz antenna is a dipole through the separation of charges, the generalization implied allows a further suggestion of the energetic state of a point-charge. Since it is due to the conservation of energy and Gauss' law that the length of propagation varies proportionally to the magnitude of the emission and that the length extends forever, in the definition of the electromagnetic force from the four forces of physics, it is relevant to point out there is a formal boundary to the fields in both the axial and lateral directions. It is also relevant to consider that the energy moving toward the boundary does not necessarily disperse from the point-charge, if it is the assumption that the point-charge only contains energy. If this condition were true, the point-charge would be exhausted after a given time. Since it does not exhaust, illustrated by the fact that electrical circuits still function, its internal modulation—or the frequency by which the energy shifts between moving toward and away from the boundary—is the attribute defining its state. Otherwise, an unseen force is applying energy to the point-charge sustaining its state feeding it as a force

holding the equilibrium, so that the field remains conservative. A modified description of the dipole is illustrated of the forces on the separation of charges given their mutual attraction a to a moment  $\mathbf{m}$  is shown in Fig.4.2.

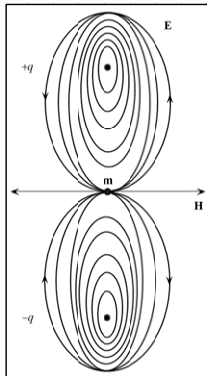


Fig.4.2. Point-charges and the wake pattern of forces.

Fig.4.2 shows point-charges  $+q, -q$  creating the wake pattern lines of attraction at the magnetic moment  $\mathbf{m}$  dispersing energy at right angles to the point charges when work is applied separating them. In Fig.4.3, forces between the point charges reveal a circulating magnetic shearing force  $\vec{F}$  analogous to the Larmor forces [6, 120]. The separation of charges, the rippling of the charges, because of the forces of separation, the wake causes the elliptical feature of the effect of point charges on free-space. The energy from the wake is expressed at right-angles as the magnetic field.

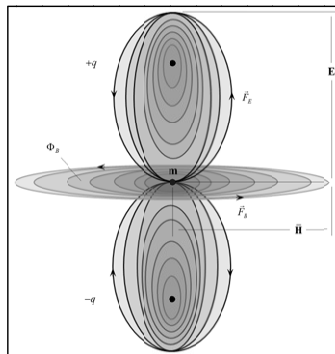


Fig.4.3. Electrostatic dipole model emitting shearing forces,  $\vec{F}_E, \vec{F}_B$ , fixed about the moment  $\mathbf{m}$  and creating the projection  $\bar{\mathbf{H}}$ .

The bending of the force lines illustrates the circulation of force across the moment  $\mathbf{m}$ . The tension between the centers of force illustrates the resulting field exchange between the two point charges and a quantized component of energy traveling along the axis of orientation between the points. The repulsive forces between the points are balanced by the attractive forces folded in the motion of the passing energy creating equilibrium in the system given the circuit potential in volts. Since the system simply either reflects or refracts the passing magnitude of energy, there is no field interaction between the points, only with those in a compatible gauge.

The dipole description has been derived exclusively from the geometry of the antenna used in the oscillator, theoretically supported by coupled-mode theory. The concept illustrated here for the dipole is to emphasize the exchange of energy between itself—as a function of the separation of charges—and other vector-based components it could possibly interact with as a Riemann surface. Greater energies in higher concentrations act to influence other dipoles not unlike gravitational forces between celestial bodies. As such, the architecture of the electrical particles is defined by

absorptions and reflections of quantized energy, in the form of electromagnetic photons. Point-charges on the manifold define each other by the exchange of photons, otherwise, they would be inert and unseen, perhaps confused for the vacuum. The definition of objects on the manifold and how they exchange energy gives rise to this description of the electromagnetic spectrum. Here, the electromagnetic spectrum is defined through two dominant processes: point-charges reflecting a photon and point-charges absorbing a photon.

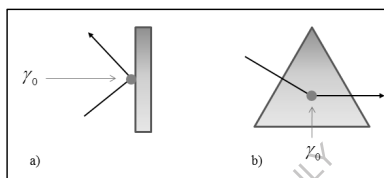


Fig.4.4. Photon reflection and absorption primitives.

Fig.4.4 shows: a) a photon refraction by the dipole field, b) photon absorption by the dipole field. On each spatial surface, a photon carrying electromagnetic energy,  $\gamma_0$ , is represented as a packet of energy moving with a constant magnitude and direction, based on the emission from the transmitter. By inspection,  $\gamma_0$  has the potential to transfer energy to the dipole or to be emitted from it by the acceleration of electrons in the conductor. The point where the photon changes direction by a factor of reflection or refraction indicates a radial point of the intensity of energy by its shift in direction giving rise to the magnitude of the free-space currents  $I_{E_\theta}$ .

### 4.3 Mapping of dipole energy circulation

Consider the contiguous system of energy in a pair of point-charges and their moment, as illustrated in Fig.4.3, to be mapped on a differentiable

manifold around the moment  $\mathbf{m}$ , where the vector,  $\vec{\omega}$ , intersecting at right-angles, is the direction of force from the displacement of  $q^+$  and  $q^-$ , resulting the separation. The big question here is: what if the projection field,  $\bar{\mathbf{H}}$ , separates the charges at a minimum distance and does not allow them to completely come back together, preserving the energy involved in the work for their initial separation?

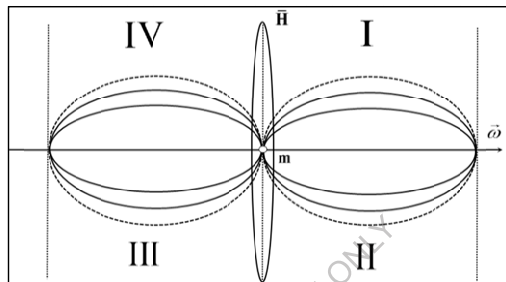


Fig.4.5. Propagation zones for dipole energy circulation.

The implicit solution for the oscillations in the circuit, in terms of charge,  $q$ , is,

$$q = q_{\max} e^{-tR/2L} \cos(\omega't + \theta). \quad (169)$$

Maximum current at any arbitrary point is,

$$i = -\omega q_{\max} \sin(\omega t + \theta) = -i_{\max} \sin(\omega t + \theta), \quad (170)$$

where the first-order angular frequency of the acceleration force, is,

$$\omega' = \sqrt{\frac{1}{LC} - \left(\frac{R}{2L}\right)^2}, \quad (171)$$

pushing the charges into these zones, separated by a distance from their shared moment,  $\mathbf{m}$ . Now, the total energy oscillating in the circuit is, as

before, a factor of the capacitance, inductance, and resonance frequency dependent upon the polarization of the material comprising the loop. If the phase between the oscillating forcive and charges are accounted for, the stored energy is expressed as,

$$\begin{aligned}
 U_C &= \frac{q^2}{2C} \cos^2(\omega t + \theta), \\
 U_L &= \frac{1}{2} L i^2 \\
 &= \frac{1}{2} L \omega^2 q^2 \sin^2(\omega t + \theta) \\
 &= \frac{q^2}{2C} \sin^2(\omega t + \theta) \\
 &= i^2 R,
 \end{aligned} \tag{172}$$

while the total energy stored in each oscillation is,

$$U_C + U_L \approx -e^{-iR/L}. \tag{173}$$

Radial contributions cancel out by the assumption of a uniform field. The resulting field  $\mathbf{B}$  is projected along  $d_B$  as  $\mathbf{B}_z$ , of Fig.2.8, where the cosine theta, of (22), is an indicator of the angle of separation of charges lying in the one of the planes illustrated in Fig.4.5. To reiterate the formulations again: because of the symmetry of the space consisting the interior of the loop and that the loop lies within zones I, II, III, and IV, the contribution

$\delta\mathbf{B}$  is  $r/d$  times  $\mu_0 \mathbf{r} \times \delta\mathbf{I} / 4\pi r^3$ , as,

$$\delta\mathbf{B}_z = \frac{r}{d} \frac{\mu_0 I}{4\pi d^2} \delta s. \tag{174}$$

All the elements,  $\delta s$ , consist the circumference for  $\mathbf{B}_z$ , as,

$$\mathbf{B}_z = 2\pi r \frac{r}{d} \frac{\mu_0 I}{4\pi d^2} = \frac{1}{2} \frac{\mu_0 I r^2}{d^3}. \quad (175)$$

The field emitted by the loop is,

$$\mathbf{B} = \frac{\mu_0 I}{2r} \alpha n, \quad (176)$$

where  $\alpha$  is an additional value due to accounting for the acceleration manifest in the projection,  $\bar{\mathbf{H}}$ ,

$$\alpha = \cos(\theta), \quad (177)$$

and  $n$  is the number of contiguous loops. If  $n = 1$ , it is a circular loop. If  $n > 1$ , it is an area loop.

If the dipole is not destroyed during the circulation of energy in the circuit via the projection of the field on the antenna at the interface of free-space, perhaps a circuit can be constructed to preserve the dipole from being destroyed at the power supply. If a way could be accounted for each of the charges in the system and suitable paths could be constructed, such is a strong theoretical possibility, given the evidence of the research conducted in this work. A proposed addition to the circuit of a single coupled-mode, shown in Fig.2.27, is illustrated in Fig.4.6.

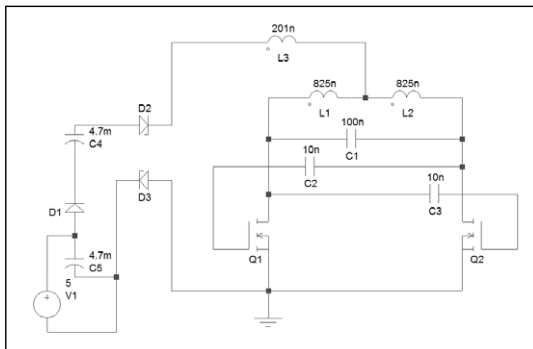


Fig.4.6. Dipole preservation circuit.

If such a circuit could be utilized in the manner described here and facilitated by future research, it could alter drastically the dynamic of how energy is expressed in our current technological era.

## 5 Application and control

The bulk of this work has discussed the theory and a prototype of wireless power by magnetic resonance. This chapter will introduce applications of the idea to control theory in the paradigm of human-machine interfaces, robotic control, and space applications.

The machine discussed in this work relates particularly to the transmission of electromagnetic energy in the form of currents through space and matter at controlled frequency, amplitude, and characteristic impedance to facilitate the transmission of power and information over medium-range distances for generalized use of powering robotic, cybernetic, and consumer devices tuned to acquire the transmission via singular and multiple receivers at singular or multiple resonant frequencies. Although this machine can be widely applied to wireless transmission in general, its main application is expected to be multiple resonance-frequency power and

communication between a single source transmitter and multiple receivers which could be robotic colonies, cybernetic implants, or collections of consumer devices in the given range allowable by the ratio of transmission frequency to length of region.

Applications, as noted earlier in this work, are vast. However, they can be restricted to particular classes of applications. Those being: in human-proximity, medical, cybernetic, wearable, direct neural interfacing or other human-integrated system, robotic power distribution and control where choice can be made an integral part of the programming of intelligent machines, and finally in this text, space applications.

### **5.1.1 A brief discourse on the potential of medical device applications**

An application of a transmitter using a single coupled-mode was examined whether or not it would be useful if coupled *directly* to the human nervous system. As noted in this work, the system described in §2 does not interact with human tissues, e.g., if I place my hand in the distance between the transmitter and receiver, the signal does not attenuate. However, using a thin sheet of metal does. Thought was given to the notion that since eddy currents are flowing in the thin metal sheet when it is placed between the distance, would it be possible to use those same currents in a different orientation and placed in contact with a point on my body?

Wireless power transfer in human proximity has been demonstrated as a viable means to transmit electrical currents between an external electrical circuit and the human body [123, 149, 150, 151]. Although these methods have examined wireless power in terms with the aim to reduce interaction of the magnetic-resonant field with tissues lying in the path between transmitter coil and the receiving implant, this section by contrast will

examine the use of the same magnetic-resonant field to exchange energy between transmitter coil and neuronal tissues *without* the consideration of an implant, following the work set out in [106]. That is, charging chains of neurons under the area of an antenna and checking their spiking responses from stimuli represented in the transmitted currents. The amount of current transferred is related to the neuronal response regarding potential and inductance parameters of the cells themselves.

Conventional wisdom has shown that when designed in such a manner as to possess a low enough frequency [124, 125], or the transmission system does not react with off-resonant objects [124, 152] a charged antenna emitting a magnetic field generally does not react strongly when placed in proximity to the human body. Rather, the energy passes through the body transferring to a strongly-coupled resonant load [124, 152, 153]. An alteration to the arrangement is required for the energy to disperse within the body. Attention must be given to the design of the antenna that it possesses the right amount of potential to allow for the electrical systems of the body to draw the currents from the circuit driving it. Beaming power onto delicate electrical cells is undesirable in this case and a passive model similar to the pattern of a set of relay resonators [106, 154], is preferred. Other methods have suggested the use of acoustically-based waves is a valid approach to transmitting energy within the body [69]. While this approach has substantial merits when describing transmission through body tissues and the transference of energy to implanted circuits, it is not interested in such high frequencies being applied, rather, it will engage transmission at a much lower range of  $< 1 \text{ MHz}$  [150].

This section will briefly describe the mechanics of linking of a magnetic resonant field to groups of neuronal cells via the membrane potential of the

cells (in volts) and the potential in the loop coil (in volts times seconds per  $\text{m}^2$ ). It will also discuss an arrangement of a loop coil powered by an external circuit which transmits ambient power, that is, by a distortions present in the inductances rather than beaming to the linked cells.

The experiment is to apply low-power currents to an area in the Psoas Minor and Psoas Major muscle group of the lower back. It is conducted to determine two things: 1. If the apparatus could transfer a steady flow of energy to the muscle group by measuring after fifteen minutes of exposure the neurons under the area of the metallic disc if the neurons manifest a fast spiking (with oscillatory) pattern, and, 2. Measure how long the neurons under the area of the disc which had been exposed they continued manifesting the fast spiking pattern. By defining the threshold of the experiment in this manner, it could be determined how efficient the apparatus is at energy transfer and demonstrate the neural response to applied magnetic-resonant fields. Data sets from the EEG device are taken for an interval of five minutes.

The area, as measured by four EEG probes, before exposure is shown in Fig.5.1. The figure shows the two channels mixed over a center rest value of 0. EEG probes numbered one (in red) and two (in blue), each with a positive and negative polarity show that the pattern in exhibiting a regular spiking pattern with a maximum average level of  $60 \mu\text{V}$ .

Next, the area was exposed to magnetic resonant fields calibrated through the magnetic potential between the apparatus and the subject's body. Calibration is achieved by manually circulating the metallic disc against the surface of the skin where exposure is planned. The motion creates charges in the disc which are absorbed by the conductor in the antenna creating a

strain in the surrounding air. The strain establishes a governing effect for a brief time on the subsequent oscillation force, giving it a characteristic impedance which is more closely matched to that of the area if the calibration had not been performed. This impedance matching increases the resonant linking between the apparatus and the area making it more tightly coupled.

The area, as measured by four EEG probes, immediately after fifteen minutes of exposure by the apparatus is shown in Fig.5.2. The figure shows the same measurement points in the graph but in this instance they are exhibiting a fast spiking pattern. It is also shown in the figure that each channel is measuring an oscillatory pattern in the firing of the neurons.

The area, as measured by four EEG probes, 76 minutes after exposure is shown in Fig.5.3. The figure shows each channel split so the pattern can be better shown. The pattern shown that the Psoas Minor is still exhibiting a fast spiking pattern while the Psoas Major has returned to its original pattern before exposure.

The area, as measured by four EEG probes, 149 minutes after exposure is shown in Fig.5.4. The pattern shows that the Psoas Minor has slowed its oscillatory pattern yet is still exhibiting a fast spiking pattern while the Psoas Major has remained in its original pattern before exposure.

The area, as measured by four EEG probes, 160 minutes after exposure is shown in Fig.5.5. The pattern shows that the Psoas Minor has slowed its oscillatory pattern and is not exhibiting a fast spiking pattern while the Psoas Major has slowed compared to its original pattern before exposure.

The area, as measured by four EEG probes, 180 minutes after exposure is shown in Fig.5.6. The pattern shows that the Psoas Minor has slowed its oscillatory pattern and is returning to its original pattern before exposure while the Psoas Major has settled to its original signal level before exposure.

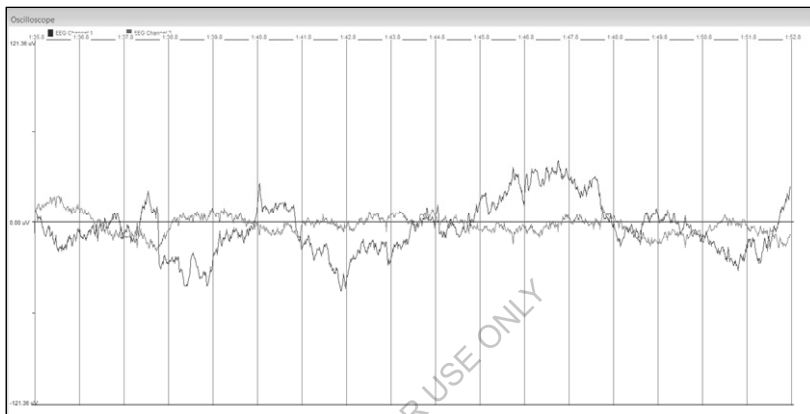


Fig.5.1. EEG measurement over the Psoas Major/Minor under ordinary conditions.

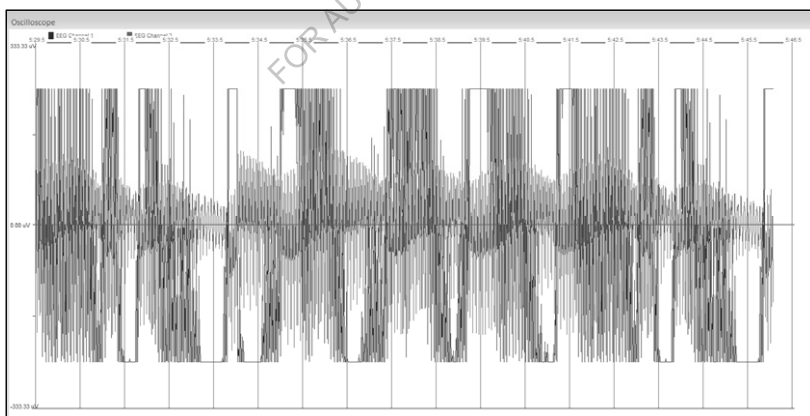


Fig.5.2. EEG measurement over the Psoas Major/Minor 15 minutes after exposure.

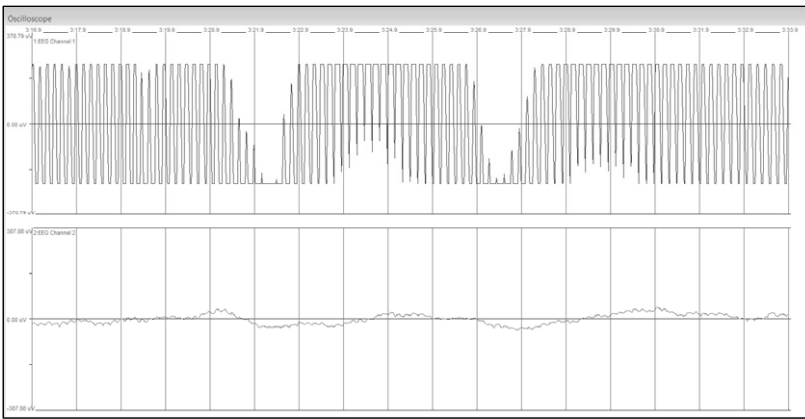


Fig.5.3. EEG measurement over the Psoas Major/Minor 76 minutes after exposure.

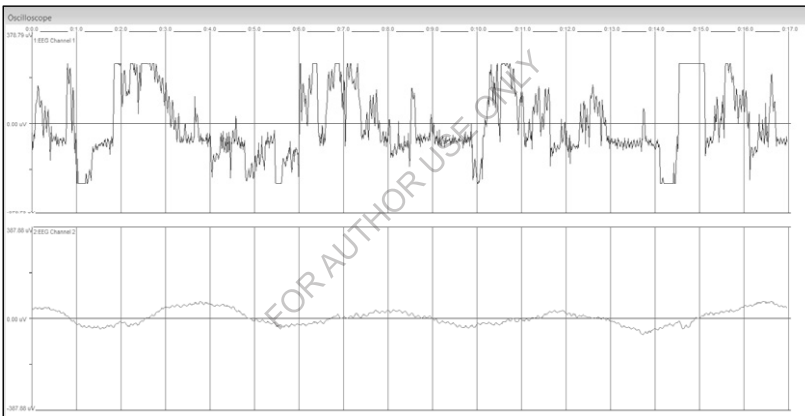


Fig.5.4. EEG measurement over the Psoas Major/Minor 149 minutes after exposure.

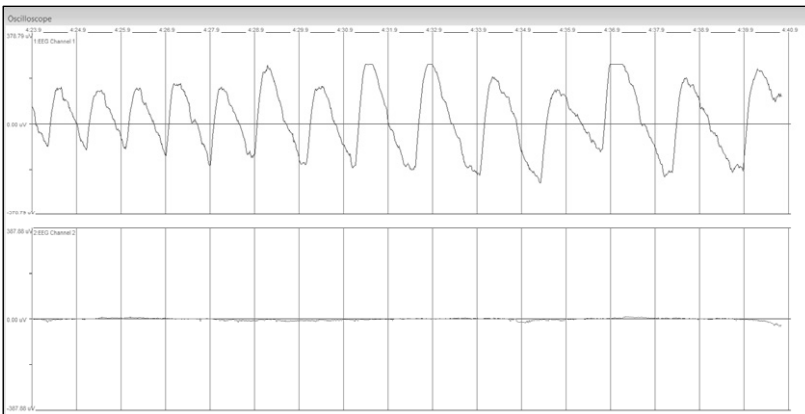


Fig.5.5. EEG measurement over the Psoas Major/Minor 160 minutes after exposure.

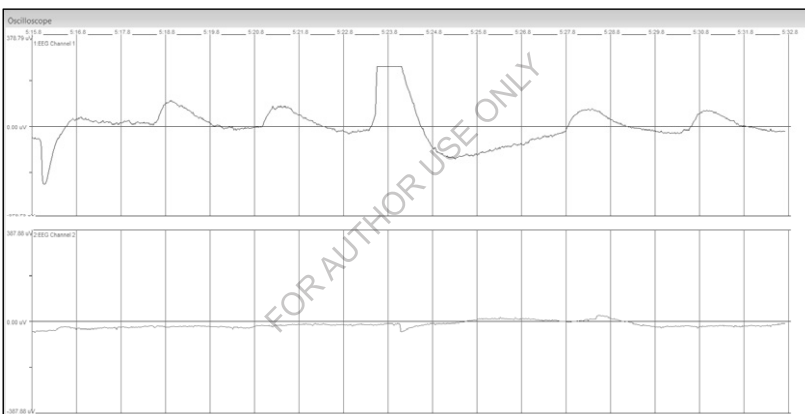


Fig.5.6. EEG measurement over the Psoas Major/Minor 180 minutes after exposure.

The experiments demonstrate the apparatus transfers energy to neurons in its field, by means of the metallic disc, and that those neurons which absorb the energy, store it for a period of time perhaps transferring it to neighboring cells before discharging and returning to their normal patterns and signal levels.

### 5.1.2 Featured power and choice in the machine

Following the discussion of the transmission of wireless energy in the form of currents through space and matter at controlled frequency, amplitude, and characteristic impedance, this section will discuss an application of the technology for controlling and powering mobile entities using singular and multiple receivers at singular or multiple resonant frequencies, illustrated in Fig.5.7.

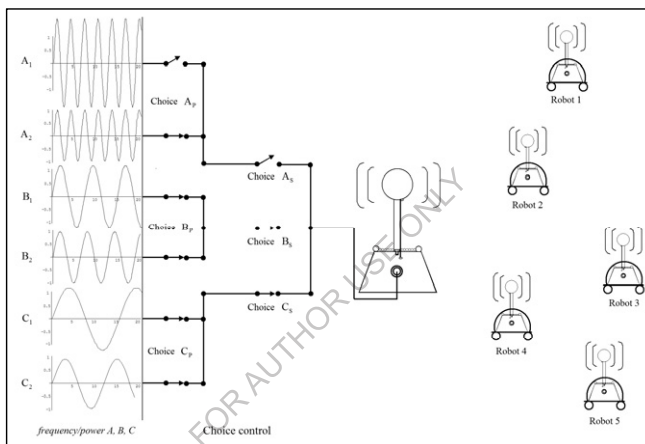


Fig.5.7. Featured power environment using choice control.

Although the description discussed throughout this work is and can be widely applied to many types of wireless transmission schemes in general, this application is multiple resonance-frequency power and communication between a single source transmitter and multiple receivers which could be robotic colonies, cybernetic implants, or collections of devices in a given range allowable by the ratio of transmission frequency to length of the region. For the purposes here, this section will discuss the application of wireless power transmission to robotic platforms.

Recharging models for autonomous robotic platforms have been classically viewed in the context of behavioral responses, yielding interesting insights [128 - 131]. A central theme is the consideration of consequential behavior to the design of a recharging model to allow freedom of emergence [132 - 135]. Given a choice, this freedom is enforced. This section will describe generalized recharging models and discuss the behavior exhibited by a robot pursuing a source of food, i.e., replenishing the energy in its onboard systems. Concepts such as transformation between states and feedback will be introduced as the mechanisms of choice, and a novel feeding model will be proposed which expands emergent freedom by an expression of the survival instinct.

W. Grey Walter first proposed feeding behavior in artificial systems as a means to understand fundamental characteristic behavior in living systems [128, 132, 133]. Owen Holland notes [136]:

In his writings about the tortoises, Grey Walter gave much weight to an attribute he called ‘internal stability’—the claimed ability of the tortoises to maintain their battery charge within limits by recharging themselves when necessary. A feature of the tortoises’ circuitry was that, as the batteries became exhausted, the amplifier gain decreased, making it increasingly difficult to produce behavior pattern N (negative phototropism).

By purposefully including circuital features to manipulate responses for an activity such as recharging, Walter was able to foster emergent behavior in his tortoises. He is suggesting that an artificial system could be designed in such a manner to study behaviors commonly witnessed in biological systems [137]. In light of Walter’s work, this section proposes two research questions:

1. Can a robot be given the ability to make its own choice?

2. Can a robot be made aware of a dependency between its choices and survival?

To facilitate answers to these questions, four goal-based assumptions [138, 139] illustrate the necessary parameters in the model:

1. The artificial system under examination is fully autonomous, that is, once the system is started it requires no further input from an operator. In order to be autonomous, the system is self-sufficient, e.g., it has the necessary components for its operation and runs continuously.
2. The artificial system exists *in situ* with its environment and composes algorithms in response to its interaction with it.
3. The artificial system possesses a system of behaviors relevant to its purpose, the ability to evolve, and a set of choices within the scope of its design.
4. The artificial system leverages behaviors indistinguishable from biological systems, from the observer's point of view. To be an effective model, a principle of equivalence illustrates the behaviors are archetypical, e.g., such behaviors are essentially identical for a biological organism with similar environmental pressures.

This section will present a characteristic model of robotic feeding. It will address the model first in a generalized form, increase its complexity, then introduce a wireless-power delivery method containing a more colorful set of feeding behaviors. Lastly, it will describe a novel circuit that introduces the capability to ascribe the survival instinct to the robot. It is the goal of this section to illustrate a method and means of the quantification in an algorithm of the consequence of choice and decision-making. It is argued

such a study is valuable not only for artificial but for biological systems to better understand primal features of life and that they are far more accessible than once believed. Such an understanding evolves designs of robotic systems that mimic natural forms giving them greater independence in environments undergoing changing conditions. It is impact of the realization that a richer set of behaviors offers the capability for study of the phenomenon of the survival instinct not only artificial systems but also for living systems.

#### **5.1.2.1 General model of robotic feeding and the application of choice**

Apart from strict considerations as a form of robust control [140] or event-driven agents [141], robotic feeding considered here is analogous in form and function to an activity [142] exhibited by organic entities, and can be reduced to a simple model of goal-seeking behavior. Such a model is illustrated in Fig.5.8.

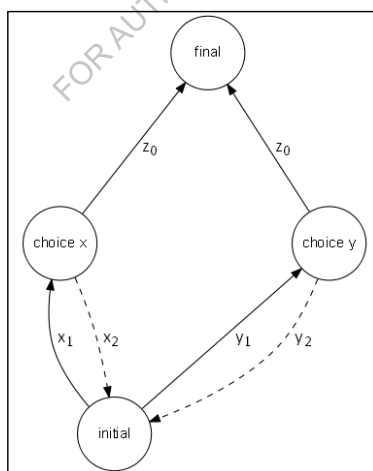


Fig.5.8. Activity of robotic feeding behavior.

A robot that is seeking power to recharge its onboard power system begins its activity at *initial* and is presented with one or more choices—in this example, two choices labeled *x* and *y*—whereby to reach its necessary goal *final*. In order to decide which path to pursue,  $x_1$  and  $x_2$  toward *x*,  $y_1$  and  $y_2$  toward *y*, weights are assigned based on either success or failure of the path leading to the pursuit of *final* at  $z_0$ . Through repetition of this activity of seeking power, consecutive weights are averaged and the robot “prefers” pursuit of one path over the other because of positive experiences as well as negative feedback. Pseudocode of this activity is shown in Fig.5.9.

```

Activity of robotic feeding behavior - Pseudocode
--Task-
Recharge the batteries present in the system before power is exhausted.

--Activity-
Notice that the power level to sustain continuous operation is low enough to require recharge.
Search stored data for available recharging types, of these types retrieve the weighted values
to determine which is most optimal. If these values are equal to zero, generate a random number
to choose which choice to pursue.

Pursue choice 'x'. If recharging is reached, store a value of one for variable 'x1'; if
recharging is not reached, store a value of zero for variable 'x1'.

If recharging is not reached from pursuit of choice 'x', pursue choice 'y'. If recharging
is reached, store a value of one for variable 'y1'; if recharging is not reached, store a
value of zero for variable 'y1'.

When the task is called, collect the weighted values for each recharging type. Sort the values
in descending order. Pursue those choices on the list which have greater values. When pursuing
a choice by greater value and recharging is not reached, divide the value by two and store
the new value.

--End Activity--

```

Fig.5.9. Activity of robotic feeding behavior – Pseudocode.

The notion of the activity as a template for robotic feeding behavior serves as the primary theme for the description of the environment containing the robot. As such, the template can be expanded to include more detail relevant to ascribed behavior. In terms of defining a set of environmental factors which facilitate the activity of power seeking behavior, the process is modeled as a run-to-completion state machine, shown in Fig.5.10.

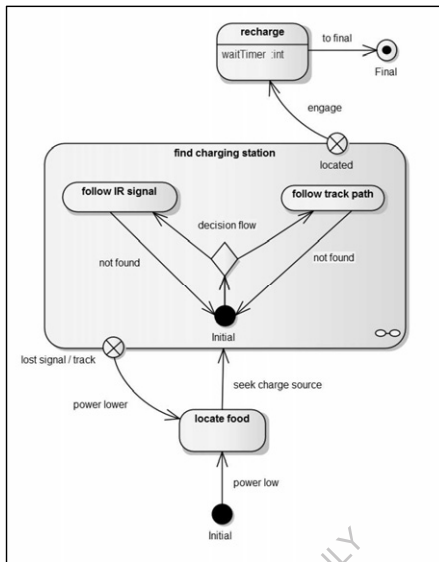


Fig.5.10. Finite-state diagram of robotic power-seeking behavior.

The components of Fig.5.10 depict the template in terms of a typical finite-state machine for a robot tasked with finding a recharging source. In ascribing behavior in an empathetic context, it is performing the task of searching for food. This activity is started when notified by the event *power low* wherein it will *locate food*. It will execute *seek charge source* entering the state machine.

The states, represented as boxes, are: *Initial*, *locate food*, *feeding*, and the state machine *find charging station* that contains *follow IR signal* and *follow track path*. The actions, represented as crossed circles, are two exits from the state machine. One is for a positive result, *located*, and one is for a negative result, *lost signal/track*. The transformations, represented as arrows: *power low*, *power lower*, *located*, are consequences of the choice following *seek charge source*. The transformation at the junction of *decision flow* indicates the decision since more than one outcome is present

and the choice is made consequential of environmental factors. The software controlling the decision stipulates, without optimization, that it based on positive sensor feedback—if the IR signal or the track path is discovered first. The first acted upon, the alternative discarded unless the former returns a negative result.

The robot enters the state machine at the *Initial* orb when the sensor responsible for monitoring battery level notifies the operating system that power is low, noted in the transformation. When within the action *locate food*, a routine in the program executes the behavior for optimal seeking of a charge source. The transition of this behavior leads to entry into the *find charging station* state machine at *Initial*. If a positive result is obtained—that either of the choices are successful—the robot exits at *located*, and the transformation *engage* leads to the state *recharge*. When *waitTimer* expires, it will exit at *Final*. In terms of the complete behavior in this diagram, most of the complex behaviors are executed in the state machine, given the choice in the decision flow between to follow an infrared (IR) signal or follow a track path. Existence of such a choice is highly dependent on multiple solutions to the charging problem, if the state machine did not have both an IR source and track path to power to guide the robot, then choice in this context is irrelevant. In Fig.5.10, the experience derived from results of trying to follow one branch or another—found or not found—is one case of behavior. The experience derived from the pursuit of the specific choice—*located* or *lost signal/track*—is a second case. In the first case, not finding an IR source or a track path could be the result of neither existing nor unable to be found due to the causality of a sensor function designed to detect them. In the second case, having found the IR source or the track path but not locating it will keep motivation to continue finding it, or the robot remaining inside *find charging station*.

When the state machine fails to return a positive result, it will exit at *lost signal/track*, the transformation then notes *power lower*, when compared to the transformation *power low*.

### 5.1.2.2 Decision-making embedded within transformation logic

Choice, in the scope detailed here, is a phenomenon isolated in the transformation between states yielding a consequence of one outcome. Given the power to select one outcome from many, the weight of consequence becomes determinate, e.g., one decision more optimal than another, to within a tolerance of 0.1 between weight values. From Fig.5.10, once the event for *locate food* is triggered, Fig.5.11 represents the behavior in the state machine *find charging station*.

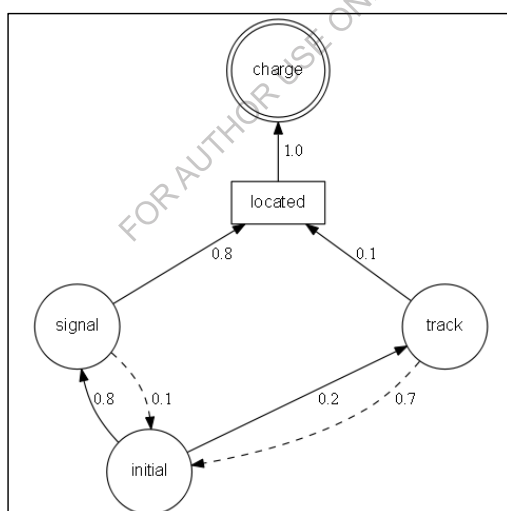


Fig.5.11. Runtime choice-weights for consequential decision-making.

The robot enters the diagram at *initial* and by reading the weights, can determine that recharging by using *signal* is better than *track* given the comparison positive weights (solid line) are 0.8 and 0.2, the comparison

negative weights (dashed line) are 0.1 and 0.7, respectively. Within the context of the program, the weights for each decision path are averaged for each successful result. Each time the robot enters the *find charging station* state machine, it will learn to choose the optimal path because of the higher value of the weight. If decision paths have the same weight, a choice that is sufficiently random would assign a decision. The ethological implication of the modeled behavior embedded in the diagram of Fig.5.11 is the dynamic of it at different points of time during the activity of seeking a feeding source. The term “feeding” is applied here with the same scope as in its original biological definition, that an entity pursuing food—in the case of the robot, energy—is exercising an adaptation for optimization of its survival.

According to Ashby [143, 144], states and their transformations are constructs of a characteristic map of behavior leading to the thinking process of entities, as noted here by the weights for each decision including positive and negative feedback. The implication is the fitness of the model and its completeness. What is illustrated in the runtime diagram are the degrees of change that the robot goes through during a finite quantity of time while attaining its goal. The model does not try to reveal the mechanisms behind the operations directly, rather, the character of the transition between states alluding to the behavior of the sequence. The goal is to reveal behavior of the robot during its power-seeking activity and gain evidence for the survival instinct in artificial systems. To accomplish this goal, in addition to a standard battery-charging station, a wireless charging model in presented next.

### 5.1.2.3 A wireless-power model of robotic feeding

In the previous model, a greater magnitude of freedom is offered by the presence of an IR signal to help guide the robot to its feeding source—as opposed to only having a track path. The presence of the signal allows the robot to receive information about the source, finding it more readily and efficiently, as illustrated by the weights in Fig.5.11. The wireless-power feeding model builds upon this, adding more degrees of freedom to the activity. The combined model in the form of a state machine is shown in Fig.5.12.

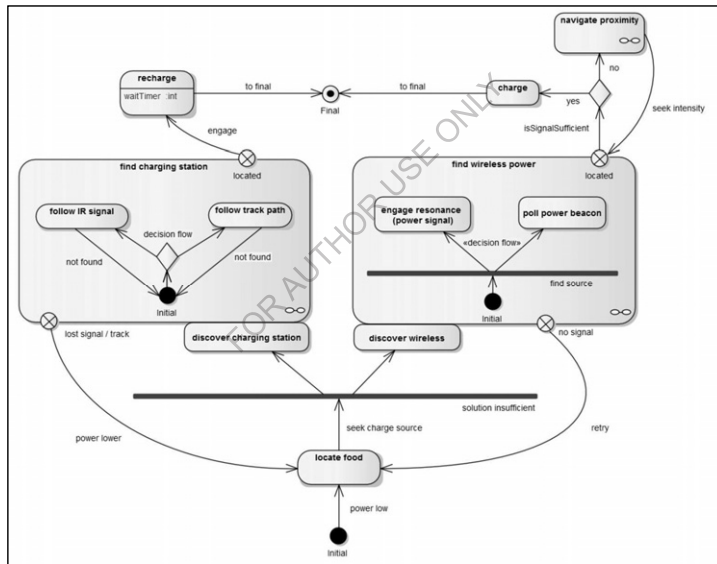


Fig.5.12. Finite-state diagram of power seeking behavior for charging station and wireless power.

The components of Fig.5.12 encapsulate behaviors in the same manner as Fig.5.10, however, seeking has an additional dimension associated with it: there is also the presence of a power signal that only requires a decision to engage a connection to feed, allowing greater cooperation between the

robot and its environment [145] and freedom in its seeking algorithm. To the left of Fig.5.12 is the *find charging station* state machine with its exit *located* leading to the transformation *engage* where it will stay in *recharge* until *waitTimer* determines when recharging is complete, wherein it leaves at *Final*. To the right of Fig.5.12 is the *find wireless power* state machine with its exit *located* leading to the Boolean decision of *isSignalSufficient* will tell the robot if it is in a suitable proximity to the power signal to perform recharging at *charge*, else to *navigate proximity* where it will *seek intensity* until the Boolean is satisfied. If true, it leaves at *Final*.

In the method demonstrated by Fig.5.12, when the robot enters at the *Initial* orb noting the transformation *power low*, it will execute *seek charge source*. It is presented with a boundary where it crosses to *discover charging station* or *discover wireless*. The boundary stipulates crossing it in the opposite direction, when the negative exits *lost signal/track* or *no signal* are noted, will place it again at *seek charge source*. After satisfying the condition at *discover wireless*, the robot enters the *find wireless power* state machine at *Initial*. Because its goal is to *find* a source, it is presented with two choices—*poll power beacon* and *engage resonance*. It can send out a polling signal to detect feedback whether or not the power signal is in range of its onboard wireless power absorption system. If the *poll power beacon* can lead the robot to the signal, it can then execute *engage resonance*, then exit at *located*.

The wireless power system used in the model relies on the physical principle of coupled modes [107], where the robot has a coil-circuit with selective components that, when engaged, determines the amount of coupling to the power signal [111, 146], translating to the intensity of the power to be absorbed. This activity is represented in Fig.5.12 by *engage*

*resonance*. In terms similar to the runtime behavior diagram of Fig.5.11, Fig.5.13 describes the wireless power scenario including the notion of the domain that encapsulates the different actions in the behavior.

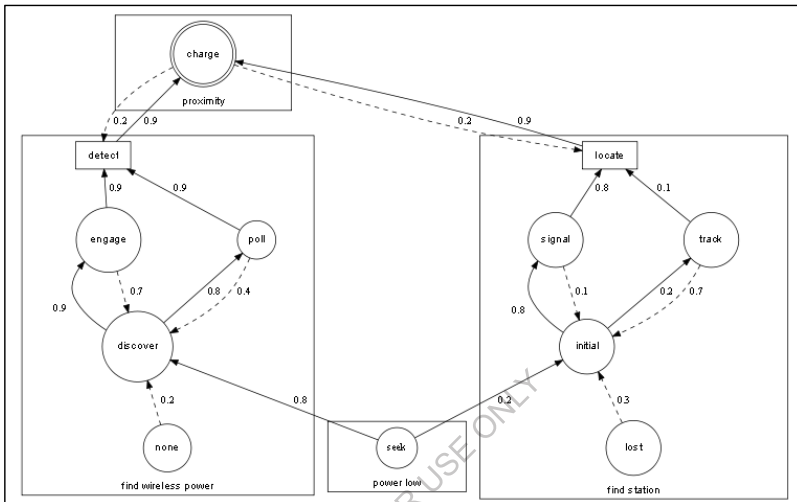


Fig.5.13. Runtime choice-weights for consequential decision-making in complex power-signaling.

The robot enters the diagram at the domain *power low* and by reading the weights at *seek*, determines that recharging by using *find wireless power* is better than *find station* given the comparison weights are 0.8 and 0.2, respectively. At the start, *discover* and *initial* also contain negative weights of 0.2 and 0.3, respectively. Following the highest weight into the domain *find wireless power*, it will read at *discover* that *engage* and *poll* have near equal values, within the tolerance of 0.1. However, since the negative weights are 0.7 and 0.4, respectively, the better choice would be to *poll* since it leads to *detect* with a higher probability, a weighted value of 0.9. The transformation between *detect* and *charge* shows the exit from *find*

*wireless power* and entry into *proximity* is strong, with a value of 0.9, with minimal negative feedback, with a value of 0.2.

In this scenario, the weights for each decision path are averaged for each successful result. Having traversed the entirety of choice, or having given the experience by seeding the weight values, the robot knows the optimal path. The ethological implication of the modeled behavior embedded in the diagram of Fig.5.13 is the additional domain wireless recharging contributes to “laziness”. Entry into the domain *find wireless power* will lead to recharging, i.e., reach the goal of *final*, with a high probability of success with the robot having to use the fewest amount of resources to attain its goal of survival. Essentially, the availability of choices to pursue in the model, subtended by weights, allows more degrees of freedom to the runtime yielding insights into how a robot would optimize its choices and how it would express the concept of “laziness” when choosing feeding sources. The array of choice lies between the extremes of charged and uncharged batteries, settling around an equilibrium of constant discharging over time, the weight of which, determined by the amount of runtime activity—searching, processing data, and using sensors. The cooperative nature of the design recalls one final contention: how does the coordination of the activity contribute to the concept of survival?

#### 5.1.2.4 The entropic circuit

Entropy is defined as the number of ways a thermodynamic system can be arranged as it experiences time. A system undergoing entropy would dissociate itself, decaying into disorder. This definition of entropy can be applied to robotic feeding models in terms of the arrangement of behavior following consequence of choice and the level of sustainability, e.g., the amount of energy the robot possesses at any point during runtime. The

measure of entropy would be the success or failure of the robot to attend to its survival, that is, maintain runtime verses shutting down due to the lack of power. Fig.5.14 depicts a circuit that introduces entropy, a dependency in the onboard energy system wherein the robot is made aware of the ability to control its own survival.

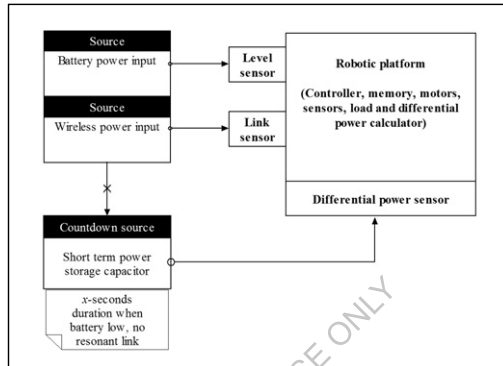


Fig.5.14. Functional diagram of an entropic circuit.

To the right side of Fig.5.14 is the robotic platform, this consists of the usual components that a robotic form would take, given its design considerations. To this is added a sensor to manage the resonant link [107, 111, 146] and a differential power sensor to monitor the value of the operating power and the value of the countdown source. The level sensor measures power stored in the batteries; compared with the value at the differential power sensor, the operating “mood” would be set: normal, seeking, charging, or distressed. To the left side of Fig.5.14 are the sources of energy—battery and wireless power—and the countdown source which is charged by the wireless power transmission. It contains a short-term storage capacitor of a value indicating the amount of available runtime if the robot had to rely solely on its energy.

Entropy, represented in the functional circuit diagram in Fig.5.14, is used to model the necessary quantitative information to specify the exact physical state of a system at any given point in time. In other words, the adaption the robot undertakes to counterbalance its effects. Similar to thermodynamic entropy, it is used as a measure of the changes in information manipulation as the runtime evolves from its initial condition at startup. The design allows the freedom for the machine to remain online indefinitely, provided it can execute the set of rules leading to the states for the best outcome. In a theoretical context, the circuit prefers to optimize equilibrium at the expense of decay, analogously to the control of the extremes of life and death by choice and experience by consequence. It reinforces causality. If the robot does not make the right choices to maintain its survival, it turns off and the data in memory is truncated, or lost, depending on the conditions of the experiment. If the robot does not follow results from weights or calls *poll* at a critical moment when it should have called *engage*, it will not receive the proper power. If the experience gained from its life cycle is held in non-volatile memory that will be stored when the power is off, this is written into the program as such. Otherwise, if volatile memory is used, cessation of activity is the result and the data erased.

#### **5.1.2.5 Thoughts on featured power and choice**

This section has described models of robotic feeding and introduced the phenomenon of choice to direct causal outcomes following consequence. It has discussed two detailed models of different feeding strategies, which have yielded an experimental paradigm to empirically test the fuzzy concept of choice, survival, and the consequence of behavior following knowledge of entropy. The models presented here yield a richer set of results and give a means to validate whether or not artificial systems

possesses what biological systems classify as the survival instinct. Some of the instincts to manifest are: where the robot has problems accessing the station, by mechanical error or environmental issues, coupling to the energy field, or that it commits suicide by giving up to the imposed condition of the entropic circuit. Decision-making is internalized by the robot and removed from an interaction with humans. The system is independent and free from external intervention apart from initial conditioning or implementation of the starter program that will provide the machine its beginning point and tasks to perform during its life cycle including sample weights to preclude consequential decisions.

A new and distinct methodology offers not to only model and quantify artificial life but to illustrate a method whereby a machine can construct an understanding about unknown events, while arriving at insights about the structure of the environment it finds itself in. The power in this approach is the artificial system more closely mimics a living system by collecting memory of each experience navigating the finite-states of feeding behavior. To facilitate this, the composite state machine presented here is contained in a modular, domain-specific language. It describes a set of features relevant to the space in which the program will operate allowing creation of members aiding in a more robust development methodology [147]. This is important in this context because, as in the case with Walter, a rigidly defined platform is a mathematical framework yielding higher orders of behavior, the quantification of which reduces the need for speculation by the observer. Theoretically, a machine would come to realize that it has the power to control its own life and death. The study of robotic feeding models, choice, and the survival mechanism contributes to the body of knowledge surrounding research into the properties of cognition in a very succinct way. Rodney Brooks notes [148]:

Researchers in artificial intelligence and artificial life are interested in understanding the properties of living organisms so that they can build artificial systems that exhibit these properties for useful purposes. AI researchers are interested mostly in perception, cognition and generation of action, whereas artificial life focuses on evolution, reproduction, morphogenesis and metabolism. Neither of these disciplines is a conventional science; rather, they are a mixture of science and engineering. Despite, or perhaps because of, this hybrid structure, both disciplines have been very successful and our world is full of their products.

The advantage for an entropic circuit lies in a continuous set of activities for the robot and its long-term behavior. It will lead to advances in understanding artificial ethological concepts executing routines in the scope of the domains. Additionally, as a composite phenomenon, it can manifest a robot in the manner of an artificial life form. Furthermore, a global picture of behavior of the sum of transformations between states and the choices can be used to describe the “personality” of the robot’s runtime. The pursuit of equilibrium between the extremes of a requisite variety of the choice between different recharging models—a station or a wireless power source—follows closely the description first set out by Walter.

### **5.1.3 Solar panels for spacecraft**

An intriguing proposition is the use of wireless power to act as a flexible joint between power connectors in energized circuits. Uses in very diverse environments allow coupling between disparate components and inhomogeneous connections. Greater freedom of design is expressed and a less rigid insistence on straight-line current delivery. There are advantages

to using wireless powered couplings. The most predominant are the ability to allow a larger ratio of error between electronic and mechanical components. In conventional circuitry, wires restrict what could be a more efficient and advantageous strategy when discovering by experience more optimal solutions to power problems. Equally, there are disadvantages to using wireless powered couplings. While there is a loss of lengths of cabling, there is an addition of circuitry and the introduction of alternating currents at radio-frequencies. In intelligent designs, circuitry is kept to a minimum and energy is contained to power transistors. By proper foresight in the application where the circuits are to be used, the currents can be contained to the paths they conduct upon. What should also be considered is the efficiency of the scheme. An excellent measure is the difference between energy input to a system compared to the energy extracted. While cabling has shown itself as a highly efficient means of transmitting currents, the direct current (dc) source of solar panel technologies over lengths and temperatures can drop significantly. Oscillating currents (ac) have proven time and time again their great advantage over dc designs. Wireless-powered schemes at stable radio-frequencies have demonstrated better efficiencies at gaps as large as twenty-five centimeters compared to those of cabled alternatives. Highly energized circuits are necessary to satisfy power-hungry equipment. Large solar arrays can generate substantial amounts of power. Converting from dc to an oscillating scheme seems daunting but with the choice of a properly designed circuit using appropriate semiconductor technologies, conversion ratios are maintained between 90 and 95%.

The information contained in this work is proposing a new approach in wireless power couplings which are reliable, high-powered, and robust

designs. The circuits described herein adapt to effects at the output frequency and stabilize energized sources to changing conditions.

### 5.1.3.1 Theory of operation

The wireless power system, in its simplest form, consists a transmission element and a receiving element. The transmission element contains an oscillator connected to a source of direct current (dc). The dc current is used to stimulate an antenna which propagates the electric force in its magnetic form across free-space. The receiving element is connected to a load and draws the current from the electromagnetic waves coalescing them into a wire. A stabilized, frequency-free current is introduced to the oscillator, shown on the left side of Fig.2.1, called the source. The source can be identified as any current-generating apparatus; for the purposes herein, this is a solar paddle array common in typical satellite deployments. The source is calibrated so that its output power, measured in watts, is regulated to be of the same tolerance as the amplifiers in the oscillator. The oscillator generates a sinusoidal wave of a particular frequency  $\omega_0$ . The resonance frequency is determined by the properties of the transmission and receiving elements designated  $L_i$  and  $L_j$  respectively in tandem with a capacitor (not shown). When the values of the inductance  $L$  and capacitance  $C$  of the  $i^{th}$  and  $j^{th}$  elements are matched, the transmission and receiving elements form a closed resonant circuit at tension with a given mutual inductance  $M_{ij}$ . When a current  $I_0$  is introduced into the transmission element, it is simultaneously observed as  $I_R$  flowing in the receiving element. The current is now available to be utilized in other power consuming circuitry, transmission-line cabling, or to a second wireless power coupler. In the latter instance, when using wireless power

couplers chained together, the oscillator element is not repeated; rather, added numbers of transmission and receiving elements project the currents across gaps, within a distance tolerance relative to the tension.

The design is generalized in the sense that it is replicated across inhomogeneous components. In the manner how a cabled system is intended in a design to transport currents, this system provides exactly the same service yet provides a dimensional flexibility to the mechanical components which rely on the transport or whose purpose is to delivery quantities of power. A particular modification to the use of cabling with this system is the insistence on transmission-line strength materials, designed specifically to allow the alternating current to continue at its manifest frequency.

Materials having higher relative permittivity support higher sensitivity because the electrical field strength is proportional to the relative permittivity, and inversely proportional to the thickness. The choice of material in the vacuum of space is a point of contention and its ability to transport alternating current valid. An oscillator driven in colder temperatures require more power to sustain them, hence, a sustained “skin” of energy aids in sustaining the circuits which manifest the energy field.

### **5.1.3.2 A sample application**

Wireless coupling provides peak performance and unparalleled utility from drawing board to prototype to manufactured craft. It provides a unique and robust means to solve power distribution problems heretofore considered unsolvable. In consideration of the expected usage of the technology described in this article, for a new satellite craft, such as the ESA Galileo,

with a paddle span of 13 meters and peak power of 1600 watts, the wireless power system is configurable to operate under these conditions.

An interesting proposal has been the invention of novel means to extend the paddle length and surface area of the solar blankets. This has been discussed at length in [118] archived by NASA and ESA. The design was used in two Japanese satellites: ADEOS I, launched in August 1996 and ADEOS II, launched in December 2002. In the first instance, the solar array paddle failed due to differential heating when the craft adjusted its attitude to control its orbit. As a result of the maneuver, the solar panel received sunlight from the rear. This caused the solar paddle mast to expand and the panel blanket to contract, placing tension on a soldered joint on the paddle, which eventually severed the wired power connection. In the second instance, the solar panel simply failed. By using wired connections in these novel and useful advancements in solar array paddles, each satellite was only able to remain operational nine months.

In current schemes and in the attempt not to repeat the failures of the ADEOS I and II projects, a folding leaf solar array paddle—similar in the manner to opening a book—has been tried with success. Increase of the length of the solar paddle as well as increase of the surface area of the solar blanket allows more power to be utilized onboard the craft. While a good alternative, folding presents problems in fatigue to cabling and reduces the number of available blanket surfaces by two (one for each paddle arm). Clearly, it is more advantageous to maximize the amount of surface areas equating to maximum power given the current state-of-the-art. Additionally, the use of a solar-array driving mechanism (SADM) that connects the solar array paddles to the spacecraft and rotating them slowly so that the surface of the arrays can remain perpendicular to the Sun's rays

at all times is more optimal. One further improvement is the inclusion of a dimensional flexibility of solar paddle arrays in that paddle segments toward the end of the span can be made flexible. A typical solar paddle array is shown in Fig.5.15.

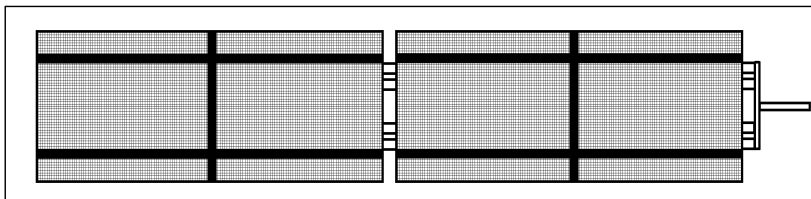


Fig.5.15. Common solar paddle array.

Such a paddle array, contained in a launch vehicle by folding, provides a stable source of dc current to the satellite craft. Generally used in pairs, these arrays provide all the electricity to the onboard computing, transmission, and sensing systems by leveraging semiconductor technology which converts solar radiation into electrical current. The size and type of the semiconductor panels, shown as closely-packed squares in Fig.5.15, determine the amount of current given the area of the panels and their orientation to the direction of solar radiation. For an optimal setting, the full value of current can be generated for the craft or vehicle using them by turning the panels if the solar radiation is less than desired. However, in most cases, only a partial current can be additionally delivered due to the array being limited to one or two degrees of freedom. Flexible mechanical structures have been explored, as previously mentioned, however, there are serious drawbacks. Altering the structure to use wireless powered couplings allows more degrees of freedom enhancing the ability of the craft to maximize its input current by aligning more succinctly with the incoming solar radiation. Modifying the common solar paddle array to leverage wireless power couplings is illustrated in Fig.5.16.

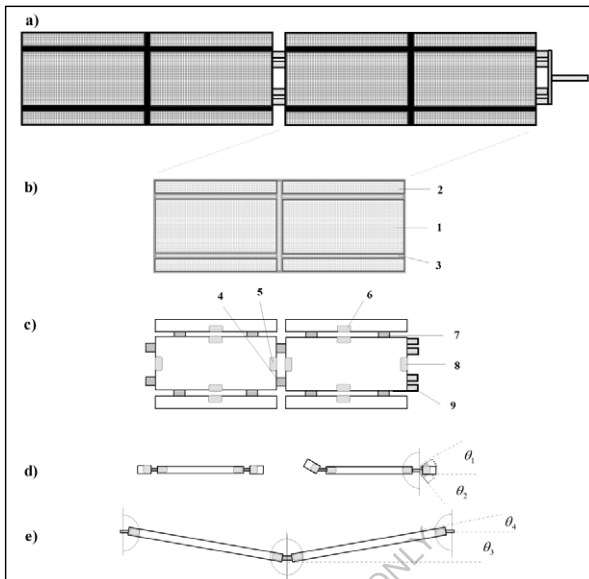


Fig.5.16. Flexive joints using wireless-power couplings.

The arrangement, shown in Fig.5.16, consists of a set of views of the breakdown of a solar paddle array into flexive mechanical joints, denoted by shading, with wireless power couplings in their expected installation points. Fig.5.16a, following Fig.5.15, shows a detail of the components of the solar paddle array for one arm of a satellite implementation. The structures inside the red boxes outline a solar panel used to convert solar energy into electrical current. A single conglomerate of a contiguous panel is shown in Fig.5.16b consisting of a center sail 1 and outer sail 2 with flexion gaps 3 separating them. Fig.5.16c illustrates what consists the connections nested inside the flexion gaps, consisting of a mechanical hinge joint 4 supporting the rotational mass of the center sail where the wireless power coupling 5 transmits the current in any position of axial flexion given by  $\theta_3$  of Fig.5.16e. Similarly, the mechanical or electro-mechanical rotational joint 7 supporting the rotational mass of the outer sail

where the wireless power coupling 6 transmits the current in any position of flexion given by  $\theta_1$  of Fig.5.16d. The array, with the components already described, are connected with a mechanical or electro-mechanical rotational joint 9, of more stiffness than the others so as to support the mass of the array, where the final wireless power coupling 8 transmits the total energy absorbed by the panels to the satellite craft. The power which is fed across the flexion gaps by the wireless power transmitters is intended to experience a minimum distortive impact, meaning where flexion in mechanical connections would not affect power being fed to the craft, in a typical manner, illustrated by the relationship between the array and the connection to the craft  $\theta_3$  and  $\theta_4$ .

As it is desirable to project currents at numerous frequencies, the wireless power system is configurable to utilize a range of frequencies. In approaching the problem of selectivity, it is worthwhile to understand which transmission frequency or frequencies are necessary given a particular transport problem. For single-instances, a “blanket” describing a contiguous field across the paddle is the model; for other instances, a pattern of frequencies where some concentrations of energy are greater than others given a particular gap ratio or folding across complex values of  $\theta_n$  is more interesting. It is feasible at design time which strategy would be most successful.

Selectivity is a crucial consideration when sending a modulated wave over the power carrier signal. Some implementations require high sensitivity where sensors are mounted away from the central control across gaps to report solar intensity, temperature, or infrared readings. Some of these sensors could be designed to behave similarly to accelerometers reporting the exact angle  $\theta_n$  for complex power optimization schemes. In order to

satisfy such conditions, the wireless power couplings are modified to contain modulation circuitry only in the last case (during a chain) when decoding the signal for processing by the computer in the craft. The energies in description emitted as a wireless transmission between couplings in the gaps has the same susceptibility to interference from the sun as the communications array in sun facing outages when thermal noise is at a maximum.

#### **5.1.3.3 Thoughts about wireless power for space activities**

Currently, humanity is standing on the threshold of a bright future. People are becoming more heavily engaged on exploiting activities in space and successful at achieving more complexities as landing a probe on a comet. As public interest and young people are more involved with creating this future, coupled with a longer lifespan, it is our responsibility now to understand how to improve conditions for not only satellite craft, but also for manned craft, such as the International Space Station (ISS). It is only by a consistent presence in space with comfortable, inhabitable dwellings can the next phase of building ships in space designed for longer journeys within our solar system ensue.

The design described in this section can overcome these issues as it relies on the properties of the materials which consist the transmission and receiving elements and their subsequent properties at the given temperatures and pressures. At its apex, used to create larger and more elaborate arrays, distinctive in how a large, fabric-like surface can bend and contort to absorb maximum solar radiation. As such, it eliminates discussions of dangerous power enhancements as nuclear fission to fill the gap between required power, craft size, and craft complexity. It is the manner in which wireless power and its implications contribute to the

understanding of tangible and realistic option in power generation and onboard environmental stability.

Although only having described one sample application, there are numerous and varied ways in which wireless power can be leveraged in space activities and it is for the future to decide which research paths are most vital to realizing those new ambitions in space technology and research. It is only a function of the imagination which technologies are most interesting and helpful to support a new era of human activities in space.

## 6 Conclusion

This work discussed a study of wireless power by magnetic resonance, in theory, application, control, and experiment. It extended the concept to include applications to aid in the increased development of humankind. It presented in this work attempts to address magnetic resonant coupling from a phenomenological point-of-view. That is, asking questions and forming hypotheses on observations of two distinctly different types of wireless power schemes. In addition, the work tries to structure its analytical arguments based on non-isolation of the phenomenon meaning the phenomenon does not exist in exclusion of other forces, rather, because of them. A novel contribution the work is presenting is exactly this point: that forces applied to an electron emitting radiation impress a pattern onto free-space and that this pattern exists only because there are counterforces simply by the connection between the original force and consequential force. It also demonstrates that the effect is linear in that an unfolded circular loop manifests the same forces equally. The main conclusion is there exists in nature a strong connection between the accelerated electron and the impression of its radiation on non-charged spaces.

In this work, a method and means of wireless power by magnetic resonance has been described. The focus of research was on the description and experimental verification of an efficient wireless power model to be used in several application areas, notably those for in a human proximity, but also for those in non-human proximity. Nevertheless, the method of power delivery is general and can be applied to other applications which require wireless power transfer on scales both large and small [30, 87] as well as many others.

The literature which contains descriptions of physical devices tends to address typical problems in wireless power transfer—antennas, inductance, coupling, and energy transfer, by clear mention of magnetic resonance or not—regardless of coil size or design of experimental setup. It can be surmised by this fact alone that the phenomenon of magnetic resonance wireless power is such that it matters little of the size of the coils or the distance apart or the pattern and number of antennas or the means by which the energy is utilized. What matters is that the phenomenon is a commonplace law of physics, although not expressly stated as such. Because of the conclusion of the similarities in analytics of other researchers, it becomes apparent that the electron affects other electrons by a connection explained in quantum mechanics. However, in none of the literature surveyed for this work has the mathematical tools of quantum mechanics been applied to magnetic resonant coupling. This work attempts to begin the framework by integrating gauge field theory to shape an understanding of the quantum mechanical implications and a thorough analysis of the magnetic potential between the coupling and free-space revealing structural equations which predict the reactive forces and subsequent observable properties.

## 6.1 Coupled-modes

While the seat of the arguments for the method of *why* for magnetic resonance lie exclusively with [23], it is used verbosely by many other examples of wireless power transfer. While the author can cite how coupled-mode theory would apply to schemes such as the one illustrated in this work, it is still not clear how the coupled-modes manifest given the simplistic model of the dipole purveyed in scholastic physics texts. For coupled-mode to be successful, it seems apparent that the dimensionality of the dipole needs to be brought into question. In terms of signaling, as it has been understood since the days of Marconi, the single dimensionality is satisfying. In terms of wireless power transfer, which is a form of signaling in the scheme of radiant transfer, the dimensionality fails to describe the system. In order to attempt to come to terms with the discrepancy, §4 introduces a dimensionally-equivalent description of the energies observed. It is anticipated that descriptions in this architecture can shed light onto current dilemmas in electromagnetism. Regardless of intention or discrepancy, couple-mode theory is a useful tool to describe mathematically wireless power schemes.

## 6.2 Circuit model and propagation

The circuit model is an attempt to present the arguments for coupled-modes into a physical paradigm. The model proposed the embodiment of coupled modes and energy exchange properties between two distant circular loops. By considering the geometry of the loops as a fundamental description of the manifest electric and magnetic fields coupled to its radiation, it has helped to extend the basic concepts of a definition of broadcast power between distant antenna forming a closed induction circuit. The extension

bundled into model properties and applied optimizations of coupled-modes as a hypothetical explanation of efficient wireless energy transmission.

If the loops are magnetic dipole antenna of a size relative to their quarter wavelength, adjustment along a descending  $\log_{10}$  scale will yield maximum power dissipation in the free-space between the antenna. In such a manner, the extant electromagnetic field creates a spherical shell whose boundary conditions interact intrinsically with the conductive properties of the medium. Because of such a seemingly high conductivity in the scheme, where there perhaps should not be given the impedance of free-space, these results lead the author to hypothesize further that at the boundary, the conductive medium on quantum scales consists of some interface of unity in the notion of space-time itself. This could be the aether or dark matter or some other nomenclature in a future science. What is clear is that *something* is going on at the boundary between the energized field and the medium.

The model in its simplicity provides stark insights that the energies that permeate the field can be expressly quantified, given enough sophistication in the methods. It is therefore interesting to explore the quantifications and to what further insights can be gleaned. Although it is very interesting to understand the physicality of what consists a coupled magnetic resonant mode, contrastingly, what reactive phenomena are responsible for providing the sustaining counter-force giving it such a strong linear equilibrium is equally so. The author suggests further research needs to be conducted on what consists the structure of “empty space”.

The transition of the mathematics from circuit to field model is a problem plaguing engineering which needs a tolerable solution. This work has

contributed to this by proposing computational methods to describe the electromagnetic problem, given the uniqueness of the model. How does the translation in mathematizing the model from circuit theory to field theory help to ease genetic fallacies [46] prevalent in electromagnetism? Can the more arbitrary components of Maxwell's theory be given substance, especially those considered as purely analytical devices such as the potential? The research opens the door to many questions by availing a means to answer them in a physical experiment. It allows the investigation of the properties of what is coupled to it as well as some masses contributed by free-space; this is the most interesting take-away knowledge from the research process.

### 6.3 Antenna at the interface

It is a valid hypothesis, given the evidence in this work, that it is possible the method is detecting something at the interface, such as the dark matter in the present accepted description of what in antiquity was called the aether. The configuration of the circuitry described for a prototype exhibited in the model is the *characteristic archetype* of all of the classes for wireless power transmission methodology. Nearly all other schemes of comparable methodologies are derived from it. The presence of currents on the wire give rise to the magnetic fields propagated into free-space because the loop antenna is a high emitter of electromagnetic photons. This presence is equal for contiguous and area loops. An interesting observation is this lack of mass of the photons and their ability to do work. However, because at some energy level, a motor is turned, some mass is entering into the system. Wired systems rely on electron masses to perform work at a distance, wireless systems rely on photons to perform work at a distance.

The unity of the potential in context with the field object is observable under measurement of an unpowered antenna and is extant at the nulls to the left and right minor lobes. It is assumed this is a loose measure of confirmation of the existence of a structure of free-space that will inevitably lead to a more detailed future description. Additional laboratory resources would be required, more than the basic equipment available a member of the public.

The movement of the oscillation through  $\pi$ , in consideration of how the antenna is coupled to an open system through the interface, suggests implications on the impedance of free-space of  $120\pi\Omega$ . Since each phase moves through  $\pi$ , a total of 60 cycles would sum up the impression of a single complex wave on free-space. Does the interface support a logarithmically-based coupling method?

#### **6.4 Commentary on the magnetic potential and final words**

The interaction of a stream of particles with the radiated field will result in a graduated ellipsoidal field growing away from the emission point. Instead of a static quantity, the momentum of the particle stream creates an elliptical area on the manifold where the relationship between the two charges, the virtual and the passing field, are in resonance with respect to each other, creating a more dense form on the manifold. Some passing particles, which could contain masses, are temporarily trapped in the sink and orbit the central axis of the field. The radius of the field and the equilibrium of the system are dependent on the magnitude of energy stored as a resonance between the transmission and receiving loop antenna. This quotient of energy is trapped in the sink as long as the system remains stable in terms of its geometry and the resonance patterns can hold it

together. The form would hold unless broken by a stronger external electric field. As a series of dipoles, analogous in the case of a short dipole, a chaining of dipoles yields the polarization of the propagating waveform—the rise and fall of current from one polarity to the other—across free-space, with a given admittance and reactance dependent upon the temperature and pressure.

What is relevant to understand at the fundamental level are that the notions of flux and propagation are absorbed into the scalar, vector, and quaternion representations of the potential of the waveguide structure, which consists and subsists the space between and of the antenna discussed throughout this work. As the phenomenon is physically observable, it indicates that the potential  $\mathbf{A}_\mu$  fields, where  $\mu = 0, 1, 2, 3, \dots$  do possess a physical significance as global-to-local operators or the case of gauge fields, subject to precisely constrained topologies [50]. The  $\mathbf{A}_\mu$  potentials are described as *physically meaningful* constructs at the classical level, numbers 2 and 3 and at long range in the case of effect 2. Coherence length limitation is noted in effects 1, 3 and 4. What this implies is that a properly constructed and well-defined topological object can manifest, along with magnetic flux, sets of potentials along its length and trajectory conditionally dependent upon the antenna creating the field object. It would be interesting in future research to explore those topologies as quantization of the field object where appropriate.

H.F. Harmuth proposed an amendment to Maxwell's equations [98, 99]. The subject having gone through much discussion [100], presents eloquently an argument of possibilities of expansion in the interpretation of the more abstract parts of the Maxwell equations. One consequence: the application of force to separate the charges by the application of current,

the current lags behind the voltage potential, the point charges are both particles and waves [101]. It is anticipated that steps toward a proof of the notions discussed in this section can be formed thusly. An electrically-charged short antenna has a trivial characteristic impedance when compared load whose impedance dominates the circuit, desirable for sending power over distances; e.g., the power is induced to traverse the free-space between the transmitter and receiver to the load where the impedance is located, a primitive form of directional finding [67]. It is this seeking effect that yields some qualified evidence that there is a possibility of a straining of the space between the antenna cited the pattern of repetitious properties not unlike a set of harmonics across space. It is suspected the observable strain is analogous to that described by Maxwell. The author hypothesizes an oscillatory reaction force permeates the waveguide. The increase of magnetic potential is the means by which to understand the force.

Throughout this work, topics for future research have been noted. Generally speaking, it would be of further interest:

1. To study the physical geometry of the scheme: the addition of a secondary coil whose winding is equidistant on the  $x-y$  plane and the addition of receivers to “chain” the power signal over longer distances.
2. To revisit the Aharonov-Bohm experiments [28], and flavors of subsequent attempts to see if the problem can be modeled on larger scales, as  $r \rightarrow \pi$ , and at higher temperatures.
3. To experiment with different lengths of component L3 of the transmitter coil and its position along the length AB. Is there a difference in projected field geometry or power?

4. To create antenna from metamaterials. The metamaterial concept is a substantial move toward practical applications in the area of antennas and wireless energy propagation. It is interesting to use collections of sub-wavelength elements in a structured medium of volumetric metamaterials (three-dimensions), meta-surfaces (two dimensions), and meta-wires (one dimension) for control over the broadcast and receiving properties of the antenna. Thusly, the medium within the loop can be carefully controlled and its exotic properties revealed: controlled in that its commonly understood properties with uncommon control over spatial variation, polarization sensitivity, and frequency dispersion. Exotic in the answers to the reasons of its behavior were not forthcoming. Nevertheless, the medium is currently inaccessible, the expansion of basic parameters and more finite granular control over the antenna and its influence at the interface would greatly aid investigation in subsequent properties of the medium of free-space beyond the interface. Of all the possible suggested research, not one is more profound than the application of metamaterials. Clearly, this approach has enormous potential for hugely efficient wireless power transfer from a central transmitter base to remote receiver stations, without incurring the losses due to wire resistance and the inherent costs of building physical transmission lines.

This work has described principle, method, and means of the transmission of wireless power by magnetic resonance.

QED

## 7 Appendix – Table, figure, and code

This section contains the large tables and figures as well as the basic *Matlab* code to create an antenna mesh as the one described in this work and ready for use with a solver of your choice. I used the method of moments (MoM). The variable names in Table 7.1 have been changed for consistency in the text.

The names affected are:  $k^2 \rightarrow u^2$ ,  $f \rightarrow \alpha$ ,  $a \rightarrow r_i$ ,  $A \rightarrow r_j$ .

Table 7.1. Values of factor  $u^2$  [31].

TABLE 13. VALUES OF FACTOR  $f$  IN FORMULA (77)

$$M = f\sqrt{Aa}.$$

$k^2$	$f$	Diff.	$\log f$	Diff.	$k^2$	$f$	Diff.	$\log f$	Diff.
0.010	0.021474	-4159	.233191	-9349	0.260	0.003805	-	3.58034	-1819
.020	.017315	-2378	.23842	-6596	.270	.003649	-	.56215	-1805
.030	.014937	-1653	.17246	-4913	.280	.003500	-	.54410	-1792
.040	.013284	-1258	.12333	-4319	.290	.003359	-	.52618	-1783
0.050	0.012026	-1009	2.08014	-3807	0.300	0.003224	-	3.50835	-1773
.060	.011017	-838	.04207	-3437	.310	.003095	-	.49062	-1767
.070	.010179	-715	2.00770	-3162	.320	.002971	-	.47295	-1760
.080	.009464	-621	3.97608	-2946	.330	.002853	-	.45535	-1757
.090	.008843	-546	.94662	-2772	.340	.002740	-	.43778	-1754
0.100	0.008297	-487	3.91890	-2627	0.350	0.0026317	-	3.42024	-1753
.110	.007810	-439	.89263	-2509	.360	.0025276	-	.40271	-1753
.120	.007371	-397	.86754	-2407	.370	.0024276	-	.38518	-1754
.130	.006974	-363	.84347	-2321	.380	.0023315	-	.36764	-1756
.140	.006611	-333	.82026	-2246	.390	.0022391	-	.35008	-1760
0.150	0.006278	-308	3.79780	-2181	0.400	0.0021502	-	3.33248	-1765
.160	.005970	-285	.77599	-2124	.410	.0020646	-	.31483	-1769
.170	.005685	-265	.75475	-2074	.420	.0019821	-	.29712	-1778
.180	.005420	-247	.73401	-2030	.430	.0019026	-	.27934	-1786
.190	.005173	-232	.71371	-1991	.440	.0018259	-	.26148	-1796
0.200	0.004941	-218	.69330	-1957	0.450	0.0017519	-	3.24352	-1807
.210	.004723	-205	.67423	-1926	.460	.0016805	-	.22545	-1819
.220	.004518	-193	.65407	-1899	.470	.0016116	-	.20726	-1832
.230	.004325	-183	.63598	-1875	.480	.0015451	-	.18894	-1846
.240	.004142	-173	.61723	-1854	.490	.0014808	-	.17048	-1862
0.250	0.003969	-164	.59869	-1835	0.500	0.0014186	-	3.15186	-1879

Note that in Fig.7.1, the  $x$  and  $y$ -scales for each waveform are  $200 \mu\text{S}$  and 2 volts per division, respectively. (a)  $\kappa = 0.002$ , (b)  $\kappa = 0.004$ , (c)  $\kappa = 0.008$ , (d)  $\kappa = 0.010$ .

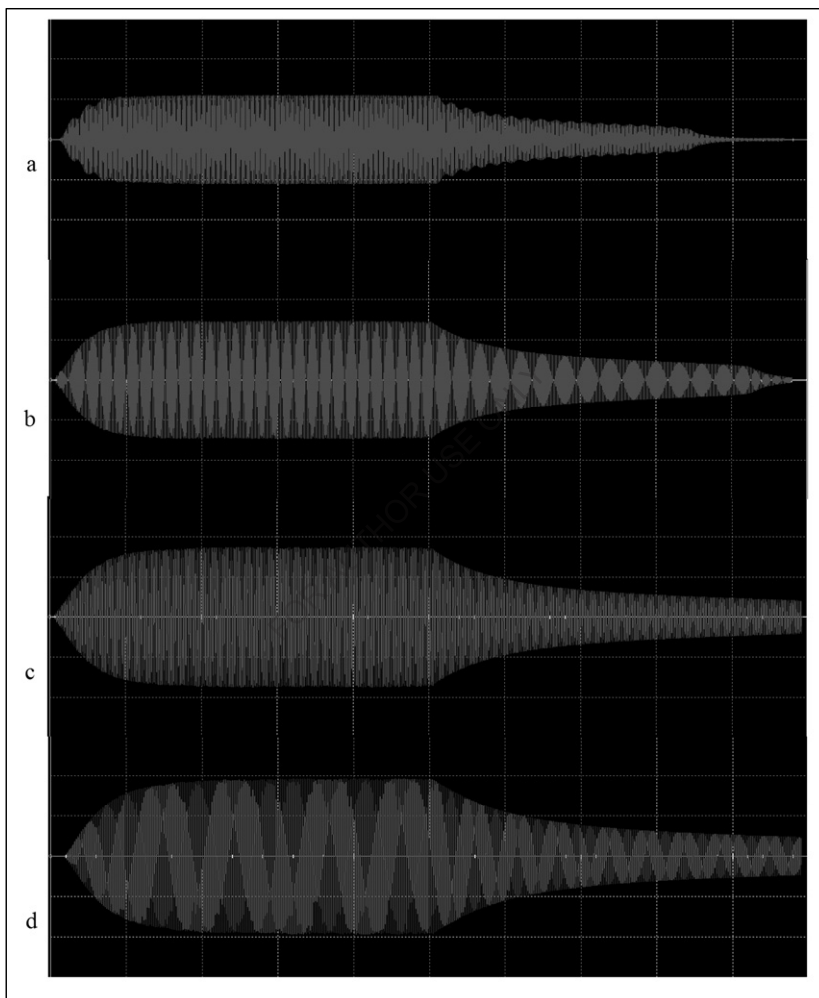


Fig.7.1. Effect on the simulated output based on changing the value of the coupling coefficient  $\kappa_{ij}$ .

Table 7.2 contains a set of instructions to use Matlab with the PDE toolbox to duplicate the mesh used to compute the antenna.

Table 7.2. Instructions to create an antenna mesh file.

Instructions to create an antenna file structure.
<ol style="list-style-type: none"><li>1. Open Matlab, type pdetool,</li><li>2. Click Options/Axes Equal,</li><li>3. Draw any ellipse, double-click on its surface,<ol style="list-style-type: none"><li>a. Set X-center to 0,</li><li>b. Set Y-center to 0,</li><li>c. Set A-semiaxes to 3 (for a radius of 3 units),</li><li>d. Set B-semiaxes to 3 (for a radius of 3 units),</li></ol></li><li>4. Draw a second ellipse, double-click on its surface,<ol style="list-style-type: none"><li>a. Set X-center to 0,</li><li>b. Set Y-center to 0,</li><li>c. Set A-semiaxes to 2.75 (for a wire thickness of 0.25 units),</li><li>d. Set B-semiaxes to 2.75 (for a wire thickness of 0.25 units),</li></ol></li><li>5. Set formula E1-E2,</li><li>6. Click Mesh/Parameters...<ol style="list-style-type: none"><li>a. Set Maximum edge size to Inf,</li></ol></li><li>7. Initialize the mesh,</li><li>8. Refine the mesh,<ol style="list-style-type: none"><li>a. Refining the mesh twice, check triangle quality by clicking Mesh/Triangle quality,</li></ol></li><li>9. The average quality should be 0.5 across the surface for an ideal mesh,</li><li>10. Save the file,</li><li>11. Export the mesh by clicking Mesh/Export Mesh,<ol style="list-style-type: none"><li>a. Leave the variable names for mesh data (points, edges, triangles) p e t,</li></ol></li><li>12. The Workspace now contains the data,<ol style="list-style-type: none"><li>a. type p(3,:)=0;</li></ol></li><li>13. Save the compiled mat file,<ol style="list-style-type: none"><li>a. Save filename p t</li></ol></li><li>14. The antenna structure file has been created.</li></ol>

The meshes are used as antenna geometry to run the MoM solution. Using a sample solution [64], run it in the order listed in Table 2.6 to generate the data discussed in §2.3.

## 8 References

---

- [1] G. Reber, *Endless, Boundless, Stable Universe*, University of Tasmania, Tasmania, 1977.
- [2] B. Hunt, *The Maxwellians*, Cornell University Press, New York, 2005.
- [3] F. Warburton, “Displacement Current, A Useless Concept,” *American Journal of Physics*, Vol. 22, Iss. 5, pp.299-305, Oct. 1954.
- [4] W. Rosser, “Displacement current and Maxwell’s equations,” *American Journal of Physics*, Vol. 43, Iss. 6, pp.807-8, Jun. 1975.
- [5] J. Larmor, “A dynamical theory of the electric and luminiferous medium,” *Philosophical Transactions of the Royal Society*, Vol. 190, 438-61, Dec. 1893.
- [6] J. Larmor, “A dynamical theory of the electric and luminiferous medium, Part II, theory of electrons,” *Philosophical Transactions of the Royal Society*, Vol. 190, pp. 695-743, Jun 1895.
- [7] P. Nahin, *Oliver Heaviside: The Life, Work, and Times of an Electrical Genius of the Victorian Age*, Johns Hopkins University Press, Maryland, 2002.
- [8] V. Stepin, *Theoretical Knowledge*, Springer, New York, 2002.
- [9] J. Poynting, “On the Transfer of Energy in the Electromagnetic Field,” Phil. Trans. 175, pp.343-61, 1884.
- [10] A. Kurs, *Power Transfer Through Strongly Coupled Resonances*, Masters of Science thesis, MIT, Sep. 2007.
- [11] K. Kodaira, *Complex Manifolds and Deformation of Complex Structures*, New York, Springer, New York, pp. 28-59, 1981.
- [12] R. Pfeifer, T. Nieminen, N. Heckenberf, and H. Rubinsztein-Dunlop, “Momentum of an electromagnetic wave in dielectric media,” *Reviews of Modern Physics*, Vol. 79, pp.1197-1216, Oct. 2007.
- [13] N. Tesla, “Experiments With Alternate Currents of High Potential and High Frequency,” IEE Address, London, February 3, 1892, contained in *Inventions, Researches and Writings of Nikola Tesla*, D. van Nostrand Company, New York , pp.186-91, 1894.
- [14] N. Tesla, *Apparatus for the Utilization of Radiant Energy*, U.S. Patent No. 685,957, filed 21 May 1901, awarded 5 Nov. 1901.
- [15] H. Yagi, “Beam transmission of ultra-short waves,” *Proceedings of the Institute of Radio Engineers*, Vol. 16, Iss. 6, pp.715-40, 1928.
- [16] E. Siering-Stumpf, “Shortwave DX Handbook: Your gateway to worldwide DXing,” Darc-Verlag, Berlin, 2005.

- 
- [17] W. Teich and W. Brown, "Design of CW amplitrons for space-borne telemetry applications," *IEEE Transactions on Electron Devices*, Vol. 10, Iss. 2, p. 108, 1963.
- [18] W. Brown, "Experiments involving a microwave beam to power and position a helicopter," *IEEE Transactions on Aerospace and Electronic Systems*, Vol. AES-5, Iss. 5, pp.692-702, 1969.
- [19] J. Schuder, "Energy transfer into a closed chest by means of stationary coupling coils and a portable high-power oscillator," *American Society for Artificial Internal Organs*, Vol. 7, pp.327-31, 1961.
- [20] R. Fano, L. Chu, and R. Alder, *Electromagnetic Fields, Energy, and Forces*, John Wiley & Sons, New York, 1969.
- [21] G. Fitzgerald, "The Ether and the Earth's Atmosphere," *Science*, Vol. 12, Iss. 328, pp.390, May 1889.
- [22] J. Maxwell, *On physical lines of force*, London: Taylor and Francis, 1861.
- [23] H. Haus and W. Huang, "Coupled-mode theory," *Proceedings of the IEEE*, Vol. 79, No. 10, pp.1505-18, Oct. 1991.
- [24] S. Schelkunoff, "General Telegraphist's Equations," *The Bell System Technical Journal*, Vol. 111, p.784-801, Jul. 1952.
- [25] R. Alder, L. Chu, and R. Fano. *Electromagnetic Energy Transmission and Radiation*, John Wiley & Sons, Inc., Cambridge, 1969.
- [26] S. Ilić, M.T. Perić, S.R. Aleksić, and N.B. Raičvić, "Quasi TEM analysis of symmetrical coupled strip line using new hybrid boundary element method," *19th Telecommunications forum TELFOR*, pp.1008-11, Nov. 2011.
- [27] S. Manić, S. Savić, M. Ilić, and B. Notaroš. "Combining finite element method and Fourier transform to analyze waveguide transients," *19<sup>th</sup> Telecommunications forum TELFOR*, pp.1004-7, Nov. 2011.
- [28] Y. Aharonov and D. Bohm, "Significance of Electromagnetic Potentials in the Quantum Theory," *Phys. Rev.*, Vol. 115, Iss. 3, Aug. 1959.
- [29] J. Kraus, *Antennas for All Applications, 3rd Edition*, McGraw-Hill, Boston, 2001.
- [30] A. Karalis, J. Joannopoulos and M. Soljačić, "Efficient wireless non-radiative mid-range energy transfer," *Annals of Physics*, Vol. 323, pp.34-48, Apr. 2008.
- [31] F. Grover, *Inductance calculations: Working formulas and tables*, New York, D. van Nostrand Company, 1946.
- [32] R. Elliott, *Electromagnetics*. New York, IEEE Press, 1993.

- 
- [33] P.K. Sharma and S.K. Guha, "Transmission of time varying magnetic field through body tissue," *Journal of Biological Physics*, Vol. 3, pp.95-102, Jun. 1975.
- [34] F. Neumann, "Allgemeine Gesetze der inducirten elektrischen Ströme," *Abhandlungen der Königlichen Akademie der Wissenschaften zu Berlin*, 1845.
- [35] L. Hannakam, "Berechnung der Gegeninduktivität achsenparalleler Zylinderspulen," *Archiv für Elektrotechnik*, Vol. 51, No. 3, pp.141-54, 1967.
- [36] I. Awai, Y. Zhang, T. Komori, and T. Ishizaki, "Coupling coefficient of spiral resonators used for wireless power transfer," *Proceedings of Asia-Pacific Microwave Conference*, pp.1328-31, Dec. 2010.
- [37] I. Awai and Y. Zhang, "Separation of coupling coefficient between resonators into electric and magnetic contributions toward its application to BDF development," *China-Japan Joint Microwave Conference*, pp.61-5, Sep. 2008.
- [38] V. Christianto and F. Smarandache, "A Note on Computer Solution of Wireless Energy Transmit via Magnetic Resonance," *Progress in Physics*, Vol. 1, Jan. 2008.
- [39] H. Lorentz, "Attempt of a theory of electrical and optical phenomena in moving bodies," *E.J. Brill*, Leiden, The Netherlands, 1895.
- [40] H. Lorentz, "Electromagnetic phenomena in a system moving with any velocity smaller than that of light," *Proceedings of Academic Science Amsterdam*, Vol. 1, pp.427-43, 1904.
- [41] H. Poincaré, "On the dynamics of the electron," *Weekly reports of meetings of the Academy of Sciences*, Vol. 140, pp.1504-8, 1905.
- [42] J. Larmor, "On a dynamical theory of the electric and luminiferous medium, Part III, relations with material media," *Philosophical Transactions of the Royal Society*, Vol. 190, 205-300.
- [43] E. Hochmair, "System optimization for improved accuracy in transcutaneous signal and power transmission," *IEEE Transactions on Biomedical Engineering*, vol. 31, pp. 177-186, Feb. 1984.
- [44] C. Zierhofer, "Geometric Approach for Coupling Enhancement of Magnetically Coupled Coils," *IEEE Transactions on Biomedical Engineering*, Vol. 43, No. 7, pp. 708-14, Jul. 1996.
- [45] H. Schey, *Div Grad Curl and all that: An informal text on vector calculus*, W.W. Norton & Company, 1997.
- [46] J. Roche, "The present status of Maxwell's displacement current," *Eur. J. Phys.*, Vol. 19, pp.155-66, 1998.

- 
- [47] E. Post. "Interferometric path-length changes due to motion," *Journal of the Optical Society of America*, Vol. 62, Iss. 2, pp.234-9, 1972.
- [48] L. de Broglie, "Researches on the quantum theory," *Annals of Physics*, Vol. 3, No. 22, 1924.
- [49] Y. Couder and E. Fort, "Single-particle diffraction and interference at a macroscopic scale," *Physical Review Letters*, Vol. 97, Iss. 15, Oct. 2006.
- [50] T. Barrett. *Topological Foundations of Electromagnetism*. World Scientific Publishing Company. 2008.
- [51] K. Corum and J. Corum, "RF Coils, Helical Resonators and Voltage Magnification by Coherent Spatial Modes", *IEEE Microwave Review*, Vol. 7, No. 2, pp. 36-45, Sep. 2001.
- [52] H. Hertz. "About very rapid electrical oscillations," *Annalen der Physik*, Vol. 267, No. 7, pp.421-48, May 1887.
- [53] H. Hertz. "On the propagation velocity of the electrodynamic effects," *Annalen der Physik*, Vol. 270, No. 7, pp.551-69, May 1888.
- [54] E. Armstrong, "Operating Features of the Audion," *Annals of the New York Academy of Sciences*, Vol. 27, No. 1, pp.215–43, Aug. 1917.
- [55] J. Hoag, *Basic Radio: The Essentials of Electron Tubes and their Circuits*, New York, D. Van Nostrand Company, 1942.
- [56] N. Malik, *Electronic circuits: analysis, simulation, and design*, Prentice Hall, New Jersey, pp.315–6, 1995.
- [57] A. Kurs, A. Karalis, R. Moffatt, J. Joannopoulos, P. Fisher, and M. Soljačić, "Wireless Power Transfer via Strongly Coupled Magnetic Resonances," *Science*, Vol. 317, pp.83-86, Jul. 2007.
- [58] S. Makarov, "MoM antenna simulators with Matlab: RWG basis functions," *IEEE Antennas and Propagation Magazine*, Vol. 43, pp.100-7, Oct. 2001.
- [59] S. Rao, D. Wilton, and A. Glisson, "Electromagnetic scattering by surfaces of arbitrary shape," *IEEE Transactions on Antennas and Propagation*, Vol. 30, No. 3, pp.409-18, May 1982.
- [60] D. Sarkar, *Vector basis function solution of Maxwell's equations*, Ph.D. dissertation, Rice University, TX, USA, May 1997.
- [61] B. Braaten, R. Nelson, and M. Mohammad, "Electric field integral equations for electromagnetic scattering problems with electrically small and electrically large regions," *IEEE Transactions on Antennas and Propagation*, Vol. 56, Iss. 1, pp.142-50, Jan. 2008.

- 
- [62] A. Peterson, S. Ray, and R. Mittra, *Computational Methods for Electromagnetics*, IEEE Press, Piscataway, NJ, 1998.
- [63] J. Shin, *Modeling of arbitrary composite objects with applications to dielectric resonator antennas*, Ph.D. dissertation, The University of Mississippi, MS, USA, Aug. 2001.
- [64] S. Makarov, *Antenna and EM modeling with Matlab*, Wiley-Interscience, 2002.
- [65] R. Paul, *Electrical fields and simple circuits*, 3rd Edition, Springer-Verlag, Berlin, 1993.
- [66] A. García, J. Carrasco, J. Soto, F. Maganto, and C. Morón, “A method for calculating the magnetic field produced by a coil of any shape,” *Physical Sensors and Actuators A*, Vol. 91, Iss. 2, pp.230-2, 2001.
- [67] R. Smith-Rose and H. Hopkins, “The application of ultra-short-wave direction finding to radio sounding balloons,” *Proceedings of the Physical Society*, Vol. 58, No. 2, Mar. 1946.
- [68] A. Pantelopoulos and N. Bourbakis, “A survey on wearable sensor-based systems for health monitoring and prognosis,” *IEEE Transactions on Systems, Man, and Cybernetics*, Vol. 40, Iss .1, pp.1-12, Jan. 2010.
- [69] K. Warwick, M. Gasson, and B. Hutt, “The application of implant technology for cybernetic systems,” *Arch. Neurology*, Vol. 60, No. 10, pp.1369–1373, 2003.
- [70] N. Neihart and R. Harrison, “Micropower circuits for bidirectional wireless telemetry in neural recording applications,” *IEEE Transactions on Biomedical Engineering*, Vol. 52, pp.1950–59, Nov. 2005.
- [71] M. Ghovanloo and K. Najafi, “A wireless implantable multichannel microstimulating system-on-a-chip with modular architecture,” *IEEE Transactions on Neural Systems and Rehabilitation Engineering*, Vol. 15, pp.449–57, Sep. 2007.
- [72] K. Warwick, M. Gasson, B. Hutt, I. Goodhew, P. Kyberd, H. Schulzrinne, and X. Wu, “Thought Communication and Control: A First Step Using Radiotelegraphy,” *IEEE Proceedings on Communications*, Vol. 151, Iss. 3, pp.185-9, Jun. 2004.
- [73] M. Gasson, B. Hutt, I. Goodhew, P. Kyberd, and K. Warwick, “Invasive Neural Prosthesis for Neural Signal Detection and Nerve Stimulation,” *International Journal of Adaptive Control and Signal Processing*, Vol. 19, Iss. 5, pp.365-75, Jun. 2005.
- [74] P. Limousin, P. Krack, P. Pollak, A. Benazzouz, C. Ardouin, D. Hoffmann, and A-L. Benabid, “Electrical Stimulation of the Subthalamic Nucleus in Advanced Parkinson’s Disease,” *New England Journal of Medicine*, Vol. 339, pp.1105-11, Oct. 1998.
- [75] E. Romero, R. Warrington, and M. Neuman, “Energy scavenging sources for biomedical sensors,” *Physiological Measurement*, Vol. 30, pp.R35-R62, 2009.

- 
- [76] M. Baker and R. Sarpeshkar, "Feedback analysis and design of RF power links for low-power bionic systems," *IEEE Transactions on Biomedical Circuits and Systems*, Vol. 1, pp.28–38, Mar. 2007.
- [77] A. RamRakhiani, S. Mirabbasi, and M. Chiao, "Design and optimization of resonance-based efficient wireless power delivery systems for biomedical implants," *IEEE Transactions on Biomedical Circuits and Systems*, Vol. 5, Iss. 1, pp.48-63, Jan. 2011.
- [78] J. Gao, "Inductive power transmission for untethered micro-robots," *IEEE Industrial Electronics Society Conference*, pp.6–11, Nov. 2005.
- [79] T. Deyle and M. Reynolds, "Surface based wireless power transmission and bidirectional communication for autonomous robot swarms," *IEEE International Conference on Robotics and Automation*, pp.1036-41, May 2008.
- [80] Z. Low, R. Chinga, R. Tseng, and J. Lin, "Design and test of high-power high-efficiency loosely coupled planar wireless power transfer system," *IEEE Transactions on Industrial Electronics*, Vol. 56, No. 5, May 2009.
- [81] J. Mur-Miranda, G. Fanti, Y. Feng, K. Omanakuttan, R. Ongie, A. Setjoadi, and N. Sharpe, "Wireless power transfer using weakly coupled magnetostatic resonators," *IEEE Energy Conversion Congress and Exposition*, pp.4179-86, Sep. 2010.
- [82] K. O'Brien, G. Scheible, and H. Gueldner, "Magnetic Field Generation in an Inductively Coupled Radio-Frequency Power Transmission System," *IEEE Power Electronics Specialists Conference*, pp.1-7, Jun. 2006.
- [83] K. Corum and J. Corum, "RF Coils, Helical Resonators and Voltage Magnification by Coherent Spatial Modes," *Telecommunications in Modern Satellite, Cable and Broadcasting Service*, Vol. 1, pp.339-48, Sep. 2001.
- [84] B. Cannon, J. Hoburg, D. Stancil, and S. Goldstein, "Magnetic Resonant Coupling as a Potential Means for Wireless Power Transfer to Multiple Small Receivers," *IEEE Transactions on Power Electronics*, Vol. 24, No. 7, pp.1819-25, Jul. 2009.
- [85] L. Wu, Z. Yang, E. Basham, and W. Liu, "An efficient wireless power link for high voltage retinal implant," *IEEE Biomedical Circuits and Systems Conference*, pp. 101-4, Nov. 2008.
- [86] L. Rindorf, L. Lading, and O. Breinbjerg, "Resonantly coupled antennas for passive sensors," in *Proc. IEEE Sensors*, pp. 1611–1614, Oct. 26-29 2008.
- [87] J. Shipley, *Incorporating Wireless Power Transfer in an LED Lighting Application*, Master's thesis, Brigham Young University, Utah, Aug. 2006.

- 
- [88] N. Hemche and A. Jaafari, "Wireless transmission of power using a PCB transformer with mobile secondary," *IEEE Electrotechnical Conference*, pp.629-34, May 2008.
- [89] S. Barker, D. Brennan, N.G. Wright, and A.B. Horsfall, "Piezoelectric-powered wireless sensor system with regenerative transmit mode," *IET Wireless Sensor Systems*, Vol. 1, Iss. 1, pp.31-8, Mar. 2011.
- [90] N. Timmons and W. Scanlon, "Improving the ultra-low power performance of IEEE 802.15.6 by adaptive synchronization," *IET Wireless Sensor Systems*, Vol. 1, Iss. 3, pp.161-70, Apr. 2011.
- [91] C. Sauer, M. Stanacevic, G. Cauwenberghs and N. Thakor, "Power harvesting and telemetry in CMOS for implanted devices," *IEEE Transactions on Circuits and Systems*, Vol. 52, Iss. 12, pp.2605-13, Dec. 2005.
- [92] H. Haus, *Waves and Fields in Optoelectronics*, Prentice-Hall, New Jersey, 1984.
- [93] R. Feynman, *QED: The Strange Theory of Light and Matter*, Princeton University Press, 1988.
- [94] D. Griffiths, *Introduction to Quantum Mechanics*, Prentice Hall, Boston, 1994.
- [95] D. Bohm, *Quantum Mechanics*, New Jersey, Prentice-Hall, 1951.
- [96] R. Stutz, *Towards measuring the electron electric dipole moment using trapped molecular ions*, Ph.D. thesis, University of Colorado, 2010.
- [97] T. Chow, *Introduction to electromagnetic theory: a modern perspective*, New York: Jones & Bartlett Publishers, 2006.
- [98] H. Harmuth. "Correction for Maxwell's equations for signals I," *IEEE Trans. Electromagnetic Compatibility*, Vol. 28, Iss. 4, pp.250-8, Nov. 1986.
- [99] H. Harmuth. "Correction for Maxwell's equations for signals II," *IEEE Trans. Electromagnetic Compatibility*, Vol. 28, Iss. 4, pp.259-66, Nov. 1986.
- [100] Comments and replies to [98, 99].
- [101] M. Abid, B. Andreotti, S. Douady and C. Nore, "Oscillating structures in a stretched-compressed vortex," *Journal of Fluid Mechanics*, 450, pp.207-13, May 2001.
- [103] N. Tesla, *Colorado Springs Notes*, Nolit, Belgrade, Serbia, 1978.
- [104] K. Selvan and S. Ehsan, "A revisiting of scientific and philosophical perspectives on Maxwell's displacement current," *IEEE Antennas and Propagation*, Vol. 51, No. 3, pp. 36-46, 2009.
- [105] J. Arthur, "An elementary view of Maxwell's displacement current," *IEEE Antennas and Propagation*, Vol. 51, No. 6, pp. 58-68, 2009.

- 
- [106] C.A. Tucker, K. Warwick, and W. Holderbaum, “Efficient wireless power delivery for biomedical implants,” *IET Wireless Sensor Systems*, Vol. 2, Iss. 3, pp.287-96, Aug. 2012.
- [107] C.A. Tucker, “Magnetic resonant modes in a wireless-powered circuit,” *19<sup>th</sup> Telecommunications forum TELFOR*, pp.977-80, Nov. 2011.
- [108] N. Tesla, *My Inventions: The Autobiography of Nikola Tesla*, Ben Johnston (ed.), Experimenter Publishing Company, Inc., New York, 1919.
- [109] N. Papanicolaou and T. Tomaras, “Dynamics of magnetic vortices,” *Nuclear Physics B*, Vol. 360, Iss. 2–3, pp. 425-62, Aug. 1991.
- [110] N. Gerson, J. Hengen, R. Pipp, J. Webster, “Radio-wave propagation to the antipode,” *Canadian Journal of Physics*, Vol. 47, No. 20, pp. 2143-59, Oct. 1969.
- [111] C.A. Tucker, K. Warwick, and W. Holderbaum, “A contribution to the wireless transmission of power,” *International Journal of Electrical Power and Energy Systems*, Vol. 47, pp.235-42, May 2013.
- [112] N. Tesla, “The transmission of electrical energy without wires,” *Electrical World and Engineer*, 5 Mar. 1904.
- [113] N. Tesla, “World system of wireless transmission of energy,” *Telegraph and Telephone Age*, pp.457-60, 16 October 1927.
- [114] N. Tesla, *Apparatus for Transmitting Electrical Energy*, U.S. Patent No. 1,119,732, filed 18 Jan. 1902, awarded 1 Dec. 1914.
- [115] J. Hettinger, *Aerial Conductor for Wireless Signaling and Other Purposes*, U.S. Patent No. 1,309,031, filed 4 Jun. 1917, awarded 8 Jul. 1919.
- [116] J.C. Baggesen and L.B. Madsen, “On the dipole, velocity and acceleration forms in high-order harmonic generation from a single atom or molecule,” *Journal of Physics B: Atomic, Molecular and Optical Physics*, Vol. 44, No. 11, May 2011.
- [117] H. Bentati, R. Abdelmoula, A. Maalej, and K. Maalej, “Numerical analysis solving the elastic dynamic problem,” *International Journal of Modelling, Identification, and Control*, Vol. 19, No. 3, pp. 299-305, 2013.
- [118] R. Kuramasu, K. Inoue, and I. Kanazawa, “Development of Mechanism to Extend the Solar Array Paddle for the Advanced Earth Observing Satellite (ADEOS)”, *Sixth European Space Mechanisms & Tribology Symposium*, Zurich, Switzerland, ESA SP-374, August 1995.
- [119] S. Hong, *Wireless: From Marconi's Black-box to the Audion*, MIT Press, 2001.
- [120] C.A. Tucker, “Power transfer in velocity-vortex acceleration,” *International Journal of Modelling, Identification, and Control*, Vol. 21, Iss. 4, Jun. 2014.

- 
- [121] N. Tesla, "The disturbing influence of solar radiation on the wireless transmission of energy," *Electrical Review*, 6 July 1912.
- [122] J.C. Stark, "Wireless power transmission using a phased array of Tesla coils," Masters of Electrical Engineering in Electrical Engineering thesis, MIT, May 2004.
- [123] J. Altman, "Are new neurons formed in the brains of adult mammals?" *Science*, Vol. 30, No. 135, pp.1127-8, Mar. 1962.
- [124] S. Pacini, G. Vannelli, T. Barni, M. Ruggiero, I. Sardi, P. Pacini, M. Gulisano, "Effect of 0.2T static magnetic field on human neurons: remodeling and inhibition of signal transduction without genome instability," *Neuroscience Letters*, 267, 185 – 188, Apr. 1999.
- [125] D. Formica and S. Silvestri, "Biological effects of exposure to magnetic resonance imaging: an overview," *Biomedical Engineering*, Vol. 3, No. 11, Apr. 2004.
- [126] K. Warwick and M. Gasson, "Practical experimentation with human implants", *Uberveillance and the Social Implications of Microchip Implants: Emerging Technologies*, IGI Global, 2013.
- [127] Q. Yuan, C. Qiang, and S. Kunio, "Effect of human body on near-field resonant coupling wireless power transmission system," *Proceedings Of the 2009 International Symposium on EMC*, pp.25-28. 2009.
- [128] W.G. Walter, "An Electromechanical Animal," *Dialectica*, Vol. 4, pp. 42-9, 1950.
- [129] O. Holland, "Grey Walter: The Pioneer of Real Artificial Life," *Proceedings of the 5th International Workshop on Artificial Life*, MIT Press, Cambridge, pp. 34-44, 1997.
- [130] L. Smith and C. Breazeal, "The Dynamic Life of Developmental Process," *Developmental Science*, (1), 61-68, 2007.
- [131] R. Brooks, "Intelligence without representation," *Artificial Intelligence*, 47 (1-3): pp. 139–59, doi:10.1016/0004-3702(91)90053-M.
- [132] W.G. Walter, "An imitation of life," *Scientific American*, 182(5): 42-5, 1950.
- [133] W.G. Walter, "A machine that learns," *Scientific American*, 185(2): 60-3, 1951.
- [134] O. Holland and R. Goodman. "Robots with internal models: a route to machine consciousness?" *Journal of Consciousness Studies, Special Issue on Machine Consciousness*, Vol. 10, No. 4, 2003.
- [135] S. Coradeschi, H. Ishiguro, M. Asada, S. Shapiro, M. Theilscher, C. Breazeal, M. Mataric, and H. Ishida. "Human-Inspired Robots," *IEEE Intelligent Systems*, 21(4), 74-85, 2006.
- [136] O. Holland, "Exploration and High Adventure: The Legacy of Grey Walter," *The Royal Society*, Aug. 2003.
- [137] W.G. Walter, *The Living Brain*, New York, 1953.

- 
- [138] G. Schönera, M. Doseb, and C. Engelsb, “Dynamics of behavior: Theory and applications for autonomous robot architectures,” *Robotics and Autonomous Systems*, Vol. 16, Issues 2–4, pp. 213–45, Dec. 1995.
- [139] M. Proetzsch, T. Luksch, and K. Berns, “Development of complex robotic systems using the behavior-based control architecture iB2C,” *Robotics and Autonomous Systems*, Vol. 58, Iss. 1, pp. 46–67, Jan. 2010.
- [140] R. Brooks, “A robust layered control system for a mobile robot,” *IEEE Robotics and Automation*, Vol. 2 Iss. 1, Sep. 1985.
- [141] J. Košeckà and R. Bajcsy, “Discrete event systems for autonomous mobile agents,” *Robotics and Autonomous Systems*, Vol. 12, Issues 3–4, pp. 187–98, Apr. 1994.
- [142] M.J. Matarić, “Learning social behavior,” *Robotics and Autonomous Systems*, Vol. 20, No. 2, pp. 191–204, Jun. 1997.
- [143] W.R. Ashby, *Introduction to Cybernetics*, London, Chapman & Hall, Second Impression, 1957.
- [144] W.R. Ashby, *Design for a Brain*, New York, Wiley, 1954.
- [145] C.R. Melhuish, O. Holland, and S.E.J. Hoddell, “Using chorusing for the formation of travelling groups of minimal agents,” *Robotics and Autonomous Systems*, Vol. 28, pp. 207–16, 1999.
- [146] C.A. Tucker, “System of transmission of wireless power,” U.S. Patent 8,274,178, Sep. 2012.
- [147] A. Van Deursen and P. Klint. “Domain-specific language design requires feature descriptions,” *CIT. Journal of computing and information technology*, 10.1, pp. 1-17, 2002.
- [148] R. Brooks, “The relationship between matter and life,” *Nature*. Vol. 409, No. 6818, pp. 409-11, 2001.
- [149] P. Fromherz, “Interfacing neurons and silicon by electrical induction,” *Berichte der Bunsengesellschaft für physikalische Chemie*, Vol. 100, Iss. 7, pp.1093–1102, Jul. 1996.
- [150] S. Vassanelli and P. Fromherz, “Neurons from rat brain coupled to transistors,” *Applied Physics A: Materials Science & Processing*, Vol. 65, No. 2, pp.85-88, June 1997.
- [151] E. García-Pérez, M. Vargas-Caballero, N. Velazquez-Ulloa, A. Minzoni, and F. De Miguel, “Synaptic Integration in Electrically Coupled Neurons,” *Biophysics Journal*, Vol. 86, No. 1, pp.646–55, Jan. 2004.
- [152] C. Walton, E. Pariser, F. Nottebohm, “The Zebra Finch Paradox: Song Is Little Changed, But Number of Neurons Doubles,” *Journal of Neuroscience*, Vol. 32, Iss. 3, pp.761-774, Jan. 2012.

- 
- [153] M. Kaplan, “Environment complexity stimulates visual cortex neurogenesis: death of a dogma and a research career,” *Trends in Neuroscience*, Vol. 24, Iss. 10, pp.617-20, Oct. 2001.
- [154] J. Ho et al., “Wireless power transfer to deep-tissue microimplants,” *Proceedings of the National Academy of Sciences*, 2014, DOI: 10.1073/pnas.1403002111.

FOR AUTHOR USE ONLY



# More Books!



# yes i want morebooks!

Buy your books fast and straightforward online - at one of the world's fastest growing online book stores! Environmentally sound due to Print-on-Demand technologies.

Buy your books online at  
**[www.get-morebooks.com](http://www.get-morebooks.com)**

---

Kaufen Sie Ihre Bücher schnell und unkompliziert online – auf einer der am schnellsten wachsenden Buchhandelsplattformen weltweit!  
Dank Print-On-Demand umwelt- und ressourcenschonend produziert.

Bücher schneller online kaufen  
**[www.morebooks.de](http://www.morebooks.de)**

OmniScriptum Marketing DEU GmbH  
Heinrich-Böcking-Str. 6-8  
D - 66121 Saarbrücken  
Telefax: +49 681 93 81 567-9

[info@omniscriptum.de](mailto:info@omniscriptum.de)  
[www.omniscriptum.de](http://www.omniscriptum.de)

OMNI**S**criptum





